

Development of spray drying technology for microencapsulation of bioactive materials

by

Bangping Wang

A dissertation submitted to the Graduate Faculty of
Auburn University
in partial fulfillment of the
requirements for the Degree of
Doctor of Philosophy

Auburn, Alabama
December 12, 2015

Key words: Microencapsulation, Spray drying, Gelatin, Shrinkage behavior, Capacitance sensor, PIV

Copyright 2015 by Bangping Wang

Approved by

Yifen Wang, Chair, Professor of Biosystems Engineering
Steve R. Duke, Co-chair, Associate Professor of Chemical Engineering
Timothy McDonald, Professor of Biosystems Engineering
Brian S. Thurow, Associate Professor of Aerospace Engineering

Abstract

Lipophilic bioactive components, such as carotenoids, have received increasing attention in food and pharmaceutical industries because of their potential health benefits. They have been recognized to exhibit physiological activities in metabolic and nutritional studies. However, the utilization of carotenoids as functional ingredients is currently limited due to high susceptibility to adverse environment conditions (such as oxidant, heat, light, pH value and enzyme). To overcome these problems, microencapsulation technology has been proposed in order to make the bioactive component more stable during handling, processing, storage and delivering. In the food industry, the most common procedure for microencapsulation is spray drying. Low cost, easy to scale, wide choices of wall materials and the possibility of producing micro-sized particles with adjustable size and morphology make this means ideal for particle encapsulation. Proper selection of wall materials is of the utmost importance for spray drying so that required functional characteristics are met for the final microcapsules. Gelatin is a natural bitterless, odorless hydrocolloid that has received great attention in food and pharmaceutical industries due to its biocompatible, biodegradable and “generally regarded as safe (GRAS)” characteristics.

This study attempts to develop a feasible spray-drying process to prepare gelatin microspheres as viable wall materials to protect bioactive materials from degradation and improve their uptake and bioavailability. The lab-scale spray dryer Buchi B-290 was used to produce particles under various operating conditions and the spray characteristics were visualized by high magnification imaging system for better understanding of the heat and

mass transfer and particle formation process during the spray drying. The effect of the processing conditions on dried particle properties (size, morphology, yield, moisture content) was investigated. Data from visualization experiments was collected and used for gelatin shrinkage model development. This study is helpful in the industrial application of gelatin as potential wall material for food and pharmaceutical microencapsulation. A stable oil-in-water (O/W) emulsion system to microencapsulate bioactive materials by spray drying was then developed. Effects of emulsification methods (high-energy and low-energy homogenization methods) on emulsion stability were characterized at various surfactant to oil ratios (SOR) with different types of oil (MCT oil, olive oil) and emulsifiers (gelatin, Tween 80). High-energy method was preferred for safety concerns, as it was able to produce fine stable emulsions at low SOR. O/W emulsions, using MCT oil as core material, gelatin as wall material and Tween 80 as secondary emulsifier, were prepared and spray dried to create micron-size microcapsules. Effects of operating conditions, including inlet temperature, on the resultant microcapsules properties (e.g. size, morphology, moisture content (MC), encapsulation efficiency (EE) and yield (Y)) were investigated. The results demonstrated that spray drying technology could be applied to transform the stable O/W emulsions into powders with desired properties. So it is feasible to use this emulsion-based system to microencapsulate carotenoids in the near future.

The residual moisture content (MC) of spray dried powders is of great importance to define the product quality, since it is directly related to drying conditions and it affects particle deposition and yield. Several methods (oven drying, NIR (near infrared spectroscopy)) have been developed to measure MC offline. However, many are not appropriate for spray drying

where an online (real-time) assessment of MC is required. The objective of this study was to develop a sensor for measuring moisture content of a moving stream of spray dried powders. A capacitance sensor was built for this purpose using pairs of copper plate electrodes attached to the perimeter of the spray dryer product collection vessel. The plates formed capacitors that were sensitive to changes in dielectric properties of the material within the collection vessel, which in turn were related to MC. Each electrode was connected to a capacitance-to-voltage transducer, the output of which was sampled using a commercial data acquisition system. The amplitude of the sensor output signal was calculated using software LabVIEW and correlated with MC. The self-built system was tested in two modes: a) an offline (non-moving sample) mode in which a mass-based MC prediction model was built to validate the capability of the sensor to measure variation in MC; and b) an online (moving sample) mode to measure MC of sample moving through the sensor enclosure. Tests were made on spray dried gelatin powders ranging in moisture content of 5% to 50% (w.b.). Results indicated a high correlation between sensor output and moisture content ($R^2 > 0.9$). The capacitance sensor also showed the ability to characterize the distribution of MC (permittivity) within the sensor enclosure, which could reflect spatial variation in deposition of dried powders during spray drying. Overall, the capacitance sensor system was feasible to measure MC for online sampling with acceptable accuracy, and can be applied in quality control applications for continuous spray drying processes.

To evaluate the airflow pattern (velocity field) inside a co-current lab scale spray dryer, air velocity magnitudes were measured by a particle image velocimetry (PIV) system at numerous locations in the spray dryer chamber in the absence of spray. Analysis at varied

drying air flow rate strongly suggested the flow in the chamber has high turbulence intensity.

The PIV analysis also provided information on how drying air flow rate affects fluid flow profiles, which could help to collect data for validation of the CFD simulated results.

Acknowledgements

First and foremost, I would like to express my deep and sincere gratitude to my advisor Dr. Yifen Wang and my co-advisor Dr. Steve Duke for their constant guidance, support and patience throughout my degree program. Their scientific attitude and philosophy have had a profound influence on me. Under their supervision, I learned how to do scientific research. Their encouragement and support certainly help me in my determination to finish this dissertation on time. I am also grateful to Dr. Timothy McDonald, Dr. Brian Thurow for being on my committee. Thanks Dr. Brian Via for being my dissertation reader. Their suggestions and feedbacks greatly improve my research. Sincere thanks will also go to professors, colleagues in the department and laboratory, especially for Dr. Rajeshwar Chinnawar, Dr. Pengmin Pan and Dr. Johnathan Bolton for their help, collaboration, and friendship. I would like to also express my gratitude to the Chinese Scholarship Council for the scholarship that made my studies possible.

Finally and as always, I want to give a special acknowledgement to my parents and my girlfriend for their love, support and encouragement.

Table of Contents

Abstract.....	ii
Acknowledgements.....	vi
List of Figures.....	xi
List of Tables.....	xiv
Chapter 1 Introduction.....	1
References.....	8
Chapter 2 Study on spray drying of gelatin as potential material for encapsulation.....	10
Abstract.....	10
2.1 Introduction.....	11
2.2 Materials and Methods.....	13
2.2.1 Gelatin solution preparation.....	13
2.2.2 Overall mass and heat balance in the spray dryer.....	14
2.2.3 Spray drying of gelatin solutions.....	16
2.2.4 Visualization of spray characteristics.....	16
2.2.5 Powder analysis.....	18
2.3 Results and discussion.....	19
2.3.1 Effect of concentration, temperature and pH value on gelatin solution.....	19

2.3.2 Selection of the operating conditions	21
2.3.3 Particle moisture content and yield	26
2.3.4 Initial droplet size distribution.....	29
2.3.5 Shrinkage behavior of 5 wt% gelatin droplets.....	30
2.3.6 Gelatin properties before and after spray drying	38
Conclusion.....	41
References	42
Chapter 3 Study on the feasibility of microencapsulation of bioactive materials by spray	
drying	50
Abstract	50
3.1 Introduction	51
3.2 Materials and methods	57
3.2.1 Materials	57
3.2.2 Preparation of wall solution and infeed emulsion	58
3.2.3 Emulsion characterization	59
3.2.4 Microencapsulation of emulsions by spray drying.....	59
3.2.5 Powder analysis	59
3.3 Results and discussion.....	61
3.3.1 Preparation of O/W emulsions	61

3.3.2 Microcapsule characterization	70
Conclusions	76
References	77
Chapter 4 Monitoring moisture content of spray dried powders using capacitance sensor.....	94
Abstract	94
4.1 Introduction	96
4.2 Capacitance sensing system configuration.....	97
4.3 Materials and Methods	101
4.3.1 Offline mode (4-electrode capacitance sensing system)	101
4.3.2 Online mode (Dual frequency capacitance sensing system)	104
4.3.3 Electric capacitance tomography (ECT) mode.....	105
4.4 Results and Discussion.....	106
4.4.1 Validation of the capability of the sensor	106
4.4.2 Measurement of MC of moving samples	111
4.4.3 Visualization of the deposition status of spray dried powders	112
Conclusion.....	115
References	116
Chapter 5 PIV measurements of airflow patterns in a lab-scale spray dryer.....	117
Abstract:	117

5.1 Introduction	118
5.1.1 Seeding	120
5.1.2 Laser and optics	121
5.1.3 Camera and synchronization	122
5.1.4 Imaging analysis	126
5.2 Materials and Methods	128
5.3 Results and discussion.....	133
Conclusion.....	139
References	140
Chapter 6 Conclusion and future work	147

List of Figures

Fig. 1.1 Schematic representation of encapsulation systems	2
Fig. 1.2 Number of papers published in Web of Science database with topic “spray drying” in the last decade	4
Fig. 2.1 Image showing experimental setup for visualization studies of the spray dryer and schematic diagram of the apparatus setup	18
Fig. 2.2 Viscosity of gelatin solutions at various conditions	21
Fig. 2.3 Influence of pH on electrical charge (zeta potential) of gelatin solutions.....	21
Fig. 2.4 Corresponding outlet temperature (T_o) versus inlet temperature (T_i)	22
Fig. 2.5 Plot of UA as a function of log mean temperature difference (ΔT_{LM}) between inlet (T_i), outlet (T_o) and the ambient temperature (T_{amb}).....	24
Fig. 2.6 Estimation of drying gas required for different amount of liquid feed	25
Fig. 2.7 Effects of variation in T_i on residual moisture content.....	27
Fig. 2.8 Effects of variation in T_i on particle yield	27
Fig. 2.9 Initial droplet size distribution approximation	30
Fig. 2.10 Droplet size change along the spray dryer as a function of the distance from nozzle outlet	33
Fig. 2.11 Comparison of d_{peak} and d_{50} value	34
Fig. 2.12 Estimation of MC change histories of 5 wt% gelatin droplets.....	36

Fig. 2.13 SEM image of raw gelatin and spray-dried gelatin powder	40
Fig. 3.1 Schematic representation of spontaneous emulsification	56
Fig. 3.2 Effect of SOR and oil type on mean droplet size of emulsion formed by high-energy method.....	63
Fig. 3.3 Droplet size distribution of MCT oil-in-water emulsion formed by high-energy method.....	64
Fig. 3.4 Droplet size distribution of olive oil-in-water emulsion formed by high-energy method	65
Fig. 3.5 Effect of SOR on mean droplet size of emulsion produced by spontaneous emulsification (SE)	66
Fig. 3.6 Droplet size distribution of MCT oil-in-water emulsion formed by spontaneous emulsification.....	67
Fig. 3.7 Particles size distribution of spray dried powders	74
Fig. 3.8 SEM image of microcapsulated MCT oil with gelatin as wall materials.....	75
Fig. 4.1 Schematic diagram of the Capacitance-to-voltage transducer circuit	99
Fig. 4.2 Image showing experiment setup for MC measurement	101
Fig. 4.3 Illustration of the offline mode	102
Fig. 4.4 Illustration of online mode	105
Fig. 4.5 Sensor output at empty and full state.....	107
Fig. 4.6 Measured sensor output (V) against water content (g).....	109
Fig. 4.7 Measured sensor output (V) against spray dried gelatin powder content (g).....	109

Fig. 4.8 Measured sensor output (V) against spray dried gelatin plus water content (g)	110
Fig. 4.9 MC Prediction with dual frequency method	112
Fig. 4.10 Sensitivity matrix simulated by ANSYS APDL for (left) C ₁₂ and (right) C ₁₃	113
Fig. 4.11 Simulated deposition status inside the spray dryer.....	114
Fig. 5.1 Timing diagram for double shutter camera and double pulsed laser.....	121
Fig. 5.2 Timing diagram for a PIV system using double-pulsed laser and double-shutter camera.....	124
Fig. 5.3 PIV data analysis via cross correlation.....	128
Fig. 5.4 PIV setup along with the spray dryer B-290	129
Fig. 5.5 Schematic diagram of the PIV system apparatus setup	130
Fig. 5.6 PIV image of the region 14 to 17 cm from the nozzle inlet for 50% aspirator rate	134
Fig. 5.7 PIV image of the region 5 to 8 cm from the nozzle inlet for 100% aspirator rate ..	135
Fig. 5.8 PIV image of the region 8 to 11 cm from the nozzle inlet for 100% aspirator rate	136
Fig. 5.9 PIV image of the region 14 to 17 cm from the nozzle inlet for 100% aspirator rate	136
Fig. 5.10 PIV image of the region 29 to 32 cm from the nozzle inlet for 100% aspirator rate	137
Fig. 5.11 PIV image of the region 38 to 41 cm from the nozzle inlet for 100% aspirator rate	137
Fig. 5.12 PIV image of the region 41 to 44 cm from the nozzle inlet for 100% aspirator rate	138

List of Tables

Table 2.1 Comparison of T_o versus estimated T_g and T_s	29
Table 2.2 Droplet diameter as a function of distance from nozzle outlet	32
Table 2.3 Gelatin properties before and after spray drying	39
Table 3.1 Recent publications for microencapsulation of carotenoids by spray drying	55
Table 3.2 Effect of drying temperature on the properties of the spray dried microcapsules ...	73
Table 4.1 Comparison of various MC measurement method	97
Table 4.2 SNR for each electrode combination	107
Table 4.3 Sensitivity test (t-test) and location test (ANOVA test) of the sensor output.....	108
Table 4.4 P-value of the coefficient in the regression model	111
Table 5.1 Effect of aspirator settings on drying gas performance	130
Table 5.2 Detailed information about the PIV system set-up.....	131

Chapter 1

Introduction

Bioactive materials, such as carotenoids and vitamins, are important nutritional substances with health promoting and disease preventing benefits. Insufficient supply of these materials may lead to many disorders or deficiency diseases (Murugesan & Orsat, 2012). Consumption of these materials as functional ingredients will therefore have very broad application prospects. However, difficulties in utilization of these materials in food and pharmaceutical industry may be encountered due to their instability during processing and storage (Desai & Park, 2005). In order to overcome this problem, microencapsulation technology has been proposed. It can help to protect the bioactive materials from adverse environments, and improve their biological properties. Moreover, microencapsulation also allows controlled release of these functional components at targeted sites, and masks unpleasant taste and odor of the substances (de Vos et al., 2010).

Microencapsulation consists a process to entrap one substance within another substance, thereby producing spherical particles with diameters of a few nanometers to a few millimeters. The substance that is encapsulated is called the core material. The substance that is encapsulating is called the wall material. Microencapsulation allows formation of a physical barrier between the core material and its surroundings (Burgain et al., 2011).

Depending on the physico-chemical properties of the core and wall material, and the method used for microencapsulation, different types of encapsulates can be obtained. Fig. 1.1 shows three major morphologies of encapsulates. Microcapsules with a single core surrounded by a layer of wall material is called the reservoir type. Microspheres with the core homogeneously dispersed in a continuous matrix network is called matrix type. A combination of these two

types gives a third type of capsule: coated matrix type. For simplification, Fig. 1.1 only shows spherical shaped encapsulates, but they can also be cylindrical, oval or irregular shaped.

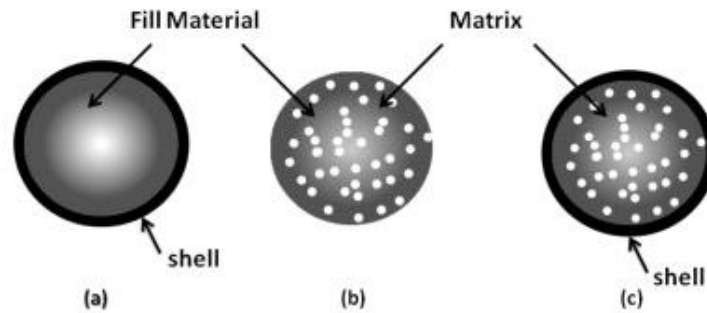


Fig. 1.1 Schematic representation of encapsulation systems: (a) reservoir type, (b) matrix type, and (c) coated matrix type (Modified from Burgain et al., 2011).

Although various techniques are available for microencapsulation of bioactive components (including spray drying, emulsification, coacervation, extrusion), spray drying is the most common technology used in food industry due to it is a rapid, continuous, reproducible, cost-effective, and easily scalable properties (Zuidam & Shimoni, 2009). Fig. 1.2 shows the number of publication with the topic “spray drying” in the last decade. Spray-drying is a continuous dehydration process to convert an initial feed liquid (containing wall and core materials) into a solid powder formed by atomizing the feed into a hot drying medium. There are four main steps in the spray-drying operation: (1) preparation and homogenization of the liquid feed; (2) atomization of the liquid feed; (3) dehydration of the atomized particles; and (4) separation and collection of the dry product. First, the liquid is fed into the drying chamber by a pump through different types of atomizers (pneumatic atomizer, pressure nozzle, spinning disk, fluid nozzle and sonic nozzle). The initial feed liquid can be a solution, an emulsion, or a suspension. Increasing the energy provided to the atomizer decreases the size of the formed droplets. For the same energy amount, the size of formed particles increases with increasing feed rate. On the other hand, the size of particles also increases with

the viscosity and surface tension of the feed liquid. The small droplets generated are subjected to fast solvent evaporation, leading to the formation of dry particles. The gas generally used is air or inert gas such as nitrogen. Regarding the direction of the drying gas flow with respect to the direction of the liquid atomization, there exist two possibilities: co-current flow (same direction) and counter-current flow (opposite direction). In the first case, the final product is in contact with the coolest air, hence is preferable for the drying of heat-sensitive materials. In the second case, the dry product is in contact with the hottest air and therefore it cannot be used with temperature-sensitive materials, but is desirable in terms of higher thermal efficiency. In addition, there are intermediate configurations with mixed flow between co-current and counter-current. Although spray-drying is often considered as a dehydration process, it can be used to encapsulate bioactive materials within a protective matrix. A remarkable advantage of spray-drying is the possibility to dry a broad spectrum of compounds including heat-sensitive substances without major detrimental effects. The atomization of the liquid into small droplets with high surface area-to-volume ratio results in very fast solvent evaporation. The fast drying process avoids significant degradation of the encapsulated materials and allows the preservation of their activity after the process (Ezhilarasi et al., 2013; Gharsallaoui et al., 2007; Sosnik & Seremeta, 2015).

The choice of a wall material for spray-drying is very important for microencapsulation efficiency and microcapsule stability. Depending on the core material and the characteristics desired in the final product, wall materials can be selected from a wide variety of natural and synthetic polymers. Since almost all spray-drying processes in the food industry are carried out from aqueous feed formulation, the wall material must be soluble in water at an acceptable level. In addition to its high solubility, a wall material should possess good properties of emulsification, film forming, and the wall concentrated solutions should have

low viscosity. Many different wall materials have been used for spray drying, including proteins (gelatin, casein, milk serum, soy and wheat), polysaccharides (starch, maltodextrins, corn syrups and gum Arabic), lipids (stearic acid, mono and diglycerides) and synthetic polymers (acrylic polymers, polyvinylpyrrolidone). Utilization of protein/polysaccharide mixtures allows the possibility of combining the specific properties of each of these polymers. Proteins can serve as an emulsifying and film-forming agent, while polysaccharides can act as a matrix forming material (Estevinho et al., 2013).

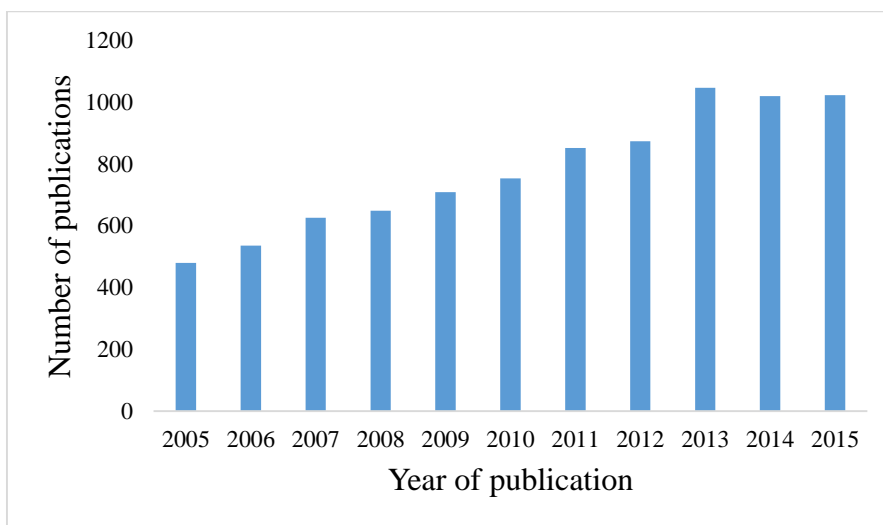


Fig. 1.2 Number of papers published in Web of Science database with topic “spray drying” in the last decade (visited Nov, 2015)

In the case of lipophilic core microencapsulation, such as carotenoids, a fine and stable oil-in-water emulsion is prepared before the spray drying step. The formed emulsion must be stable over a certain period of time. These emulsion are often fabricated either using high-energy or low-energy approach. High-energy approach utilizes mechanical devices (homogenizers) capable of generating intense disruptive forces that are capable of disrupting and intermingling the oil and aqueous phases into tiny oil droplets. High pressure homogenization is preferred because of its interesting results in terms of emulsion properties and stability. Moreover, increasing homogenization pressure gives a slight decrease in oil droplet size and emulsion viscosity. High viscosities interfere with the atomization process and lead to the

formation of elongated and large droplets that adversely affect the drying rate. Low energy approach relies on the spontaneous formation of tiny oil droplets within mixed oil-water-emulsifier system (McClements & Rao, 2011).

In order to improve microencapsulation efficiency and obtain products with desirable characteristics, optimization of spray drying process is quite necessary (Fang & Bhandari, 2010; Kandansamy & Somasundaram, 2012; Krishnaiah et al., 2014; Nesterenko et al., 2013). The main factors in spray-drying that must be optimized are feed temperature, air inlet temperature, and air outlet temperature. Feed temperature modifies the viscosity of the emulsion. When the feed temperature is increased, viscosity and droplets size should be decreased but high temperatures can cause degradation of some heat-sensitive ingredients. Appropriate adjustment of the air inlet temperature and flow rate is also important. In fact, air inlet temperature is directly proportional to the drying rate and the final moisture content (MC). When the air inlet temperature is low, the low evaporation rate causes the formation of microcapsules with high moisture content, poor fluidity, and easiness of agglomeration. However, a high air inlet temperature may cause an excessive evaporation and results in cracks in the membrane or a degradation of encapsulated ingredient. Traditionally, optimization of these spray drying parameters is achieved by trial-and-error procedures, in which the operation variables and dried product properties are correlated with the help of statistical experimental design techniques (design of experiments (DOE)). The most common approaches used include Plackett–Burman factorial design, response surface methodology (RSM), artificial neural network (ANN) and etc. However, the complexity of the spray drying process makes this procedure time consuming and costly. Let alone the measurement of some parameters are very difficult. The traditional methods also do not allow determination of the drying phenomena and kinetics that govern particle formation. All these drawbacks have

heightened the expectation for better understanding and controlling the spray drying process.

In the spray drying process, droplets shrink as moisture is removed, while the change in droplet size affects mass and heat transfer that determine the drying behavior. Drying kinetics is a key element in predicting a material's drying behavior and product quality. Drying kinetics models allow for predicting constant and falling drying periods in the dryer chamber. Due to increased resistances to heat-mass transfer during drying, the drying rate significantly slows down during the falling drying period and will affect the overall drying time.

Measurement of drying kinetics and fitting of measured data with an appropriate drying kinetics model are important steps to understand the shrinkage behavior of droplets during drying. Even though there are many reported works on microencapsulation, there has been a lack of this fundamental mechanistic information on this process. If a quantitative understanding of the drying process can be gained, it is possible to simulate different spray drying conditions to optimize the process (Kuriakose & Anandharamakrishnan, 2010; Patel et al., 2010).

The moisture content of spray dried product is of great importance to define product quality, and also it is a good indicator to evaluate the spray dryer performance. Several methods like oven drying and near infrared spectroscopy (NIR) have been applied in spray drying system to measure MC offline. However, these methods are not suitable to measure MC for spray dried products, which are usually moving samples. There is also lack of approaches for quality control of continuous spray drying processes.

Due to the complexity of the physical mechanisms (e.g. heat transfer, flow behavior) involved in spray drying processing, understanding of the underlying processes has still been

poor. Since the introduction of fast computers and computational fluid dynamics (CFD), it is now possible to evaluate spray dryer performance without undertaking expensive experimental tests. Although simulation of the complex transport phenomena that occurs in a spray dryer cannot yet be modeled with high accuracy, the results are nevertheless useful to guide design and operation of spray dryers when coupled with some empirical experience. However, there are still some limitations to the CFD approach since it does not typically include reliable and validated models. This requires measurement of local properties using experimental techniques such as hot wire anemometry and laser Doppler anemometry and hence, validation of CFD simulations.

The aim of this study is to develop spray drying technology for microencapsulation of bioactive materials. In chapter 2, the potential of gelatin as wall material for encapsulation is evaluated. Effect of operating conditions on the resultant particles was investigated in order to optimize the spray drying process. The gelatin droplet shrinkage behavior during spray drying was also visualized. In chapter 3, an emulsion-based system was developed for further microencapsulation of bioactive materials. Both high and low energy emulsification methods were applied to fabricate emulsions and their performance was characterized. The obtained emulsion was then spray dried and microcapsules properties was investigated to find the optimal conditions for microencapsulation. In chapter 4, a self-built capacitance sensor was developed for measuring MC of the moving stream of spray dried powders. The capacitance sensor was tested in three different modes for different purposes in order to determine its feasibility for MC measurement as well as quality control of the spray drying process. In chapter 5, a particle image velocimetry (PIV) system was introduced to visualize the airflow pattern in a lab-scale spray dryer, which aimed to investigate the airflow profile and collect data for CFD simulation results.

References

- Burgain J, Gaiani C, Linder M, Scher J, 2011. Encapsulation of probiotic living cells: From laboratory scale to industrial applications. *Journal of Food Engineering*. 104(4):467-483.
- Desai KGH, Park HJ, 2005. Recent Developments in Microencapsulation of Food Ingredients. *Drying technology*. 23:1361-1394.
- de Vos P, Fass MM, Spasojevic M, Sikkema J, 2010. Encapsulation for preservation of functionality and targeted delivery of bioactive food components. *International Dairy Journal*. 20(4):292-302.
- Estevinho BN, Rocha F, Santos L, Alves A, 2013. Microencapsulation with chitosan by spray drying for industry applications – A review. *Trends in Food Science & Technology*. 31(2):138-155.
- Ezhilarasi PN, Karthik P, Chhanwal N, Anandharamakrishnan C, 2013. Nanoencapsulation Techniques for Food Bioactive Components: A Review. *Food Bioprocess Technology*. 6:628-647.
- Fang ZX & Bhandari B, 2010. Encapsulation of polyphenols – a review. *Trends in Food Science & Technology*. 21(10):510-523.
- Gharsallaoui A, Roudaut G, Chambin O, Voilley A, Saurel R, 2007. Applications of spray-drying in microencapsulation of food ingredients: An overview. *Food Research International*. 40(9):1107-1121.
- Kandansamy K, Somasundaram PD, 2012. Microencapsulation of Colors by Spray Drying - A Review. *International Journal of Food Engineering*. 8(2): Article 1.
- Krishnaiah D, Nithyanandam R, Sarbatly R, 2014. A critical review on the spray drying of fruit extract: effect of additives on physicochemical properties. *Critical Reviews in Food Science and Nutrition*. 54(4):449-473.
- Kuriakose R & Anandharamakrishnan C, 2010. Computational fluid dynamics (CFD)

- applications in spray drying of food products. *Trends in Food Science & Technology*. 21(8):383-398.
- McClements DJ & Rao JJ, 2011. Food-Grade Nanoemulsions: Formulation, Fabrication, Properties, Performance, Biological Fate, and Potential Toxicity. *Critical Reviews in Food Science and Nutrition*. 51(4):285-330.
- Murugesan R & Orsat V, 2012. Spray Drying for the Production of Nutraceutical Ingredients- A Review. *Food and Bioprocess Technology*. 5(1):3-14.
- Nesterenko A, Alric I, Silvestre F, Durrieu V, 2013. Vegetable proteins in microencapsulation: A review of recent interventions and their effectiveness. *Industrial Crops and Products*. 42(2013):469-479.
- Patel K, Chen XD, Jeantet R, Schuck P, 2010. One-dimensional simulation of co-current, dairy spray drying systems — pros and cons. *Dairy Science & Technology*. 90(2):181-210.
- Sosnik A, Seremeta KP, 2015. Advantages and challenges of the spray-drying technology for the production of pure drug particles and drug-loaded polymeric carriers. *Advances in Colloid and Interface Science*. 223(2015):40-54.
- Zuidam NJ & Shimoni E, 2009. Overview of Microencapsulates for Use in Food Products or Processes and Methods to Make Them. *Book: Encapsulation Technologies for Active Food Ingredients and Food Processing*. 3-29.

Chapter 2

Study on spray drying of gelatin as potential material for microencapsulation

Keywords

Gelatin, Spray drying, Wall material, Shrinkage behavior

Abstract

This study attempts to develop a feasible spray-drying process to prepare gelatin microspheres as viable wall materials to protect bioactive elements from degradation and improve their uptake and bioavailability. The lab-scale spray dryer Buchi B-290 was used to produce gelatin particles under various operating conditions. Analysis of the resultant particles indicates the importance of optimizing the operating conditions, in order to obtain products with desired properties. For better understanding of the heat and mass transfer and particle formation process during the spray drying, a high magnification imaging system was introduced in the present work to investigate the droplet/particle shrinkage behavior of gelatin droplets during spray drying. 5 wt% gelatin solution was atomized and heated at 3 different drying temperatures (120, 150, 180°C), the spray characteristics were visualized at various vertical distances (~0, 7, 14, 21, 28, 35, 42 cm) from the nozzle outlet, and the drying temperature effects on droplet/particle diameter change were studied. Changes in droplet/particle size were correlated with the moisture content, and compared with the final particle size determined by scanning electron microscopy (SEM). This study provides a better understanding of the drying behavior of gelatin droplets, which aids the design of the system for the production of gelatin-based microcapsules by spray drying. This study demonstrates the potential for the industrial application of gelatin as potential wall material for food and pharmaceutical microencapsulation.

2.1 Introduction

Spray-drying is a rapid, continuous and easily scalable dehydration process that is used as a means of producing micro particles with adjustable size and morphology. It is the most common microencapsulation technology in food and pharmaceutical industries because of its low cost, wide choices of wall materials and capability of drying even heat-sensitive materials (Gharsallaoui et al., 2007; Santos & Meireles, 2010; Verma & Singh, 2015). Proper selection of wall materials is of the utmost importance for spray drying to obtain the required functional characteristics for the final microcapsules. Gelatin is a natural, bitterless, odorless hydrocolloid that has received great attention in food and pharmaceutical industries due to its biocompatible, biodegradable and “generally regarded as safe (GRAS)” characteristics (Hanani 2014; Kapoor & Dhawan, 2013; Pignatello 2011; GRAS Substances, 1975). It also exhibits good emulsifying and drying properties (film forming properties, relative high glass transition temperature (T_g)), which allows its use as both surface-active agent and wall material (Karim & Bhat, 2008). This study attempts to develop a feasible spray-drying process to prepare gelatin microspheres as viable wall materials to protect bioactive elements from degradation and improve their uptake and bioavailability. In order to produce a product with desired characteristics, the operating conditions must be carefully selected. A greater control of the spray drying process can lead to higher production rates, improvements in energy efficiency, and more consistent powder quality.

Even though there are many reported works on gelatin microencapsulation (Calvo et al., 2010; Han et al., 2008; Hee et al., 2015; Huang et al., 2014; Li et al., 2008; Paramita et al., 2010; Pourashouri et al., 2014a,b; Prata & Grosso, 2015; Tran et al., 2014; Wang et al., 2009, 2012; Xie et al., 2010), fundamental mechanistic information on this process is lacking, particularly on the droplet drying process itself. During the spray drying process, droplets are

expected to shrink due to the evaporation of water, and this shrinkage behavior exhibits significant effects on the particle characteristics, such as size and morphology (Fu et al., 2013; Vehring et al., 2007), which may further affect the quality of the final products (Kim et al., 2009; Islam & Langrish, 2010). Therefore, the understanding of shrinkage behavior of droplets under different operating conditions is of great importance for quality control in order to produce products with desired properties.

Droplet shrinkage behavior can be studied by single droplet drying (SDD) technique, where a single droplet is generated and dried under a controlled environment, and changes in droplet drying behavior are monitored as drying progresses. Depending on the methodologies used, the droplet can be either suspended at a fixed position (e.g. suspended on a thin glass filament (or glass capillary tube) (Che et al., 2010; Fu et al., 2012b, 2013; Woo et al., 2011), deposited on a flat surface (Perdana et al., 2013), levitated by acoustic fields (Mondragon et al., 2011, 2012; Sloth et al., 2006, 2010), or studied as a free falling droplet (Amelia et al., 2011; Wu et al., 2011). The SSD technique could mimic the actual spray drying conditions to some extents (Fu et al., 2012a, 2013; Rogers et al., 2012; Schutyser et al., 2012). However, during a conventional spray drying process, billions of droplets are simultaneously generated, the complexity in droplet sizes and trajectories (Patel & Chen, 2007) makes it difficult for SSD to develop an environment that can represent the actual drying profile each droplet experiences within the spray dryer. In addition, the SSD experiments are often restricted due to the relatively large initial droplet size, for example, droplets generated from the conventional spray dryer generally have a size range between 10-500 μm (Oakley, 1997), while the glass filament SSD experiments are only feasible when droplets are greater than 800 μm (Rogers et al., 2012), as it is more difficult to measure the drying kinetics of a smaller droplet. The presence of the glass filament or acoustic field in the SSD system could also lead to some

unwanted effects, such as additional heat convection from the supporting glass filament or possible effect of acoustic waves on the mass and heat transfer rate (Schutyser et al., 2012). Apart from the SSD technique, Alamilla-Beltrán et al. (2005) designed a unique device for capturing spray samples at different heights of the drying chamber, such set-up allowed better understanding of the intermediate droplet changes inside the spray dryer. However, semi-dried droplets collected were usually crushed into a thin smear, which limited its use for further quantitative analysis (Fu et al., 2013). In order to achieve an accurate measurement on the droplet shrinkage behavior within the spray dryer, a high magnification imaging system was used in the present study to monitor the atomized spray droplets. The effects of drying temperature on the spray characteristics and particle characteristics were also investigated.

The objectives of this study are to 1) produce micro-sized gelatin particles through spray drying and investigate the effect of operating conditions on particle characteristics (particle size, morphology, moisture content) and 2) study spray characteristics during spray drying by high magnification visualization technique, which will facilitate the understanding of droplet shrinkage behavior during the drying process. This study will be helpful in the industrial application of gelatin as potential wall material for food and pharmaceutical microencapsulation.

2.2 Materials and Methods

2.2.1 Gelatin solution preparation

Aqueous gelatin solutions were prepared by dispersing the desired amount (1-20 wt%) of raw gelatin powders (Amresco LLC, Solon, OH) into distilled water and magnetic stirring (PC-101 Hot Plate Magnetic Stirrer, Corning Incorporated, Corning, NY) overnight to ensure complete dissolution. The viscosity of aqueous gelatin solution was determined using a

Cannon-Fenske viscometer (Cannon Instrument Co., State College, Pa., U.S.A.) at 40, 50, 60 and 70°C, respectively. Influence of pH on electrical charge (zeta-potential) was determined using an Electrophoretic Light Scattering (ELS) instrument (Zetasizer Nano ZS, Malvern Instruments, Malvern, UK). Samples were diluted in deionized water prior to analysis to avoid scattering effects.

2.2.2 Overall mass and heat balance in the spray dryer

The overall mass and energy balance equations were applied in assisting selection of appropriate operating conditions for spray drying (Ivey & Vehring, 2010; Langrish, 2009; Pu et al., 2011). The connections in B-290 are screw thread connections with rubber seals, so the gas leakage can be negligible (Hanus & Langrish, 2007), the mass of water entering the spray dryer is assumed to be equal to the mass of water leaving the spray dryer (Equation 1). The energy entering the dryer is through hot gas and liquid feed, while the energy leaving the dryer is mainly through both humid gas and solids. Heat loss was considered in this work as the spray dryer (B-290) had a large surface area and no insulation on the dryer chamber (Hanus & Langrish, 2007). So the energy balance over the spray dryer follows the principles that the total energy entering the dryer (Q_i) (Equation 2) equals to the energy leaving the dryer (Q_o) (Equation 3) plus energy (heat) loss (Q_{loss}) ($Q_i = Q_o + Q_{loss}$). The spray dryer was first operated with heated gas only (no liquid), the inlet and outlet gas temperatures were measured experimentally and the energy (heat) loss values were calculated using equation (4). The Q_{loss} values obtained were then used to determine overall heat transfer coefficient (UA) in equation (5).

$$M_g \cdot 1/(1+Y_i) \cdot Y_i + M_f \cdot 1/(1+X_i) \cdot X_i = M_g \cdot 1/(1+Y_o) \cdot Y_o + M_f \cdot 1/(1+X_o) \cdot X_o \quad (1)$$

$$Q_i = M_g \cdot 1/(1+Y_i) \cdot \{C_{pg} (T_{gi} - T_{ref}) + Y_i \cdot [\Delta H_v + C_{pv} (T_{gi} - T_{ref})]\}$$

$$+ M_f \cdot 1 / (1 + X_i) \cdot (C_{ps} + X_i \cdot C_{pw}) \cdot (T_{fi} - T_{ref}) \quad (2)$$

$$Q_o = M_g \cdot 1 / (1 + Y_i) \cdot \{ C_{pg} (T_{go} - T_{ref}) + Y_o \cdot [(\Delta H_v + C_{pv} (T_{go} - T_{ref}))] \} \\ + M_f \cdot 1 / (1 + X_i) \cdot (C_{ps} + X_o \cdot C_{pw}) \cdot (T_{so} - T_{ref}) \quad (3)$$

$$Q_{loss} = M_g \cdot C_{pg} \cdot (T_{gi} - T_{go}) \quad (4)$$

$$Q_{loss} = UA \cdot \Delta T_{LM} = UA \cdot [(T_i - T_{amb}) - (T_o - T_{amb})] / \ln[(T_i - T_{amb}) / (T_o - T_{amb})] \quad (5)$$

Where M_g and M_f are the mass flow rates of drying gas and liquid feed entering the dryer ($\text{kg} \cdot \text{s}^{-1}$), respectively. X_i , X_o are the inlet and outlet solids moisture content (dry basis, $\text{kg water} \cdot (\text{kg solids})^{-1}$), Y_i , Y_o are the inlet and outlet gas humidity (dry basis, $\text{kg water} \cdot (\text{kg dry gas})^{-1}$), respectively. T_{gi} , T_{li} are the gas inlet temperature and feed inlet temperature ($^{\circ}\text{C}$). T_{ref} is the reference temperature ($^{\circ}\text{C}$). C_{pg} , C_{pw} , C_{ps} , C_{pv} refer to the specific heat capacity of drying gas, water, feed solid and pure water vapor ($\text{kJ} \cdot \text{kg}^{-1} \cdot \text{K}^{-1}$), respectively. ΔH_v is the latent heat of vaporization for water ($\text{kJ} \cdot \text{kg}^{-1}$). U refers to the overall heat transfer coefficient ($\text{W} \cdot \text{m}^{-2} \cdot \text{K}^{-1}$), A is the surface area of the spray dryer (m^2). T_i , T_o are the spray dryer inlet and outlet temperature displayed in the control panel, respectively. T_{amb} is the ambient temperature. ΔT_{LM} is the log mean temperature. An advantage of using a dry solids basis is that the dry gas and dry solids flow rates are identical at the inlet and the outlet of the dryer if the leakage is negligible. (M_g , M_s is the same at inlet and outlet). For a well-mixed dryer, the outlet solids are close to being in equilibrium with the outlet gas, so the outlet gas and solids temperature can be assumed to be same ($T_{go} = T_{so} = T_o$) (Langrish, 2009).

Closure of the balance equations was achieved using experimental data generated by spray drying of 5 wt% gelatin solutions. Once the reliable correlation for the energy (heat) loss was determined, the balance equations could be solved by using the commercially available software package Excel (Microsoft, Redmond, Washington). For a given amount of liquid

feed to be dried to a certain level of moisture content, the amount of drying gas required can be calculated by rewriting the above equations into Equation (6):

$$\begin{aligned}
 M_g &= (Q_{\text{evap}} + Q_{\text{powder}} + Q_{\text{loss}}) / [(C_{p,g,i} T_i - C_{p,g,o} T_o) + (Y_i - Y_o) (C_{p,v,i} T_i - C_{p,v,o} T_o)] \\
 &= \{M_f(X_i - X_o) / (1 + X_i) [\Delta H_v + C_{p,v} (T_o - T_{fi})] + M_f / (1 + X_i) [C_{p,s} + X_o * C_{p,w}] (T_o - T_{fi}) + UA \cdot [(T_i - T_{\text{amb}}) - (T_o - T_{\text{amb}}) / \ln[(T_i - T_{\text{amb}}) / (T_o - T_{\text{amb}})]]\} / [(C_{p,g,i} T_i - C_{p,g,o} T_o) + (Y_i - Y_o) (C_{p,v,i} T_i - C_{p,v,o} T_o)]
 \end{aligned}$$

(6)

2.2.3 Spray drying of gelatin solutions

Spray drying process was performed using a laboratory-scale spray dryer (B-290, BÜCHI Labortechnik AG, Flawil, Switzerland). Dehumidified air, which was provided by a dehumidifier (B-296, BÜCHI Labortechnik AG, Flawil, Switzerland), was used as the drying medium to improve the drying rate per unit time. The inlet air temperature was set from 110°C to 180°C to find the optimum drying temperatures. The aspirator setting was maintained at 100% aspirator rate, which indicated the pressure drop across the cyclone was 55 mbar and the drying gas flow rate was ~39 m³/h. The rotameter height was kept at 35mm, which corresponds to the spray gas flow rate at 414 L/h as suggested by the manufacturer for better protection of the nozzle. After conditioning, the gelatin solutions were pre-warmed to 50°C and then delivered to the nozzle by the peristaltic pump at a feed flow rate from 6-9 mL/min. The resultant spray dried samples were collected and stored in air tight desiccators for further analysis.

2.2.4 Visualization of spray characteristics

5 wt% aqueous gelatin solution was used as the spray solution. The solution temperature was maintained at 50 °C to ensure that the viscosity was consistent during each run. Experiments

were conducted under the following operating conditions: inlet air temperatures of 120 °C (regarded as low-temperature drying), 150 °C (regarded as intermediate temperature drying) and 180 °C (regarded as high-temperature drying), while drying gas flow rate was kept constant at 100% aspirator rate ($\sim 39 \text{ m}^3/\text{h}$) during all experiments. After the dryer reached steady state, the gelatin solution was delivered to the nozzle at 6 mL/min and atomized into fine droplets with the atomizing airflow kept constant at 414 L/h. The atomizing airflow of 414 L/h corresponds to a setting of 35 mm of the rotameter. The complete drying process from the nozzle down to the product collection vessel was visible through the B-290 glassware. A high magnification imaging system was used to visualize the atomized droplets in the spray chamber at different distances ($\sim 0, 7, 14, 21, 28, 35, 42 \text{ cm}$) from the nozzle outlet. Visualization at $\sim 0 \text{ cm}$ distance represented the initial droplet size (d_0). Due to apparatus obstructions, images could not be captured at the tip of nozzle (0 cm). Visualization was taken at 7 cm instead. The droplet size emerging from the two-fluid nozzle depends upon liquid properties and the mass ratio of atomizing air to liquid feed, but it is independent of drying temperature (Hede et al., 2008). To obtain visualization at $\sim 0 \text{ cm}$, the operating condition was set at room temperature ($\sim 25^\circ\text{C}$) and the diameter obtained from these conditions was assumed to be a good approximation of d_0 . The imaging system consists of a high speed camera (PCO 1200 hs, PCO AG, Kelheim, Germany), a long distance microscopic lens (Questar QM100 MKIII, Company Seven, Montpelier, MD), and a light source (Ultralight 2-20, Anton/Bauer, Shelton, CT) for backlight illumination of the object. The software CamWare (PCO AG, Kelheim, Germany) was used to export the recorded videos into a series of images. The use of the backlighting enabled capture of the image of the gelatin droplet being dried, which could generate a clear contrast between the droplet/particle and its background, facilitating the visualization of the contour of projected droplet/particle. The changes in droplet diameter during spray drying were recorded and analyzed using image

processing software ImageJ (National Institutes of Health, U.S.A). During analysis of droplet diameter, at least 500 droplets were measured for droplet size distribution. The spray dried samples were collected into the product vessel and analyzed by SEM (EVO 50 VP, Zeiss, Oberkochen, Germany). An image and schematic diagram showing detailed experimental setup for visualization studies of the spray dryer are presented in Fig. 2.1 (Bell et al., 2005; Chinnawar, 2015).

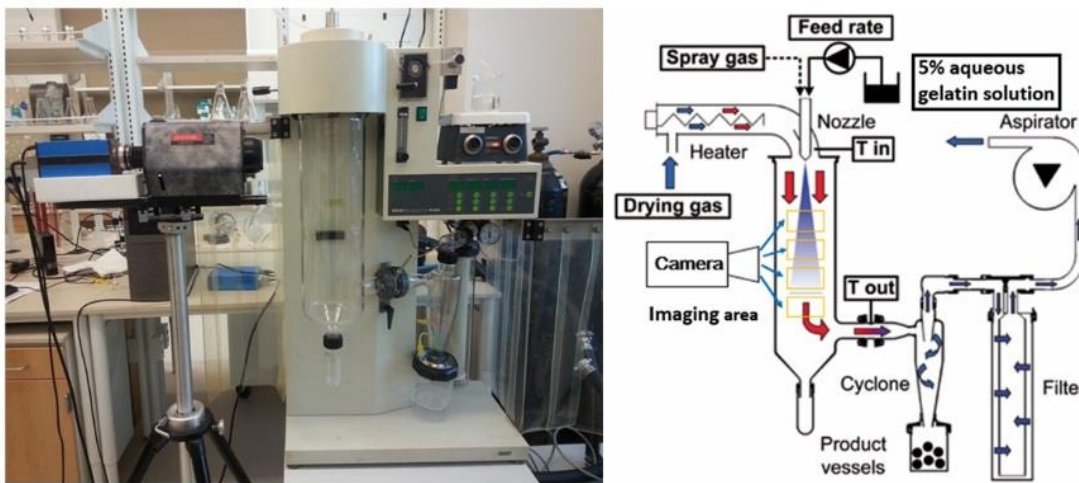


Fig. 2.1 (Left) Image showing experimental setup for visualization studies of the spray dryer. (Right) Schematic diagram of the apparatus setup (adapted from BÜCHI Labortechnik AG).

2.2.5 Powder analysis

2.2.5.1 Moisture content (MC) and production yield (Y)

The moisture content (MC, d.b.) of samples were determined gravimetrically by MF-50 Moisture Analyzer (A&D, San Jose, CA). The production yield (Y) is expressed as weight fraction (%) of powders recovered from the production vessel with respect to the weight of dry matter originally added to the feed solution. Any powders adhering to the walls of dryer chamber or cyclone were not considered. Each measurement was carried out in triplicate, and averaged MC and Y were reported.

2.2.5.2 Powder density

The solid true density of the powders (microcapsules) were measured by Accupyc 1330 pycnometer (Micromeritics, Norcross, GA) which used a gas displacement technique to determine the volume of sample under test. The density is calculated as the ratio of sample weight and the volume.

2.2.5.3 Particle size and morphology

The size and morphology of the spray dried particles were investigated using a scanning electron microscope (SEM) (EVO 50 VP, Zeiss, Oberkochen, Germany). The specimens were loaded on the SEM stubs (attached to a metal holder) using a two-sided adhesive tape, and sputtered with gold using a magnetron sputter coater. The coated samples were then examined using SEM operating at an accelerating voltage of 20 kV. The particle size and size distributions were measured on the SEM micrographs using an imaging processing software ImageJ (National Institutes of Health, US).

2.3 Results and discussion

2.3.1 Effect of concentration, temperature and pH value on gelatin solution

Since gelatin is the major component of the microcapsule, the physicochemical properties of resultant particles are largely determined by the gelatin solutions. Effect of concentration, temperature and pH value on gelatin solutions was thus investigated as it is likely to influence its behavior during spray drying. The viscosity of gelatin solutions are shown in Fig. 2.2 at various concentrations (1-20%) and temperatures (40-70°C). The viscosity of gelatin solutions increased rapidly when concentration was greater than 10 wt%. High viscosity leads to inefficient atomization of gelatin solution because samples soon blocked the atomizer through the formation of a thick solid wall. Larger drops were formed and more difficult to

be dried, the resulting particles were more humid and observed to have agglomeration tendencies. Therefore, 5 wt% gelatin solution was selected to allow forming aqueous solutions with reasonable viscosity in order to maintain proper atomization and efficient drying of the powder during the spray drying process. And as gelatin solution gels at temperature $< 40^{\circ}\text{C}$, higher temperature (close to phase inversion temperature) may promote thermal degradation of bioactive materials and affect the emulsion stability (Gulotta et al., 2014) as well, so the inlet feed temperature was kept at 50°C .

Influence of pH on zeta-potential of gelatin solutions was also investigated (Fig. 2.3). The zeta-potential went from positive (+ 21 mV) to negative (-12 mV) when the pH increased from 2 to 10. Zeta-potential became zero (isoelectric point) at a pH between 6 and 7. Droplets with large zeta potential (surface charge) repel each other, thereby improving the solution stability (Tantra et al., 2010). For this reason, pH of the gelatin solutions was adjusted to 3 using HCl prior to spray drying to achieve maximum surface charge. The positive (cationic) droplets could also repel iron (Fe^{2+} and Fe^{3+}) and inhibit iron (Fe^{2+} and Fe^{3+}) catalyzed oxidation of lipids in the emulsions (McClements, 2014).

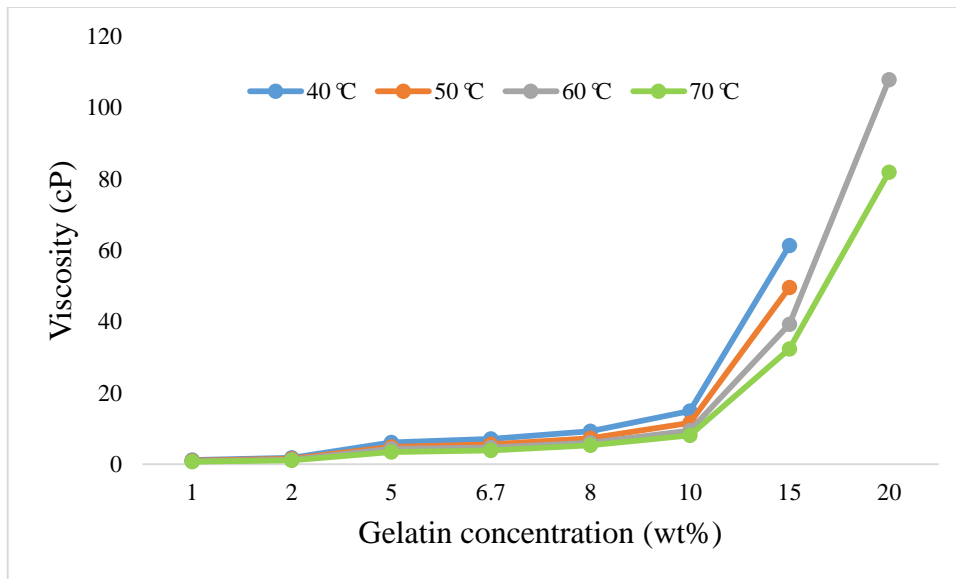


Fig. 2.2 Viscosity of gelatin solutions at various conditions

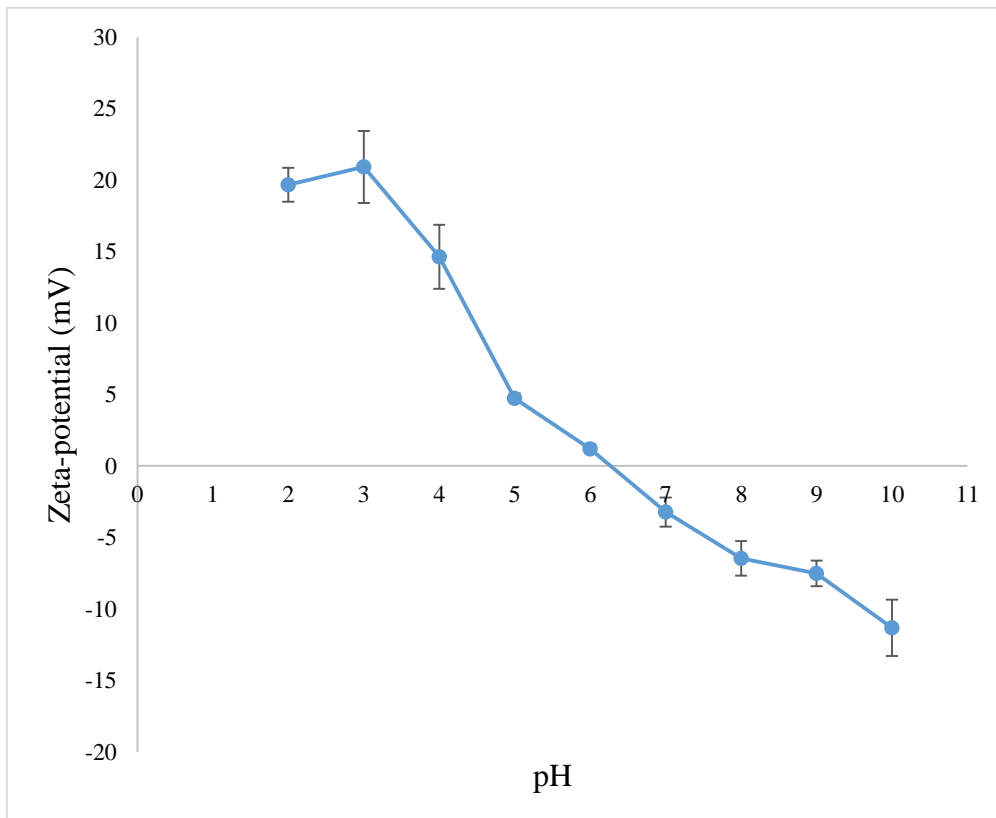


Fig. 2.3 Influence of pH on electrical charge (zeta potential) of gelatin solutions

2.3.2 Selection of the operating conditions

The inlet (T_i) and outlet temperature (T_o) play crucial role in spray drying process as they influence the properties of the dried particles. Higher inlet temperature, which is proportional

to the drying rate, can result in sufficient droplet/particle drying. However, too high inlet temperature may destroy heat sensitive components. In contrast, if the inlet temperature is too low, the water will not evaporate completely in short time. In addition, the outlet temperature, which is the resulting temperature of the heat and mass transfer between droplet/particle and drying gas, can be regarded as the maximum temperature the particle experienced during the spray drying process. So cares need to be taken to make sure the dried product is not damaged by excessively high outlet temperature.

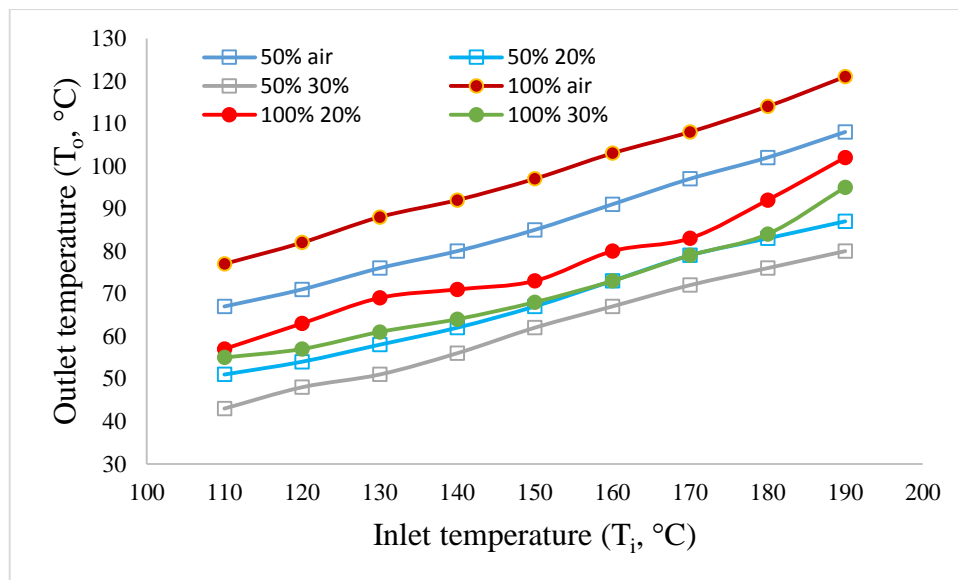


Fig.2.4 Corresponding outlet temperature (T_o) versus inlet temperature (T_i) at different feed pump rate (0% (air only), 20% (6 mL/min) and 30% (9 mL/min)) and drying air aspirator rate (50% (20 m³/h) and 100% (39 m³/h)).

Fig. 2.4 shows the T_o versus T_i curves for the spray dryer. T_o is always lower than T_i because of the heat loss through the spray dryer and higher T_i will result in higher T_o . When run on gelatin solution over the same range of T_i , T_o is lower than on air because of consumption of enthalpy to evaporate the water. When $T_i > 190^\circ\text{C}$ (100% aspirator rate, 20% pump rate), T_o will be above the boiling point of water ($>100^\circ\text{C}$), overpressure effects could occur and may further result in inflation or cracking, which is harmful for the microcapsule (Chen et al., 2013; Kemp et al., 2013; Shen & Quek, 2014). Therefore, spray drying at lower temperature

is preferable in this work to avoid overheating of the microcapsules. Drying at lower temperatures is also more cost effective.

The overall mass and energy balance used in this study assumed complete evaporation of liquid components. The energy (heat) loss (Q_{loss}) through the B-290 spray dryer is substantial in this case due to the heat convection and conduction through the large surface area of the glass spray dryer chamber (Hanus & Langrish, 2007). The spray dryer was first operated with heated gas only (no liquid). The inlet and outlet gas temperatures were measured experimentally and the energy (heat) loss (Q_{loss}) was calculated by equation (4). As the Q_{loss} value varies with changing spray dryer operating conditions, these obtained Q_{loss} values were used to determine the overall heat-transfer coefficient for heat loss (UA) in equation (5), which is independent of the operating conditions. Fig.1.5 shows UA as a function of log mean temperature difference (ΔT_{LM}). Although there is a slight variation in UA values, there is no discernable trend between UA and the ΔT_{LM} . Thus, using an average of the values found, the lumped parameter, UA, of the Buchi-B290 spray dryer was estimated to be $4.77 \text{ W}\cdot\text{K}^{-1}$. As a result, the energy (heat) loss under any operating conditions could be correlated (Equation 7).

$$Q_{\text{loss}} = 4.77 \cdot [(T_i - T_{\text{amb}}) - (T_o - T_{\text{amb}})] / \ln[(T_i - T_{\text{amb}}) / (T_o - T_{\text{amb}})] \quad (7)$$

Therefore, the amount of drying gas required to dry the liquid feed to a certain level of moisture content can be calculated by Equation (6). It can be seen from Fig.1.7 that 100% aspirator rate (M_g) is usually higher than the minimum requirement to dry the gelatin solution, while 50% aspirator rate is insufficient to dry the product in most of the cases, despite the increased residence time in the spray dryer. Thus, the drying gas flow rate should be set at or close to the maximum gas flow rate (100% aspirator rate) to ensure complete

solvent evaporation. For a spray dryer operated at fixed aspirator settings, the maximum achievable liquid feed flowrate (M_f) can also be approximated by the balance equations. Considering all the factors discussed above, the inlet temperature range was set from 110°C to 180°C for the experiments in this study.

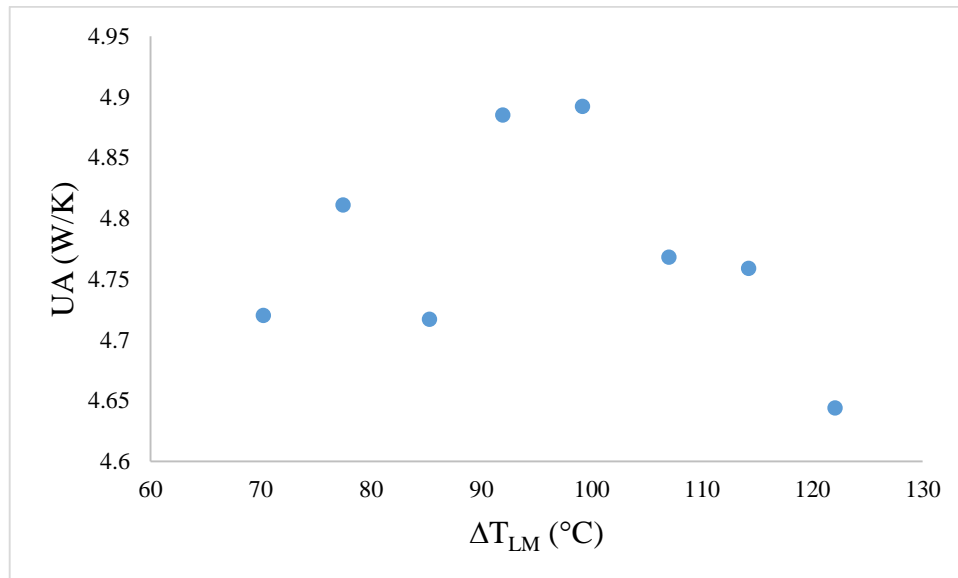
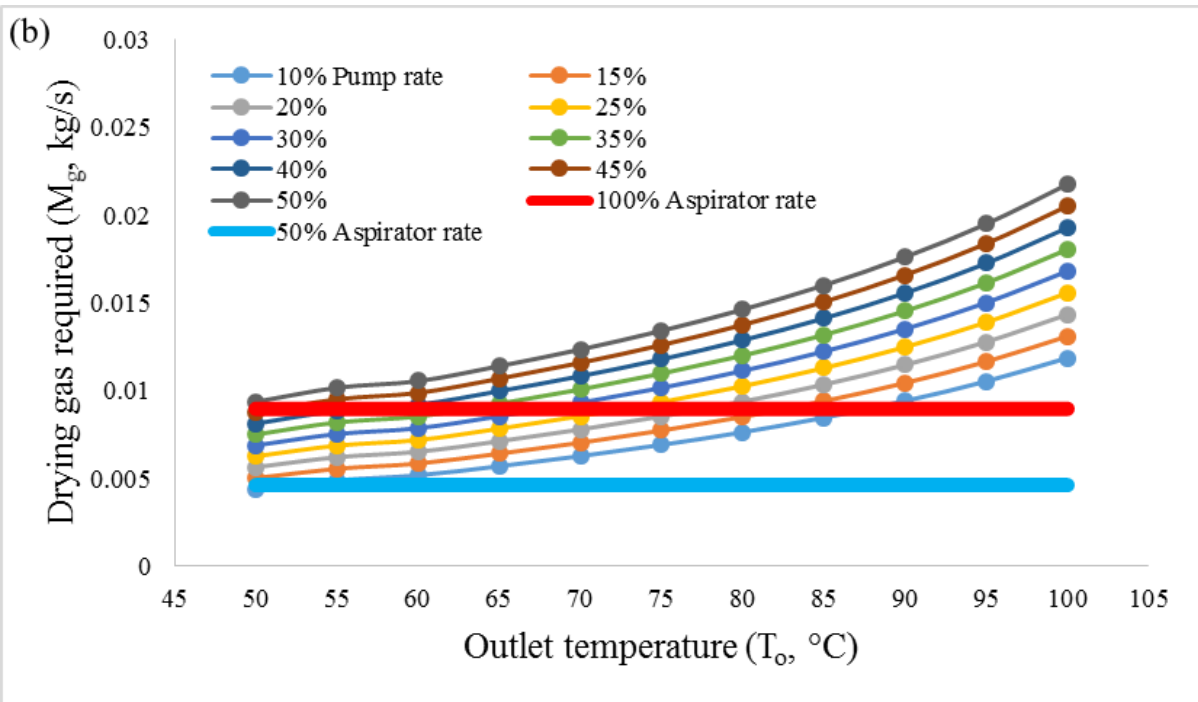
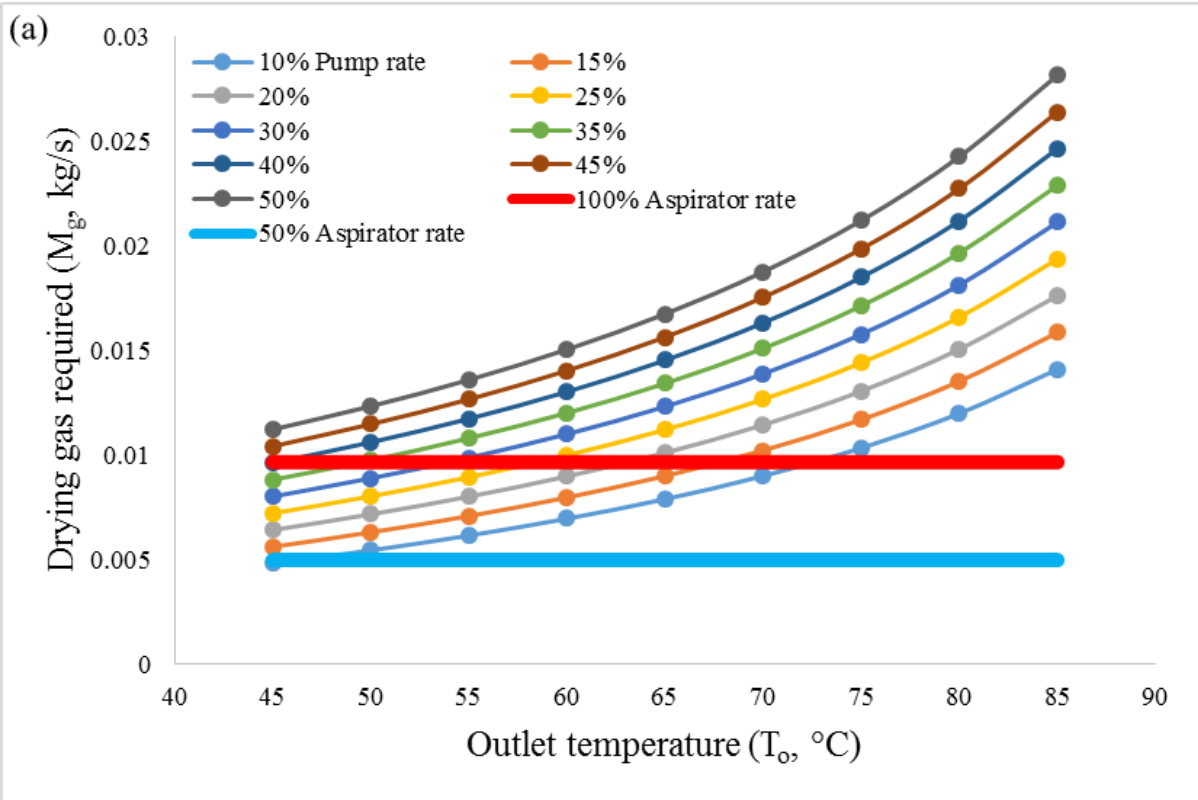


Fig.2.5 Plot of UA as a function of log mean temperature difference (ΔT_{LM}) between inlet (T_i), outlet (T_o) and the ambient temperature (T_{amb}).



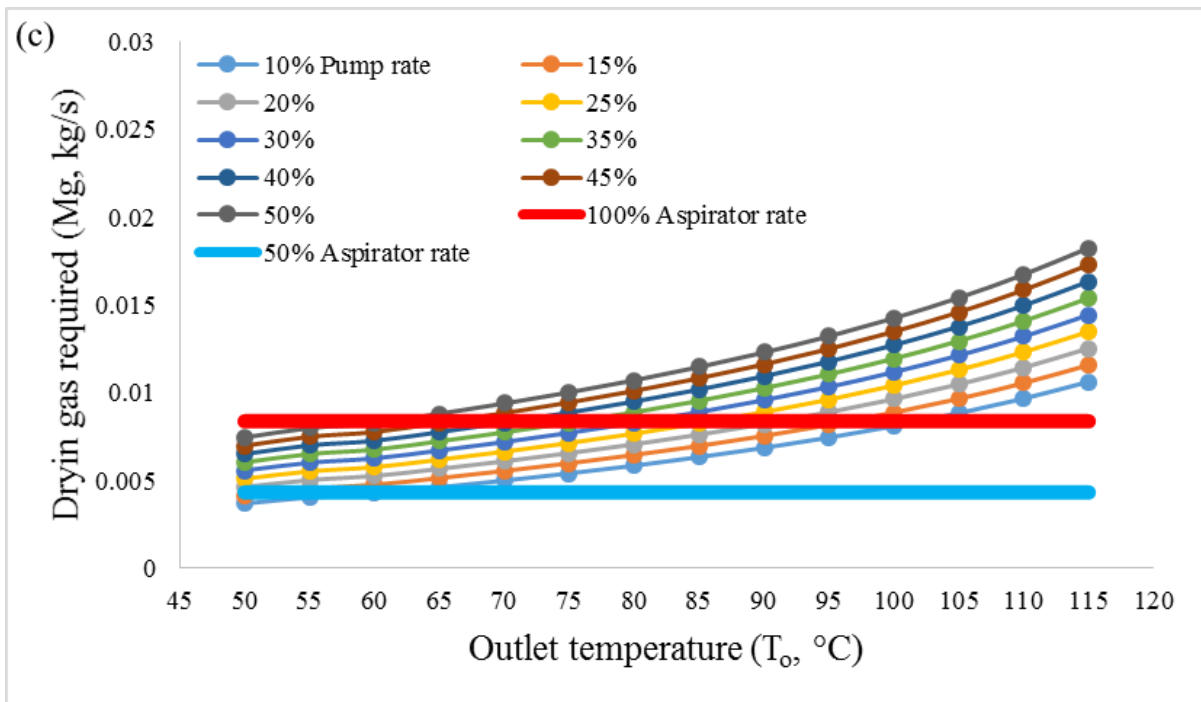


Fig.2.6 Estimation of drying gas required for different amount of liquid feed (10-50% pump rate; inlet temperature (a: $T_i=120^\circ\text{C}$, b: 150°C , c: 180°C); liquid feed temperature ($T_f=50^\circ\text{C}$), moisture content ($X_i=19$, $X_o=5\%$) and outlet temperature ($T_o=45-115^\circ\text{C}$).

2.3.3 Particle moisture content and yield

Fig.2.7 and 2.8 show the residual moisture content and yield of the final particles as a function of drying temperatures (T_i and T_o). MC can play an influential role in determining the physical and chemical stability of the dried powder. Usually, a dry product with a moisture content as low as possible is aimed for. Current results show that the MC of the powders decreases gradually with increasing T_i (T_o). A lower pump setting should result in a higher outlet temperature and therefore more efficient drying, resulting in lower residual moisture contents. Although the product MC can be lowered by simply increasing the temperature, exposing the material to excessive temperatures should in general be avoided to prevent thermal degradation.

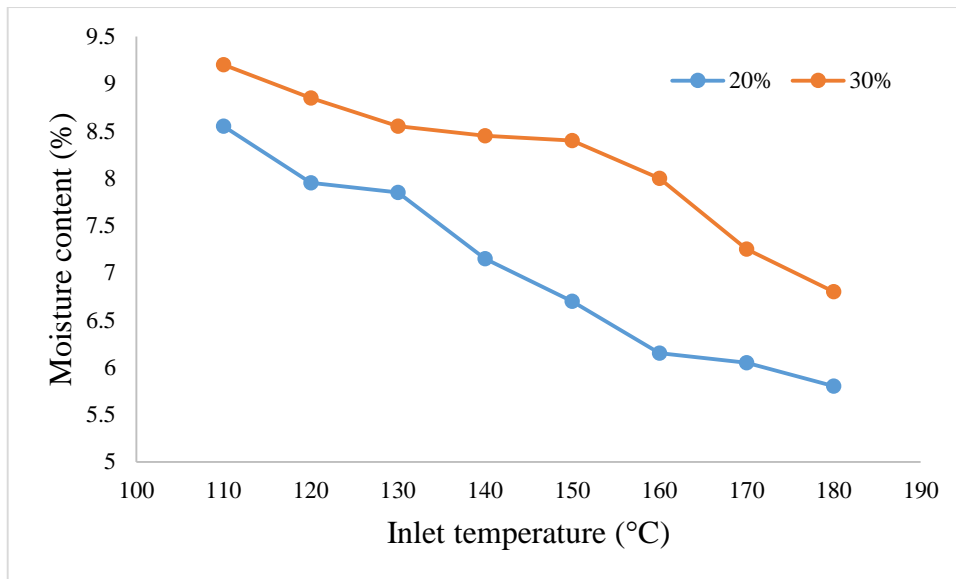


Fig.2.7 Effects of variation in T_i on residual moisture content of spray-dried gelatin at different feed rate (20% pump rate: 6 mL/min and 30% pump rate: 9 mL/min).

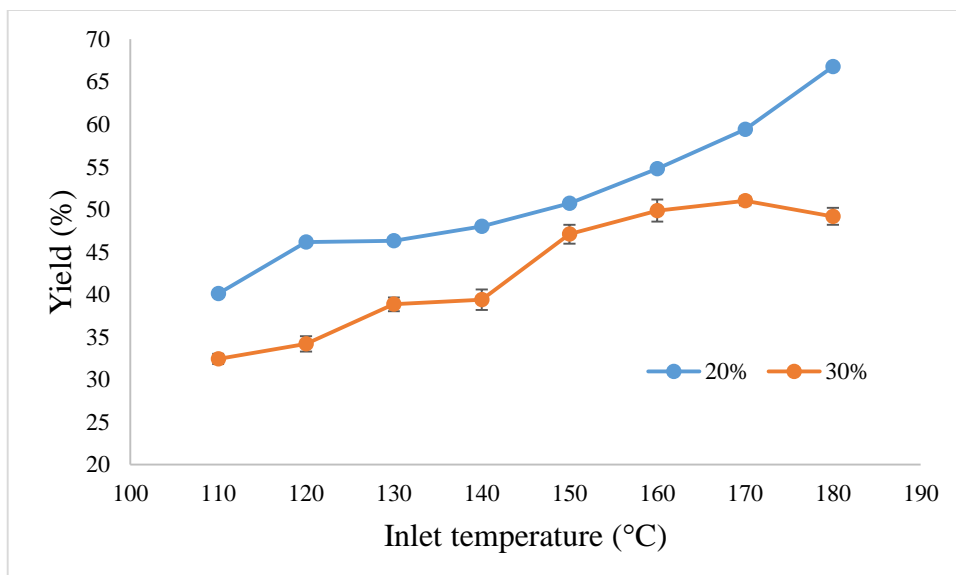


Fig.2.8 Effects of variation in T_i on particle yield of spray-dried gelatin at different feed rate (20% pump rate: 6 mL/min and 30% pump rate: 9 mL/min).

For the yield of microcapsules, most of the product loss was found as wet deposits of semi-wet particles on the chamber wall and cyclone. When the pump rate was set at 9 mL/min, at low drying temperatures droplet/particles were insufficiently dried and easily deposit (sticky) when they hit the wall, hence a reduced powder yield. The powder yield increased with higher process temperatures, owing to improved droplet/particle drying before impact with

the wall and reduced droplet/particle deposition on the walls of the drying chamber. The powder yield declined with further increase in T_i ($>180^\circ\text{C}$), although the residue moisture content remained at a low level. Spray dried products often exist in an amorphous state, which show great sensitivity to moisture content and temperature fluctuations during processing (Heldman et al., 2006). Therefore, typically, outlet temperature (T_o) is chosen to stay below glass transition temperature (T_g). Otherwise, when T_o exceed their T_g , the amorphous particle (glassy state) changes to rubbery state and become viscous, when the particle is heated above the so-called 'sticky point' ($T_s > T_g + 10^\circ\text{C}$), it tends to stick on the walls of the spray dryer and decrease the yield (Jayasundera et al., 2009). According to Kasapis & Sablani (2005) (Table 2.1), although the glass transition temperature of gelatin is relatively high (161°C , $k=6.1$), it can be greatly reduced by adsorbed moisture. For 30% pump feed rate ($M_f=9\text{mL}/\text{min}$), when $T_i=180^\circ\text{C}$, the T_o (84°C) is more than 10°C above T_g (73.5°C). As a consequence, the rubbery gelatin is more likely to stick to the chamber and cyclone walls, reducing the yield of the product. Therefore, a maximum yield can be obtained at T_o which prevents wet deposits because of insufficient drying, but not so high to cause molten deposits above T_s (Maury et al., 2005). Moreover, powders also have higher shelf life if stored under glass transition temperature. However, for hygroscopic materials like gelatin, care needs to be taken because easy re-absorption of vapors from the air phase could reduce the glass transition temperature. Therefore, for good conservation of these powders without risk of caking during storage, spray dried gelatin powders were sealed and stored at 4°C until analysis. The relative humidity of the drying gas is also an important parameter need to be controlled during spray drying. Not only does humid air cause the water droplets to evaporate/dry slower, it also lowers the glass transition temperature of amorphous products as adsorbed moisture acts as a plasticizer. To decrease and maintain the relative humidity in the

inlet air, the dehumidifier B-296 was used. This additional dehumidification accessory could improve the drying efficacy and allow the removal of water more quickly.

Table 2.1 Comparison of T_o versus T_g and T_s estimated from Kasapis & Sablani (2005).

T_i (°C)	20% pump rate			30% pump rate		
	T_o (°C)	T_g (°C)	T_s (°C)	T_o (°C)	T_g (°C)	T_s (°C)
110	57	58.9	68.9	55	54.0	64.0
120	63	63.7	73.7	57	56.6	66.6
130	69	64.5	74.5	61	58.9	68.9
140	71	70.4	80.4	64	59.7	69.7
150	73	74.4	84.4	68	60.1	70.1
160	80	79.5	89.5	73	63.3	73.3
170	83	80.5	90.5	79	69.5	79.5
180	92	82.9	92.9	84	73.5	83.5

Compared with industrial spray dryers (yield over 90%), the production yield (50-70%) in the current study appears to be relatively low. However, yields of around 60% are considered to be good for small-scale spray dryers, such as these Buchi designs (Fang & Bhandari, 2011; Intiaz-Ul-Islam & Langrish, 2009; Langrish & Premarajah, 2013). The fundamental reason for these low yields with small-scale spray dryers can be found from the work of Hanus and Langrish (2007). The narrow dryer chamber of B-290 results in a high level of inertial deposition of small droplets/particles, and hence a reduced production yield. High liquid feed flow rates were also detrimental to powder yield. On increasing the feed rate value (>12 mL/min), large deposits of powder were visible in the spray chamber, and liquid water was also observed on the inner wall of the collection vessel. Lower feed rate (< 3mL/min) gave higher yield, but also resulted in lower productivity.

2.3.4 Initial droplet size distribution

Generally, the spray generated by two-fluid nozzles contains droplets of varied size (Parikh, 2005; Patel & Chen, 2007). As seen from Fig.2.9 and Table 2.2, the initial gelatin solution droplets emerging from the nozzle showed a circular (spherical) contour, and a narrow size

distribution, with peak ($d \approx 30 \mu\text{m}$) representing a predominant size. This peak value is also equal to the medium value (d_{50}) of the droplet size distribution, evident by the cumulative distribution curve in Fig.2.9. Since it was difficult to track the precise size change for each individual droplet as the spray progresses, the peak size of droplet during the spray drying under different drying temperatures was investigated in section 2.3.5. SAS software (SAS Institute Inc, Cary, NC) was used to determine P-values for lognormal curve fit. Three different methods based on EDF Goodness-of-Fit test (Anderson-Darling, Cramer-von Mises, Kolmogorov-Smirnov) and Chi-Square Goodness-of-Fit test (chi-square) were used. The P-values for all four tests are larger than 0.10, indicating that the lognormal model is appropriate for the curve fit.

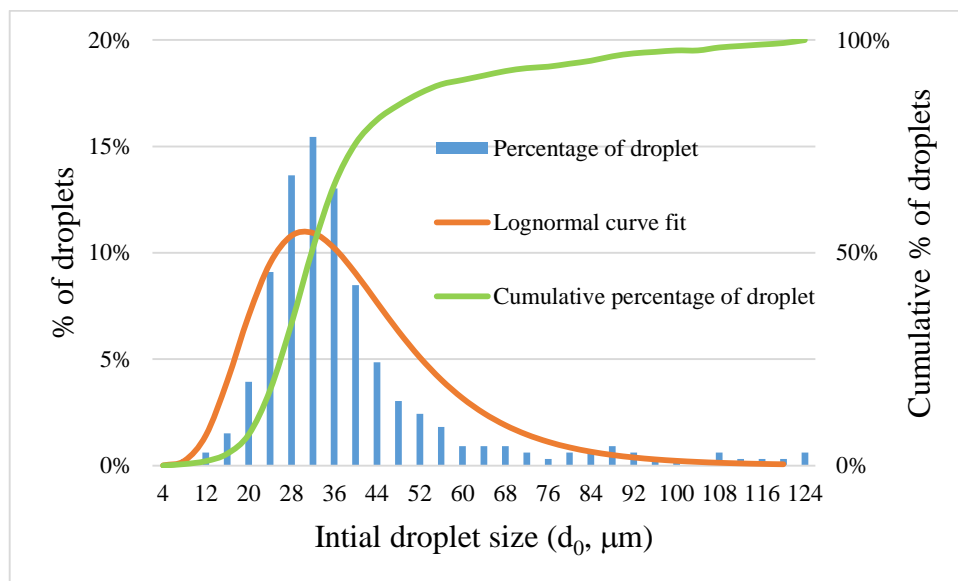


Fig.2.9 Initial droplet size distribution approximation for 5% aqueous gelatin solution.

2.3.5 Shrinkage behavior of 5 wt% gelatin droplets

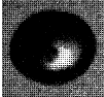
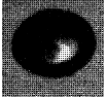
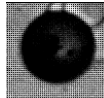
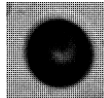


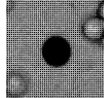

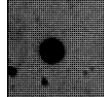
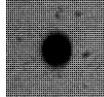
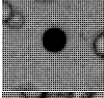
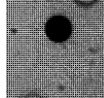
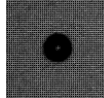
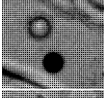
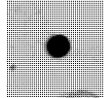
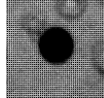
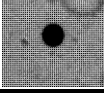
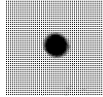
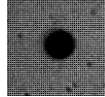
The measured diameter of 5 wt% gelatin droplets along spray dryer at 120, 150 and 180°C are shown in Table 2.2. Fig.2.10 shows the lognormal distribution curve fit for droplet size at 120, 150 and 180°C. As drying progressed, most droplets/particles maintained spherical and smooth contours. The droplet diameter rapidly decreased at the initial stage of drying (Table

2.2 and Fig. 2.10), associated with a rapid decrease in MC ($MC = m_0 - m_p = 1/6\pi \cdot \rho_d \cdot (d_{d,0}^3 - d_d^3)$) as will be discussed later (Fig. 2.12), and less so as drying approached the final stage. Although with the same initial MC and droplet size, the effect of drying temperature plays an important role in the overall droplet shrinkage behavior and particle formation process (Vehring et al., 2007 and Yao et al., 2008). Larger particles were produced at a higher drying temperature as observed in the present study (Table 2.2 and Fig. 2.10). For material like gelatin, droplet drying is generally divided into two different drying stages, namely, the constant-rate and falling-rate drying periods. The constant-rate drying period is dictated by the presence of free moisture on the droplet-air interface, the droplet shrinks drastically during this stage. When the outer free moisture could not be further maintained, a surface skin would start to appear with the accumulation of dissolved materials on the outer layer. As the outer layer 'solidifies' with the formation of crust under the skin, further droplet shrinkage becomes less apparent (Walton & Mumford, 1999a, b). Therefore, the extent of the difference between initial droplet size and final particle size depends on the point when crust formation occurs.

When the droplets dried at low temperatures (120 °C), our measurements were consistent with the notion that the crust formation was delayed until the concentration within the entire droplet has reached the solubility limit, so that the reduction of droplet diameter was more pronounced, resulting in the smallest size particles. As was seen in Alamilla et al (2005), the peak droplet size decreased along the length of the spray dryer within 28 cm from the nozzle outlet. In contrast, although diameter reduction was still observed, the total reduction was negligible between 28 cm to 35 cm. Presumably the particle surface could be still moist, allowing the particle to shrink to a small extent. However, the surface shell gradually thickened as drying progressed (Nešić and Vodnik, 1991). After 35 cm, the shell became

sufficiently solidified to resist further shrinkage, even though the drying was still in progress. The shrinkage may not be homogenous as the moisture distribution on the particle surface may not be even. When the MC reduced, others observed that the projected area of the semi-dried particle was no longer a regular circle, the contour became undulated, indicating the formation of a surface shell. The contour of the projected particle area became slightly rougher at the final drying stage.

Table 2.2 Droplet diameter as a function of distance from nozzle outlet

Distance (cm)	120°C			150°C			180°C		
	Droplet Image	d _{peak} (μm)	d ₅₀ (μm)	Droplet Image	d _{peak} (μm)	d ₅₀ (μm)	Droplet Image	d _{peak} (μm)	d ₅₀ (μm)
~0		29.9	29.9	Experiments were taken at 7cm instead of 0 cm, at room temperature (~25°C)					
7		27.6	28.2		26.3	26.3		23.7	23.7
14		24.0	24.0		21.1	23.6		10.7	10.7
21		19.9	19.9		9.8	10.2		10.7	11.2
28		8	8		9.8	9.8		10.7	12.6
35		8	9		9.8	9.8		12.4	13.1
42		8	8		9.8	10.9		10.7	12.8

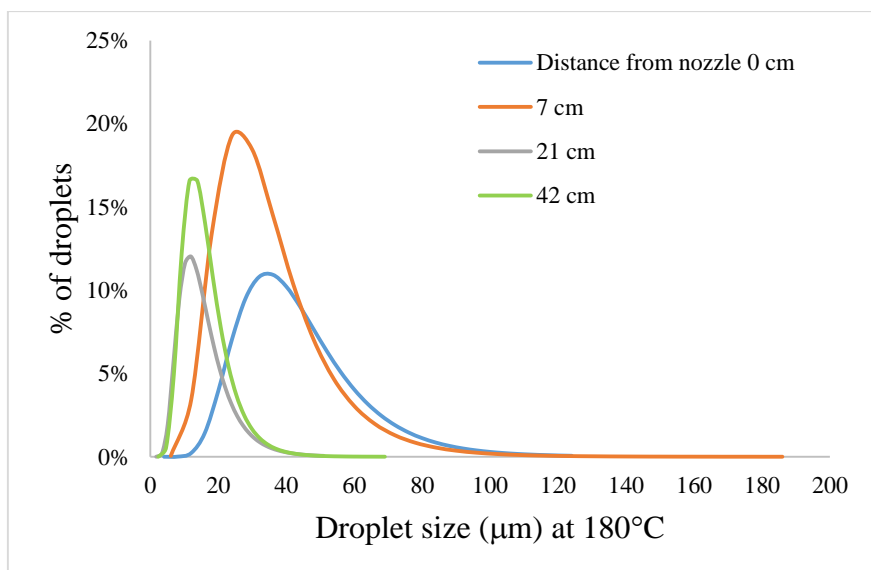
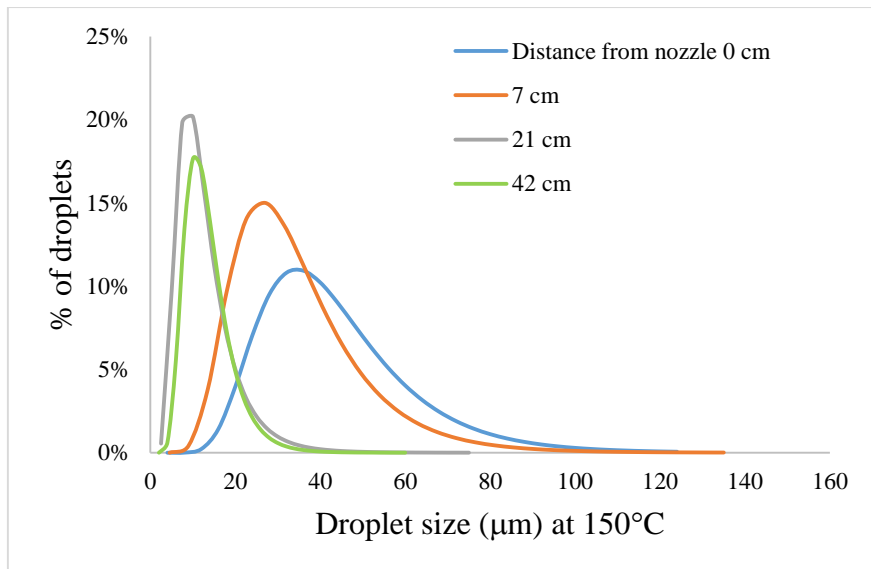
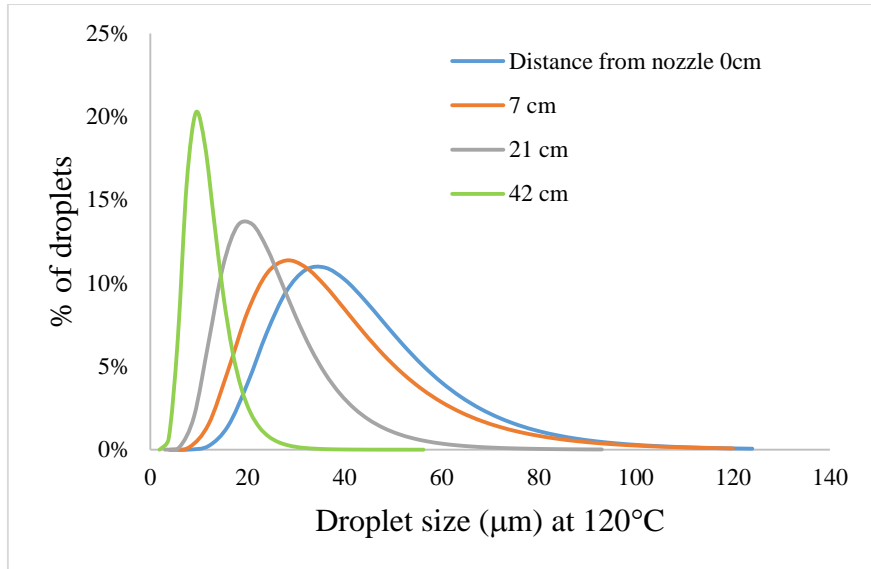


Fig.2.10 Droplet size change along the spray dryer as a function of the distance from nozzle outlet: (top) $T_i=120^\circ\text{C}$, (middle) $T_i=150^\circ\text{C}$, (bottom) $T_i=180^\circ\text{C}$.

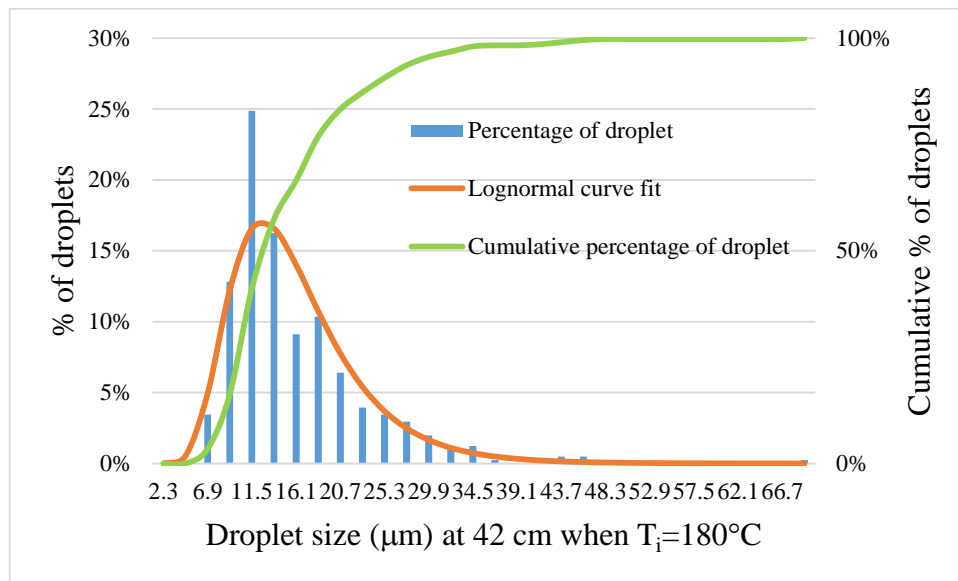


Fig. 2.11 Comparison of d_{peak} and d_{50} value at 42 cm when $T_i=180^\circ\text{C}$

For intermediate temperature drying (150°C), the droplet dried more rapidly than at 120°C , as expected. This difference is shown even clearly when the shrinkage behavior is plotted against MC removal (Fig. 2.12). Apart from reducing the MC of the final products, higher drying temperature also led to higher droplet size. The larger size in 150°C is partly due to a quicker crust formation than lower temperatures (Kim et al., 2009), which could hinder further shrinkage and thus influence diameter reduction (Wang et al., 2014). Compared with 120°C , the droplet showed a faster shrinkage at the beginning (0-21cm), while no apparent change in peak droplet diameter after 21 cm, despite a continuous reduction in MC. The area contour at 35 cm looked similar to that at 42 cm, indicating a possible sustaining of the semi-dried particle structure by solids fraction.

For high-temperature drying (180°C), the drying behavior was different from that found at 120 and 150°C . The atomized droplets first shrank as they traveled away from the nozzle and a more rapid crust formation occurred very close to the initial droplet size (nozzle outlet). Then a phenomenon known as droplet inflation (Handscomb & Kraft, 2010; Rogers et al.,

2012), caused by the build-up of internal vapor pressure when the droplet/particle temperature exceeded boiling temperature, has been observed at 35 cm from the nozzle outlet. As seen from Fig.2.4, when the inlet temperature was at 180°C, the outlet temperature (at 42 cm) was below the boiling temperature (<100°C), which was generally regarded as the maximum temperature the particle could reach in the spray dryer. However, common to many co-current dryers, that the maximum particle temperatures occur not at one of the end points of the dryer (inlet or outlet) but in the middle of the dryer. This result is due to the differing rates of heat and mass transfer, with heat transfer being more rapid than mass transfer, leading to the particle being initially heated up to boiling temperature very quickly at 35cm, followed by a period where both the particle and the gas temperatures decrease due to energy being used in evaporation and heat loss (Langrish & Premarajah, 2013). In some cases, those inflated droplets/particles may break up under the drying stress (Handscomb & Kraft, 2010). However, in this case, the surface crust showed good elasticity, which may be because the crust formed very early when the droplet had a larger diameter and may have been thicker before boiling, hence able to expand further without breaking. After the temperature cooled down to below the boiling temperature, the expanded droplet/particle deformed again back to the unexpanded state. The difference between d_{peak} (10.7 μm) and d_{50} (12.8 μm) at 42 cm (Fig.2.11) may due to the existence of several small peaks around 16.1-18.4 μm , resulting in the right shift of d_{50} , so that d_{peak} was more representative than d_{50} . Large droplet/particles were formed probably because of the recirculation of the airflow inside the dryer chamber, which enhanced the mixing between hot air and the droplet and increased the contact time. A quicker crust formation occurred and led to larger droplet/particle size.

Specifically, it was demonstrated that the shrinkage behaviors (dimeter reduction) of 5 wt% gelatin droplet were more pronounced at lower drying condition. While, shell formations were advanced at higher drying temperature (Kim et al., 2009; Fu et al., 2013), leading to a deviation from ideal shrinkage kinetics (Patel et al., 2010). However, at the initial stage of drying, the water fraction remained as the dominant fraction in the droplet (MC =19 d.b.), so that the resultant droplet shrinkage followed the ideal shrinkage kinetics to a large extent. Once the diameter of the droplet were measured accurately, the quantity of water removed from the droplet during spray drying (MC) could be assumed proportional to the change in droplet diameter travelling through the dryer chamber. The shrinkage behavior proceeded until the point of crust formation and then stopped provided that there was no inflation.

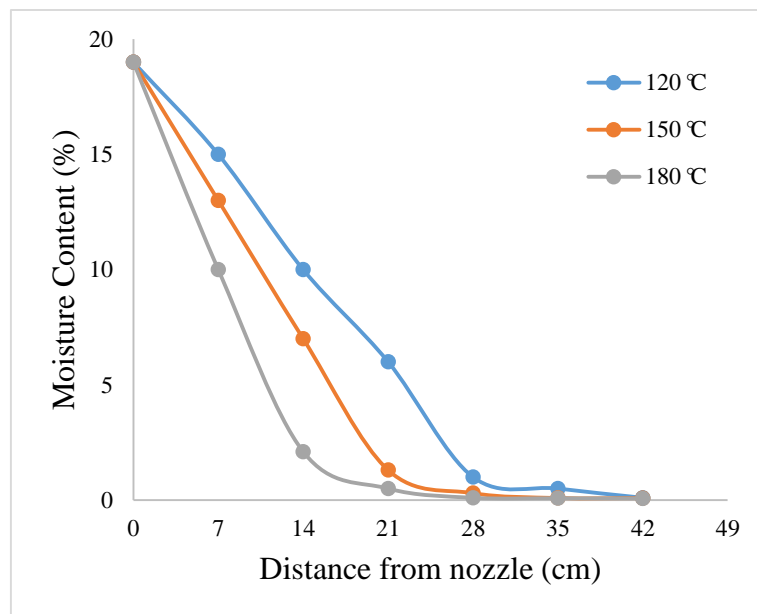


Fig.2.12 Estimation of MC change histories of 5 wt% gelatin droplets at 120, 150, 180 °C as a function of the distance from the nozzle outlet

Fig. 2.12 shows estimated MC as a function of distance from the nozzle outlet of the spray dryer at different drying temperatures. It was possible to qualitatively relate the MC with air drying temperatures along the length of the spray dryer. As would be expected, MC reduced more rapidly at higher drying temperatures. Meanwhile, higher drying temperatures also led

to lower residual moisture in the particles after drying, indicating that drying was more complete than using lower temperatures. As we can see from Fig.1.12, at the beginning, the MC reduction was approximately linear along with the decrease in droplet size. It only took around 28 cm for 95% of the total moisture to be removed at 180°C. Such a fast water removal might cause advanced shell formation (Kim et al., 2009), which resisted further shrinkage and maintained the particle shape. As drying further progressed, the curve showed a transition point and a slight MC reduction, negligible diameter reduction occurred after MC was reduced to around 1 (d.b.). When the overall droplet MC reached about 0.1 kg/kg, the particle likely reached its equilibrium moisture content (X_e); no further MC reduction was observed.

Visualization of the spray process allows for a comparison of the spray characteristics and the resulting particle characteristics. However, the imaging system did not have sufficient resolution to visualize the morphology of the droplet/particle. Spray dried particles were analyzed using a SEM to confirm and augment results observed by high speed camera. Particles produced at lower temperature tended to be smaller than the particles produced at higher temperature. Observing the morphology of each powder, most particles appeared as spherical shapes with dimpled surfaces. It is reasoned that the particles formed as a spheres and then deformed by drying stresses. The shell helped maintain the shape, producing nearly spherical particles. After the surface shell was formed during drying, the solids fraction with low initial solids levels could not support the shell, which then sank inwards as inner moisture was removed, producing concave morphology.

The drying of droplets in a spray dryer is a continuous process. However, in this work, the drying behavior along the spray dryer was investigated at different distances from the nozzle

outlet. Hence the simultaneous heat and mass transfer inside the spray chamber could not be monitored continuously. Only estimated MC curves could be drawn. Further experiments can be conducted to visualize the spray at more positions. The polydispersity of droplets generated by the two-fluid nozzle also made it more difficult to characterize the droplet shrinkage behavior (Chen & Patel, 2008; Liu et al., 2015; Patel & Chen, 2007). Mono-dispersed droplet generation techniques that capable of producing monodisperse droplets could be further used to remove the complexity of the droplet size effect (Rogers et al., 2012). In addition, the proposed methodology was suitable if regularly shaped particles (spherical, nonagglomerated particles) were produced by spray drying. However, when spray drying leads to highly irregular shaped particles (e.g. agglomerating particles), the proposed method is not always valid.

2.3.6 Gelatin properties before and after spray drying

As seen in Table 2.3, Gelatin is relatively insoluble in cold water. After spray drying, the resulting gelatin powder becomes "cold water soluble". This solubility enhancement may be due to generation of the amorphous form of gelatin and reduction of particle size in contrast to the large crystalline form of raw gelatin (Kuant et al., 2015). On contact with water, the high energy state of the amorphous powder results in faster dissolution and higher solubility (Paudel et al., 2013). The reduction in particle density may be due to the formation of crust during drying, leading to the formation of hollowed particles.

Table 2.3 Gelatin properties before and after spray drying

	Raw gelatin	Spray-dried gelatin
Solubility	Practically insoluble in cold water	Cold-water soluble
Size (diameter, μm)	>100	5-20
Density (g/cm^3)	1.35	1.2-1.3
MC (%)	12-13	5-9

The spray dried gelatin powders produced have a range of particle size from about 5 to 20 μm , and were mostly spherical in shape with dimpled surfaces, which is a typical characteristic of spray dried powders (Gallardo et al., 2013; Tonon et al., 2011). Both well-formed microcapsules (Fig. 2.13 (middle)) and agglomerated powders (Fig. 2.13 (bottom)) were observed. The appearance of particles agglomeration instead of well-formed microcapsules may be associated with the cohesion between sticky particles at high T_0 , which is coincident with experimental results of low yield (Fig.2.8). No cracks, craters or fissures on the particle surfaces indicate complete coverage of gelatin that is essential to ensure lower gas permeability, better protection and retention of the active material (Rocha et al., 2012; Aniesrani Delfiya et al., 2015). Dimpled surfaces were more likely to occur because of the slower diffusion of water, allowing more time for structures to deform, shrink and even collapse (Aniesrani Delfiya et al., 2015; Chen & Mujumdar, 2008). Addition of sucrose or mannitol may promote formation of micro-spheres with smoother outer surface (Bayram et al., 2005; Bruschi et al., 2003; Faria et al., 2010; Shu et al., 2006).

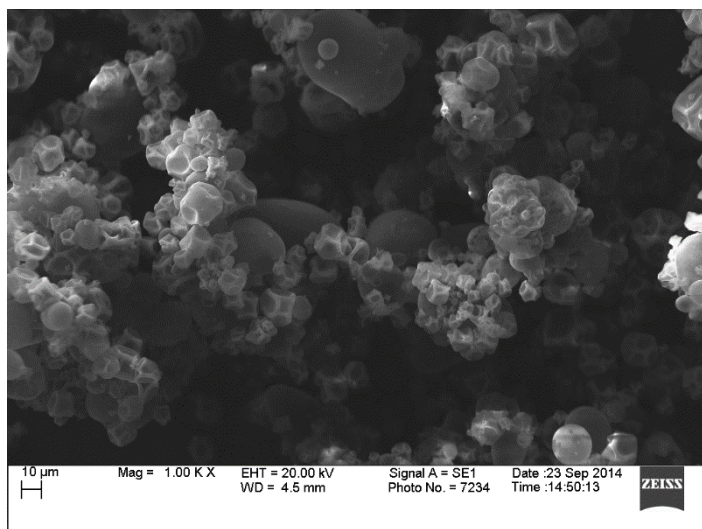
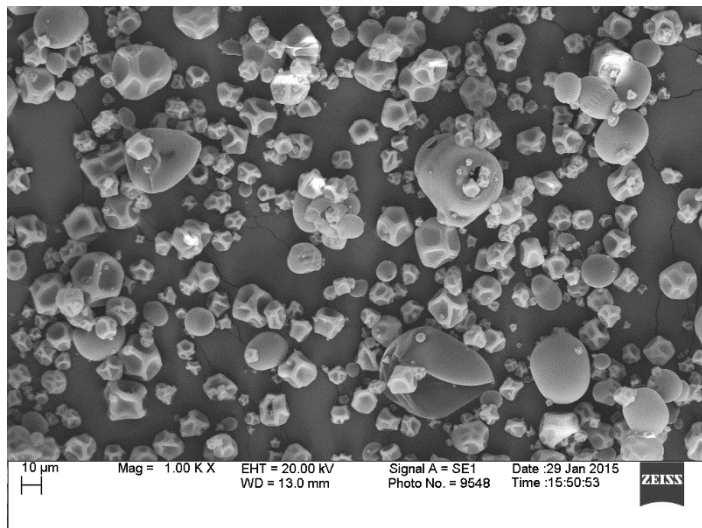
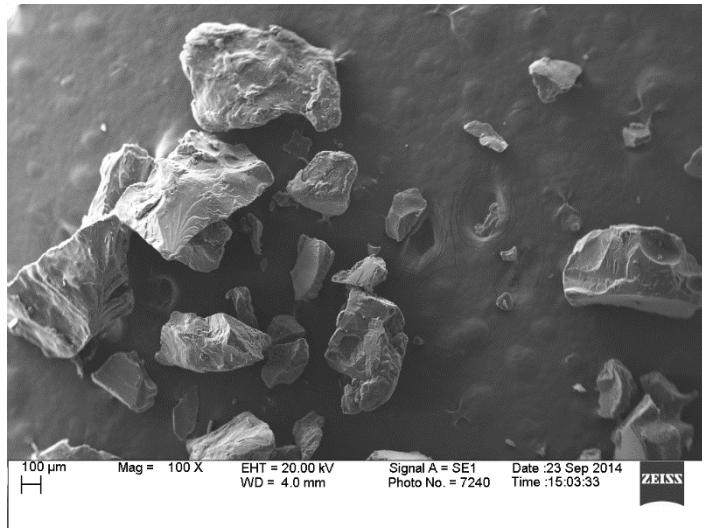


Fig. 2.13 (top) SEM image of raw gelatin; (middle) SEM image of spray-dried gelatin powder at inlet temperature=140 °C, feed rate=6mL/min; (bottom) SEM image of agglomerated spray-dried gelatin powder at inlet temperature=180 °C, feed rate=9mL/min.

Conclusion

The objective of this work was to evaluate the potential of gelatin as wall materials for microencapsulation. Spherical, dimpled and micron-sized gelatin particles or agglomerates were successfully produced through the spray drying process. Particle properties were characterized and can be affected by varying operating conditions. Feasibility of the high magnification visualization system for study of the spray characteristics during the spray drying process was demonstrated. Data from visualization experiments was collected and used for shrinkage model development. The results confirmed that different drying temperatures lead to a variation in shrinkage behavior for 5 wt% gelatin drying. Higher drying temperatures tended to have less extent of shrinkage than lower drying temperatures, resulting in larger final particles than lower temperatures, as opposed to the prediction by ideal shrinkage kinetics of smaller particles at higher temperatures. We attributed this behavior to a quicker surface crust formation. This study provides a better understanding of the drying behavior of gelatin droplets, which will benefit the production of gelatin-based microcapsules by spray drying.

References

- Alamilla-Beltrán L, Chanona-Pérez JJ, Jiménez-Aparicio AR, Gutiérrez-López GF, 2005. Description of morphological changes of particles along spray drying. *Journal of Food Engineering*. 67(1-2):179-184.
- Amelia R, Wu WD, Cashion J, Bao P, Zheng R, Chen XD, Selomulya C, 2011. Microfluidic spray drying as a versatile assembly route of functional particles. *Chemical Engineering Science*. 66(22):5531-5540.
- Aniesrani Delfiya D., Thangavel K, Natarajan N, Kasthuri R, and Kailappan R, 2015. Microencapsulation of turmeric oleoresin by spray drying and in vitro release studies of microcapsules. *Journal of Food Process Engineering*. 38(1):37-48.
- Bayram OA, Bayram M, Tekin AR, 2005. Spray drying of sumac flavour using sodium chloride, sucrose, glucose and starch as carriers. *Journal of Food Engineering*. 69(2):253-260.
- Bruschi ML, Cardoso MLC, Lucchesi MB, & Gremião MPD, 2003. Gelatin microparticles containing propolis obtained by spray-drying technique: preparation and characterization. *International Journal of Pharmaceutics*. 264:45-55.
- Calvo P, Hernández T, Lozano M, González-Gómez D, 2010. Microencapsulation of extra-virgin olive oil by spray-drying: Influence of wall material and olive quality. *European Journal of Lipid Science and Technology*. 112(8):852-858.
- Che L & Chen XD, 2009. A simple non-gravimetric technique for measurement of convective drying kinetics of single droplets. *Drying Technology*. 28(1):73-77.
- Chen Q, McGillivray D, Wen JY, Zhong F, Queka SY, 2013. Co-encapsulation of fish oil with phytosterol esters and limonene by milk proteins. *Journal of Food Engineering*. 117(4):505-512.

- Chen XD & Patel KC, 2008. Manufacturing Better Quality Food Powders from Spray Drying and Subsequent Treatments. *Drying Technology*. 26(11):1313-1318.
- Chen XD & Mujumdar AS, 2008. *Drying Technologies in Food Processing*. Wiley-Blackwell. Hoboken, NJ.
- Fang ZX & Bhandari B, 2011. Effect of spray drying and storage on the stability of bayberry polyphenols. *Food Chemistry*. 129(3):1139-1147.
- Faria AF, Mignone RA, Montenegro MA, Mercadante AZ, and Borsarelli CD, 2010. Characterization and Singlet Oxygen Quenching Capacity of Spray-Dried Microcapsules of Edible Biopolymers Containing Antioxidant Molecules. *Journal of Agricultural and Food Chemistry*. 58(13):8004-8011.
- Fu N, Woo MW, Chen XD, 2012a. Single Droplet Drying Technique to Study Drying Kinetics Measurement and Particle Functionality: A Review. *Drying Technology*. 30(15):1771-1785.
- Fu N, Woo MW, Selomulya C, Chen XD, Patel K, Schuck P, Jeantet R, 2012b. Drying kinetics of skim milk with 50 wt% initial solids. *Journal of Food Engineering*. 109(4):701-711.
- Fu N, Woo MW, Selomulya C, Chen XD, 2013. Shrinkage behaviour of skim milk droplets during air drying. *Journal of Food Engineering*. 116(1):37-44.
- Gallardo G, Guida L, Martinez V, López MC, Bernhardt D, Blasco R, Pedroza-Islasc R, Hermida LG, 2013. Microencapsulation of linseed oil by spray drying for functional food application. *Food Research International*. 52(2):473-482.
- Handscorn, C.S., Kraft, M, 2010. Simulating the structural evolution of droplets following shell formation. *Chemical Engineering Science* 65(2):713-725.
- Hanus MJ & Langrish TAG, 2007. Re-entrainment of wall deposits from a laboratory-scale spray dryer. *Asia-Pacific Journal of Chemical Engineering*. 2(2):90-107.

- Hee YY, Tan CP, Rahman RA, Adzahan NM, Lai WT, Chong GH, 2015. Influence of Different Wall Materials on the Microencapsulation of Virgin Coconut Oil by Spray Drying. *International Journal of Food Engineering*. 11(1):61-69.
- Heldman DR, Lund DB, Sabliov C, 2006. *Handbook of Food Engineering, Second Edition*. CRC Press, Boca Raton, FL.
- Huang H, Hao SX, Li LH, Yang XQ, Cen JW, Lin WL, Wei Y, 2014. Influence of emulsion composition and spray-drying conditions on microencapsulation of tilapia oil. *Journal of Food Science and Technology*. 51(9):2148-2154.
- Intiaz-Ul-Islam Md & Langrish TAG, 2009. Comparing the crystallization of sucrose and lactose in spray dryers. *Food and Bioproducts Processing*. 87(2):87-95.
- Islam MIU, Langrish TAG, 2010. An investigation into lactose crystallization under high temperature conditions during spray drying. *Food Research International*. 43(1): 46-56.
- Ivey JW, Vehring R, 2010. The use of modeling in spray drying of emulsions and suspensions accelerates formulation and process development. *Computers & Chemical Engineering*. 34(7):1036-1040.
- Jayasundera M, Adhikari B, Aldred P, Ghandi A, 2009. Surface modification of spray dried food and emulsion powders with surface-active proteins: A review. *Journal of Food Engineering*. 93(3):266-277.
- Kemp IC, Wadley R, Hartwig T, Cocchini U, See-Toh Y, Gorringer L, Fordham K, Ricard F, 2013. Experimental Study of Spray Drying and Atomization with a Two-Fluid Nozzle to Produce Inhalable Particles. *Drying Technology*. 31(8):930-941.
- Kim EHJ, Chen XD, Pearce D, 2009. Surface composition of industrial spray-dried milk powders. 2. Effects of spray drying conditions on the surface composition. *Journal of Food Engineering*. 94(2):169-181.

- Kuang P, Zhang H, Bajaj PR, Yuan Q, Tang J, Chen S, Sablani SS, 2015. Physicochemical properties and storage stability of lutein microcapsules prepared with maltodextrins and sucrose by spray drying. *Journal of Food Science*. 80(2):E359-69.
- Langrish TAG, 2009. Multi-scale mathematical modelling of spray dryers. *Journal of Food Engineering*. 93(2):218-228.
- Langrish TAG & Premarajah R, 2013. Antioxidant capacity of spray-dried plant extracts: Experiments and simulations. *Advanced Powder Technology*. 24(4):771-779.
- Li DX, Oh YK, Lim SJ, Kim JO, Yang HJ, Sung JH, Yong CS, Choi HG, 2008. Novel gelatin microcapsule with bioavailability enhancement of ibuprofen using spray-drying technique. *International Journal of Pharmaceutics*. 355(1-2):277-284.
- Lin, SXQ, Chen, XD, 2006. Prediction of air drying of milk droplet under relatively high humidity using the reaction engineering approach. *Drying Technology* 23 (7), 1395-1406.
- Liu W, Chen XD, Selomulya C, 2015. On the spray drying of uniform functional microparticles. *Particuology*. 22(2015): 1-12.
- Maury M, Murphy K, Kumar S, Shi L, Lee G, 2005. Effects of process variables on the powder yield of spray-dried trehalose on a laboratory spray-dryer. 59(3):565-573.
- Mondragon R, Hernandez L, Julia JE, Jarque JC, Chiva S, Zaitone B, Tropea C, 2011. Study of the drying behaviour of high load multiphase droplets in an acoustic levitator at high temperature conditions. *Chemical Engineering Science*. 66(12):2734-2744.
- Mondragon R, Jarque JC, Julia JE, Hernandez L, Barba A, 2012. Effect of slurry properties and operational conditions on the structure and properties of porcelain tile granules dried in an acoustic levitator. *Journal of the European Ceramic Society*. 32(1):59-70.
- Nešić S, Vodnik J, 1991. Kinetics of droplet evaporation. *Chemical Engineering Science* 46 (2), 527-537.

- Oakley DE, 1997. Produce uniform particles by spray drying, *Chemical Engineering Progress*. 93(10):48-54.
- Paramita V, Iida K, Yoshii H, Furuta T, 2010. Effect of Additives on the Morphology of Spray-Dried Powder. *Drying Technology*. 28(3):323-329.
- Patel KC & Chen XD, 2007. Production of spherical and uniform-sized particles using a laboratory ink-jet spray dryer. *Asia-Pacific Journal of Chemical Engineering*. 2(5):415-430.
- Patel KC, Chen XD, Lin SXQ, 2009. A composite reaction engineering approach to drying of aqueous droplets containing sucrose, maltodextrin (DE6) and their mixtures. *AIChE Journal* 55 (1), 217-231.
- Patel K, Chen XD, Jeantet R, Schuck P, 2010. One-dimensional simulation of co-current, dairy spray drying systems - pros and cons. *Dairy Science & Technology*. 90(2):181-210.
- Paudel A, Worku ZA, Meeus J, Guns S, Van den Mooter G, 2013. Manufacturing of solid dispersions of poorly water soluble drugs by spray drying: Formulation and process considerations. *International Journal of Pharmaceutics*. 453(1):253-284.
- Perdana J, Fox MB, Schutyser MAI, Boom RM, 2013. Mimicking Spray Drying by Drying of Single Droplets Deposited on a Flat Surface. *Food and Bioprocess Technology*. 6(4):964-977.
- Piao MG, Yang CW, Li DX, Kim JO, Jang KY, Yoo BK, Kim JA, Woo JS, Lyoo WS, Han SS, Lee YB, Kim DD, Yong CS, Choi HG, 2008. Preparation and in vivo evaluation of piroxicam-loaded gelatin microcapsule by spray drying technique. *Biological and Pharmaceutical Bulletin*. 31(6):1284-1287.

- Pourashouri P, Shabanpour B, Razavi SH, Jafari SM, Shabani A, Aubourg SP, 2014a. Impact of Wall Materials on Physicochemical Properties of Microencapsulated Fish Oil by Spray Drying. *Food and Bioprocess Technology*. 7(8):2354-2365.
- Pourashouri P, Shabanpour B, Razavi SH, Jafari SM, Shabani A, Aubourg SP, 2014b. Oxidative Stability of Spray-Dried Microencapsulated Fish Oils with Different Wall Materials. *Journal of Aquatic Food Product Technology*. 23(6):567-578.
- Prata AS & Grosso CR, 2015. Production of microparticles with gelatin and chitosan. *Carbohydrate Polymers*. 116(2015):292-299.
- Pu JN, Bankston D, Sathivel S, 2011. Developing microencapsulated flaxseed oil containing shrimp (*Litopenaeus setiferus*) astaxanthin using a pilot scale spray dryer. *Biosystems Engineering*. 108(2):121-132.
- Rocha GA, F ávaro-Trindade CS, Grosso CRF, 2012. Microencapsulation of lycopene by spray drying: Characterization, stability and application of microcapsules, *Food and Bioproducts Processing*. 90(1):37-42.
- Rogers S, Wu WD, Lin SXQ, Chen XD, 2012. Particle shrinkage and morphology of milk powder made with a monodisperse spray dryer. *Biochemical Engineering Journal*. 62(15):92-100.
- Schutyser MAI, Perdana J, Boom RM, 2012. Single droplet drying for optimal spray drying of enzymes and probiotics. *Trends in Food Science & Technology*. 27(2):73-82.
- Shen Q & Quek SY, 2014. Microencapsulation of astaxanthin with blends of milk protein and fiber by spray drying. *Journal of Food Engineering*. 123:165-171.
- Shu B, Yu WL, Zhao YP, Liu XY, 2006. Study on microencapsulation of lycopene by spray-drying, *Journal of Food Engineering*. 76(4):664-669.

- Sloth J, Kiila S, Jensen AD, Andersen SK, Jørgensen K, Schiffter H, Lee G, 2006. Model based analysis of the drying of a single solution droplet in an ultrasonic levitator. *Chemical Engineering Science*. 61(8):2701-2709.
- Tran TH, Ramasamy T, P BK, Marasini N, Moon BK, Cho HJ, Choi HGC, Yong CS, Kim JO, 2014. Preparation and Characterization of Spray-Dried Gelatin Microspheres Encapsulating Ganciclovir. *Macromolecular Research*. 22(2):124-130.
- Tonon RV, Grosso CRF, Hubinger MD, 2011. Influence of emulsion composition and inlet air temperature on the microencapsulation of flaxseed oil by spray drying. *Food Research International*. 44(1):282-289.
- Vehring R, Foss WR, Lechuga-Ballesteros D, 2007. Particle formation in spray drying. *Aerosol Science*. 38(7):728-746.
- Verma A & Singh SV, 2015. Spray drying of fruit and vegetable juices--a review. *Critical Reviews in Food Science and Nutrition*. 55(5):701-719.
- Walton DE & Mumford CJ, 1999a. Spray Dried Products—Characterization of Particle Morphology. *Chemical Engineering Research and Design*. 77(1):21-38.
- Walton DE & Mumford CJ, 1999b. The Morphology of Spray-Dried Particles: The Effect of Process Variables upon the Morphology of Spray-Dried Particles. *Chemical Engineering Research and Design*. 77(5):442-460.
- Wang YF, Ye H, Zhou CH, Lv FX, Bie XM, Lu ZX, 2012. Study on the spray-drying encapsulation of lutein in the porous starch and gelatin mixture. *European Food Research and Technology*. 234(1):157-163.
- Wang Y, Lu ZX, Lv FX, Bie XM, 2009. Study on microencapsulation of curcumin pigments by spray drying. *European Food Research and Technology*. 229(3):391-396.

- Wang Y, Che LM, Selomulya C, Chen XD, 2014. Droplet drying behaviour of docosahexaenoic acid (DHA)-containing emulsion. *Chemical Engineering Science* 106(2014): 181-189.
- Woo MW, Fu N, Che L, Chen XD, 2011. Evaporation of pure droplets in the convective regime under high mass flux. *Drying Technology*. 29(14):1628-1637.
- Wu WD, Liu W, Selomulya C, Chen XD, 2011. On spray drying of uniform silica-based microencapsulates for controlled release. *Soft Matter*. 7(24):11416-11424.
- Xie YL, Wang AR, Lu QY, Hui M, 2010. The Effects of Rheological Properties of Wall Materials on Morphology and Particle Size Distribution of Microcapsule. *Czech Journal of Food Sciences*. 28(2010):433-439.

Chapter 3

Study on the feasibility of microencapsulation of bioactive materials by spray drying

Keywords:

Spray drying, Microencapsulation, Bioactive materials

Abstract

Bioactive material, such as carotenoid, is an important class of natural pigment with various health benefits. To enhance its stability and application in food and pharmaceutical industries, microencapsulation technology was introduced. The objective of this study was to develop a stable oil-in-water (O/W) emulsion system to microencapsulate bioactive elements by spray drying. Effects of emulsification methods (high-energy and low-energy homogenization method) on emulsion stability were characterized at various surfactant to oil ratios (SOR) with different types of oil (MCT oil, olive oil) and emulsifier (gelatin, Tween 80). High-energy method was preferred for safety concerns, as it was able to produce fine stable emulsions at low SOR. O/W emulsions, using MCT oil as core material, gelatin as wall material (encapsulant and primary emulsifier) and Tween 80 as secondary emulsifier, were prepared and spray dried to create micron-size microcapsules using a lab scale spray dryer (Buchi B-290). Effects of operating conditions, including inlet temperature, on the resultant microcapsules properties (e.g. size, morphology, moisture content (MC), encapsulation efficiency (EE) and yield (Y)) were investigated. The results demonstrated that spray drying technology could be applied to transform the stable O/W emulsions (containing bioactive material) into powders with desired properties. So it is feasible to use this emulsion-based system to microencapsulate bioactive materials in the near future.

3.1 Introduction

Lipophilic bioactive components, such as carotenoids, have received increasing attention in food and pharmaceutical industries because of their promising health benefits. They have been recognized to exhibit physiological activities in recent metabolic and nutritional studies (Abidov et al., 2010; Hosokawa et al., 2004; Maeda et al., 2005, 2007a, 2008, 2009, 2015; McClements et al., 2007; Kotake-Nara et al., 2001, 2005a, 2005b; Rao & Rao, 2007; Sachindra et al., 2007; Zhang et al., 2015), including antioxidation activities (Carranco Járegui et al., 2011), antiobesity properties (Gammone & D'Orazio, 2015), antidiabetic effects (Sluijs et al., 2015), and anticancer effects (Tanaka et al., 2012). However, the utilization of these bioactive elements as functional ingredients is currently limited due to high susceptibility to adverse environment conditions, such as oxidant, heat, light, pH value and enzyme (Mercadante et al., 2008), as well as poor water solubility and low bioavailability (Ax et al., 2001; Hashimoto et al., 2012; Park 1997; Peng et al., 2011).

To overcome these problems, microencapsulation technology has been proposed to make the bioactive component more stable during handling, processing, storage and delivery. It is a technique that enables bioactive components to be enveloped as a “core” material with a “wall” matrix which helps to protect them against degradation, increase their stability during storage, mask some of their properties (unpleasant tastes and/or odors), and improve their bioavailability. In addition, it offers the possibility not only for controlled release but also for targeted delivery of encapsulated molecules to a specific site in the body (Fang & Bhandari., 2010; Nazzaro et al., 2012; Nedovic et al., 2011; Vos et al., 2010; Zuidam & Nedovic, 2010).

In the food industry, the most common procedure for microencapsulation is spray drying. Low cost, easy to upscale, broad choices of wall materials and possibility of producing

micro-sized particles with adjustable size and morphology makes this means ideal for particle encapsulation (Gharsallaoui et al., 2007; Santos & Meireles., 2010; Verma & Singh., 2015). Many researchers have used this technology to encapsulate carotenoids such as β -carotene (Faria et al., 2010; Liang et al., 2013; Loksawan., 2007), lycopene (Goula & Adamopoulos, 2012; Rocha et al., 2012; Shu et al., 2006), lutein (Kuang et al., 2015; Wang et.,2012), astaxanthin (Pu et al., 2011; Shen & Quek, 2014), and canthaxanthin (Hojjati et al., 2011, 2014). Recent publications are listed in Table 3.1. Generally, there are two main methods to encapsulate these lipophilic materials. In the first method, carotenoids are solubilized in aqueous wall solutions with the help of some organic cosolvents, such as acetone (Goula & Adamopoulos, 2012; Shu et al., 2006) and dichloromethane (Faria et al., 2010), which are toxic and raise questions for further microencapsulation applications (lead to solvent traces in microcapsules). In the second method (Hojjati et al., 2011, 2014; Liang et al., 2013; Pu et al., 2011; Rocha et al., 2012; Shen & Quek., 2014), carotenoids are emulsified and trapped within the core of the O/W emulsion. It has received growing interest for a number of reasons. First, lipids (oils) are “natural” components with many favorable nutritional functions. For example, medium-chain triglycerides (MCT) can support the immune system, and are a good substitute for carbohydrate calories (Kang & Connolly, 2006). Long-chain triglycerides (LCT) such as olive oil offer good protective effect on the cardiovascular system (Lucas et al., 2011; Ruiz-Canela & Martínez-González, 2011). Second, lipids (oils) are good solvents for lipophilic compounds, so they can work as carriers for carotenoids during processing as well as digestion, protecting them against oxidation and enzymatic hydrolysis. The absorption (bioavailability) of carotenoids also significantly improved once dissolved in lipid (oil), which facilitates its digestion in human body (Brown et al., 2004; Lemmens et al., 2014; Nagao et al., 2013; Parker., 1997).

Since it is crucial to form a stable emulsion before spray drying, the choice of an appropriate wall material with good emulsifying properties is in consideration (Nesterenko et al., 2013; Tontul & Topuz, 2013). Gelatin is one of the wall materials that is commonly used in food industry due to its biocompatible, biodegradable and “generally regarded as safe (GRAS)” characteristics (Hanani 2014; Kapoor & Dhawan, 2013; Pignatello 2011; GRAS Substances, 1975). It also exhibit good emulsifying and wall forming properties, which allows its use as both surface-active agent (emulsifier) and wall material (Karim & Bhat, 2008). The emulsification step also plays an important role in microencapsulation. Two methods are currently available to fabricate stable O/W emulsion, the high-energy and low-energy approaches. High-energy approach utilizes mechanical devices (such as high pressure homogenizers, rotor-stator homogenizers, microfluidizers and ultrasound generators) capable of generating intense disruptive forces to breakup and intermingle the oil and water phases into tiny oil droplets (McClements & Rao, 2011; Santana et al., 2013b; Yang et al., 2012). It is the most versatile method to produce food grade emulsions as it allows the use of a broad variety of different types of oils (triacylglycerol oils, essential oils and flavor oils) and emulsifiers (biopolymers and surfactants) at relatively low concentrations (~1-2%). Emulsion can also be fabricated using the low-energy method. It is easy and cost efficient since emulsification can occur under simple stirring, no expensive homogenization equipment is required. A number of different low-energy methods have been developed, including spontaneous emulsification (SE), phase inversion temperature (PIT), and phase inversion composition (PIC) methods (McClements & Rao, 2011). Among them, spontaneous emulsification (SE) is probably the easiest one to carry out since it simply involves titration of an organic phase (containing oil-surfactant mixture) into an aqueous phase with constant agitation, which leads to the spontaneous formation of fine oil droplets at the oil-water boundary (Saberri et al., 2014a) (Fig.3.1). However, there are also some potential

disadvantages of low-energy approach. For example, limited types of oils and emulsifiers can be used in food industry. To the best of our knowledge, it is currently not possible to form stable emulsions using biopolymer emulsifiers (e.g. proteins) with the low-energy approach, the small molecular weight surfactants frequently used in low-energy process are usually either not food grade or need to be used at relative high concentration (sometimes even at toxic level).

Table 3.1 Recent publications for microencapsulation of carotenoids by spray drying

Carotenoids	Solvent	Wall materials	Particle characteristics	Reference
β -carotene, apocarotenal	Dichloromethane	GA, MD	6.4-10.7 μm spherical microcapsules with irregular surfaces (for GA) or smooth surfaces (for MD)	Faria et al., 2010
Carotenoids from chilli	Corn, Sunflower, Safflower oil	GA, MD	Semi-spherical microcapsules with dents and rough surfaces, but no fracture. MC 3.9-5%, $d_{32}=11.1\pm 1.4-12.7\pm 0.5 \mu\text{m}$.	Guadarrama-Lezama et al., 2012
Carotenoids from Gac aril	Gac oil	WPC, GA	Spherical shape and concave surface with various sizes (less than 20 μm). EEs of the oil, β -carotene, lycopene, Y and MC were validated as 87.22%, 82.76%, 84.29%, 52.78%, and 4.90%, respectively.	Kha et al., 2014a, 2014b
β -carotene	MCT oil	HI-CAP, CAPSUL, CAPSUL TA	Microcapsules showed rounded surface with grooves.	Liang et al., 2013
Lycopene	Oil	Capsul [®]	A matrix type of microcapsules had a rounded outer surface with the formation of teeth or concavities. No fissures, cracks or interruptions.	Rocha et al., 2012
Lutein	Ethanol	Porous starch gelatin mixture	Uniform spherical microcapsules, $94.4 \pm 0.4\%$ EE (%), $92.6 \pm 1.7\%$ Y (%).	Wang et al., 2012
Astaxanthin	Sunflower oil	WPI, SC, SCF 70	2-25 μm particles, mostly spherical in shape.	Shen & Quek, 2014
Canthaxanthin	pure corn oil	SSPS, GA, MD	7.94 \pm 0.14 μm microcapsules for SSPS (EE (90.3 \pm 0.7) and higher stability), 9.08 \pm 0.07 μm microcapsules for GA and 10.42 \pm 0.14 μm microcapsules for MD (1.035 \pm 0.008), respectively.	Hojjati et al., 2014

Note: GA refers to Gum Arabic, MD refers to Maltodextrin, WPI refers to whey protein isolate, WPC refers to whey protein concentrate, SC refers to sodium caseinate, SCF 70 refers to soluble corn fiber, SSPS refers to soluble soybean polysaccharide, MC refers to moisture content, EE (%) refers to the encapsulation efficiency, Y(%) refers to the yield.

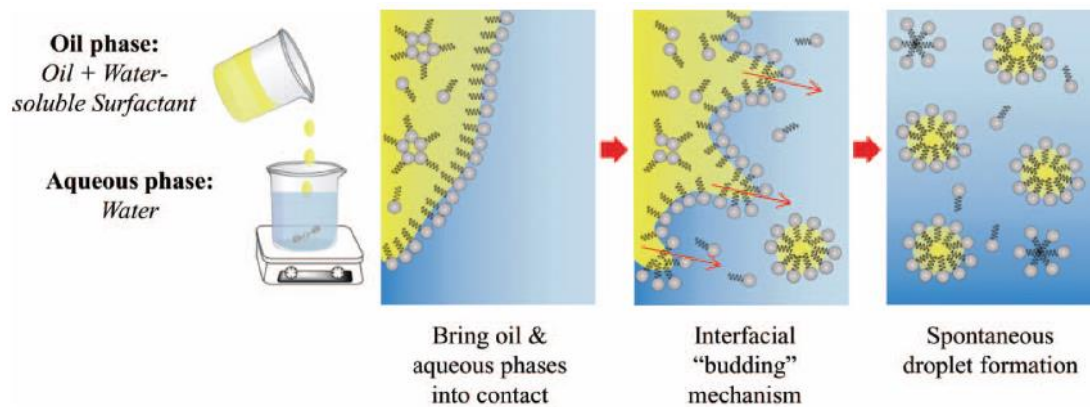


Fig. 3.1 Schematic representation of spontaneous emulsification (adapted from McClements & Rao, 2011)

The objective of this study was to develop a stable O/W emulsion system for microencapsulation of bioactive materials by spray drying. The effectiveness of a high-energy method was compared with a low-energy method (spontaneous emulsification) at various combination of SOR, oil type (MCT/Olive oil) and emulsifier type (Gelatin/Tween 80). The emulsion formed was then spray dried and the resultant microcapsules were characterized for moisture content (MC), yield(Y), encapsulation efficiency (EE), particle size and morphology. The use of both high and low energy emulsification method prior to spray drying process was a relatively new attempt. This research might be useful for identifying the most appropriate homogenization method for bioactive materials microencapsulations.

3.2 Materials and methods

3.2.1 Materials

The food grade gelatin powder and non-ionic surfactant Tween 80 were purchased from Amresco LLC (Solon, OH). A variety of different oils and emulsifiers are available for the formulation of emulsions in the food industries. In the current study, MCT oil and olive oil were selected as carrier oils as they are the source of medium chain triglycerides and long chain triglycerides, respectively and have been highlighted to be efficient in enhancing carotenoid bioaccessibility (facilitate digestion of carotenoids) in food systems (Colle et al., 2012; Nagao et al., 2013). MCT oil is a saturated fat (no double bonds) so it can tolerate higher temperatures. Olive oil, which contains mostly monounsaturated fatty acids (only one double bond), is fairly resistant to high temperature as compared with the polyunsaturated fats (many double bonds) and essential oils (Grootveld et al., 2001; Prabhu, 2000), so they can offer better protection of carotenoids against thermal treatment during spray drying process. Food-grade nonionic surfactant Tween 80 (Hydrophilic-lipophilic balance (HLB) =15) was employed since this type of surfactant is usually considered most suitable for the formation of emulsions by low energy methods (Chang et al., 2013, 2014; Gulotta et al., 2014; Mayer et al., 2013; Ostertag et al., 2012; Saberi et al., 2013a, 2014; Yang et al., 2012). Olive oil was provided by Bertolli (Houston, TX). The supplier reported the olive oil (smoke point, 468 °F (242°C)) contained 14% saturated fat, 14% polyunsaturated fat and 72% monounsaturated fat. Medium-chain triglycerides (MCT) oil was obtained from NOW Foods (Bloomington, IL), the fatty acid composition of MCT was 56% caprylic acid (C8:0) and 44% capric acid (C10:0) according to the manufacture's report. Deionized water was used to prepare all solutions and emulsions. All chemicals used in this research were of food grade.

3.2.2 Preparation of wall solution and infeed emulsion

Wall material gelatin was dissolved in distilled water at 50°C with magnetic stirring (PC-101 Hot Plate Magnetic Stirrer, Corning Incorporated, Corning, NY) overnight to ensure complete dissolution. As described in Section 2.3.1, 5 wt% gelatin solution was selected to allow forming aqueous solutions with reasonable viscosity in order to maintain proper atomization and efficient drying of the powder during spray drying process. The gelatin solution was kept at 50%, even higher temperature may promote thermal degradation of bioactive materials and affect the emulsion stability. The pH value of gelatin solutions was adjusted to 3 using HCl prior to spray drying to achieve maximum surface charge (zeta-potential) to improve the solution stability. These positive (cationic) droplets could also repel iron (Fe^{2+} and Fe^{3+}) and inhibit iron (Fe^{2+} and Fe^{3+}) catalyzed oxidation of lipids in the emulsions (McClements, 2014).

The infeed oil-in-water (O/W) emulsions were prepared using two methods. In the high energy method, core material, including olive or MCT oil, was mixed with the gelatin solution at the core to wall ratio of 1:4, and blended using a rotor-stator homogenizer (T18 digital Ultra-turrax, IKA, Wilmington, NC) at 20,000 rpm for 5 min to form a coarse emulsion. The resulting coarse emulsion then passed through a microfluidizer (M-110EH-30, Microfluidics, Newton, MA) 3 times at 12,000 psi to form finer emulsions. To create O/W emulsion using spontaneous emulsification (SE) procedure, an organic phase (containing Tween 80 and MCT oil) was titrated by a syringe pump (KDS 200, KD Scientific, Holliston, MA) at a rate of 2 mL/min into an aqueous phase (pure water or gelatin solution) with continuous stirring (500 rpm) using a

magnetic stirrer to ensure system homogeneity. Each emulsion sample was sealed and stored for at least 1h before emulsion characterization.

3.2.3 Emulsion characterization

The emulsion droplet size were measured by a commercial dynamic light scattering (DLS) instrument (Zetasizer Nano ZS, Malvern Instruments, Malvern, UK). Emulsion samples were diluted with deionized water prior to analysis to avoid multiple scattering effects. The final emulsion size and size distribution were averaged from three measurements with each measurement set for 50 runs. The emulsion stability was also observed by the phase separation of water and oil phase.

3.2.4 Microencapsulation of emulsions by spray drying

The infeed emulsions were pre-warmed to 50°C and then spray dried using a laboratory-scale spray dryer (B-290, Buchi, Flawil, Switzerland), equipped with a dehumidifier (B-296, Buchi, Flawil, Switzerland). Dehumidified air was used as the drying medium to improve the drying rate. The inlet air temperature was set from 150°C to 180°C with interval of 10°C to determine the optimum drying temperatures. The resultant spray dried samples were collected and stored in an air tight desiccators for further analysis.

3.2.5 Powder analysis

3.2.5.1 Moisture content (MC) and production yield (Y)

The moisture content (MC, d.b.) of samples were determined gravimetrically by MF-50 Moisture Analyzer (A&D, San Jose, CA). The production yield (Y) is expressed as weight fraction (%) of

powders (microcapsules) recovered from the production vessel with respect to the weight of dry matter originally added to the feed solution. Any powders adhering to the walls of dryer chamber or cyclone were not considered. Each measurement was carried out in triplicate, and averaged MC and Y values were reported.

3.2.5.2 Encapsulation efficiency (EE)

Encapsulation efficiency (EE) was calculated based on the retention of oil contents in the encapsulated powder as follows:

$$EE\% = [(TO - SO)/TO] \times 100$$

Where TO is the total oil content and SO is the surface oil content of encapsulated powders. The total oil (TO), which includes both the encapsulated oil (EO) and surface oil (SO), is assumed to be equal to the initial oil, since MCT oil is not volatile. Surface oil (SO), or extractable non-encapsulated oil content, was determined according to Bae & Lee (2008) with slight modifications. Hexane (50 ml) was added to the microcapsule samples (5 g) and gently shaken with a vortex mixer (Fisher Scientific, Pittsburgh, PA) for 10 min. The suspension was then filtered with Whatman No.1 filter paper (GE Healthcare Bio-Sciences, Piscataway, NJ) and the powder residue was rinsed three times with 20 mL of hexane by passing it through the powder. The residual powder was then air dried at 70°C until constant weight. The amount of surface oil (SO) was calculated based on the difference in weights of the microcapsules, before extraction and after washing. The experiment was conducted in duplicate.

3.2.5.3 Particle size and morphology

The size and morphology of the spray dried particles were investigated using a scanning electron microscope (SEM) (EVO 50 VP, Zeiss, Oberkochen, Germany). The specimens were loaded on the SEM stubs (attached to a metal holder) using a two-sided adhesive tape, and sputtered with gold using a magnetron sputter coater. The coated samples were then examined using SEM operating at an accelerating voltage of 20 kV. The particle size and size distributions were disclosed from the SEM micrographs using an imaging processing software ImageJ (National Institutes of Health, US). The volume median particle size (d_{50}) was calculated and the width of size distribution was indicated by Span ($\text{Span} = (d_{90} - d_{10})/d_{50}$, where d_{50} , volume median size; d_{90} , 90% of the volume has a size smaller than d_{90} , d_{10} , 10% of the volume has a size smaller than d_{10}). A smaller Span value indicates a narrower size distribution.

3.3 Results and discussion

3.3.1 Preparation of O/W emulsions

3.3.1.1 O/W emulsions by high-energy method (Effect of carrier oils and SOR on emulsion size)

Initially, we examined the influence of system composition (surfactant-to-oil ratio (SOR)) and oil type on the formation of oil-in-water (O/W) emulsion. The emulsion droplet size and the minimum amount of emulsifier needed to produce fine emulsions were investigated. As seen in Fig. 3.2, the emulsion size was highly dependent on the initial system compositions (SOR and carrier oil type). Gelatin alone (SOR=0:1.5) could help to form tiny emulsions ($d=339\pm 1.8$ nm) in MCT O/W system, however, it is incapable of making olive O/W emulsion with smaller mean droplet size ($d=735\pm 5.3$ nm). This observed differences in emulsion size may be due to the difference in the bulk physicochemical properties of these two carrier oils, such as viscosity. Previous research suggested that the viscosity of the oil phase was expected to influence droplet

disruption and the mass transport rate of emulsifier molecules from the organic to aqueous phase (Israelachvili, 2011; López-Montilla et al., 2002; Song et al., 2011). Therefore, the lower viscosity of MCT oil (32.8 ± 0.45 cP at 25 °C) may lead to the faster movement of the gelatin molecules, which facilitated the formation of smaller droplets. Conversely, the higher viscosity of olive oil (84.8 ± 0.87 cP at 25 °C) limited droplet disruption within the rotor-stator homogenizer (Saber et al., 2013a, 2014), which made the breakup of the droplet more difficult (Yang et al., 2012).

Once Tween 80 was introduced in the system, there was a steep decrease in the emulsion size of the olive O/W system, while the emulsion size in MCT O/W system was only slightly decreased. This phenomenon may be related to the Hydrophilic-lipophilic balance (HLB) value of the surfactants, which appeared to play an important role in surfactants' ability to form small droplets (Chang et al., 2013; Wang et al., 2009). Tween 80 has a HLB value at 15, which was closer to "required" HLB for olive oil to form O/W emulsion (HLB =14) (Ma & Hadzija, 2013), so it was more efficient in emulsifying the olive O/W system.

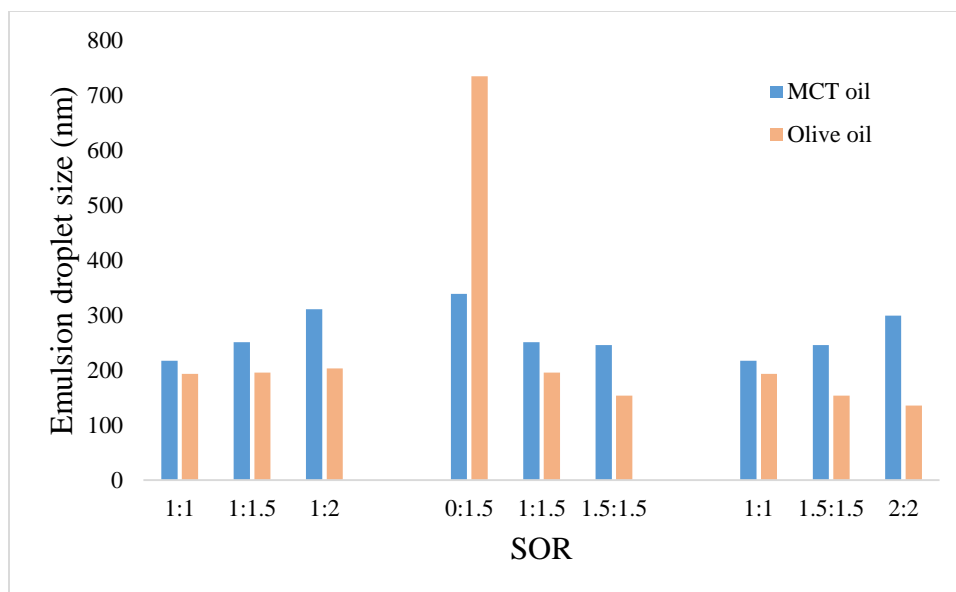


Fig. 3.2 Effect of SOR and oil type on mean droplet size of emulsion formed by high-energy method (no microfluidization). Gelatin concentration is fixed in the O/W system (5%), SOR is ratio between surfactant Tween 80 and carrier oil (MCT oil or Olive oil).

The droplet size distribution of MCT and Olive O/W emulsions are shown in Fig. 3.3 and Fig. 3.4, respectively. A bimodal droplet size distribution with a small population of large droplets were observed in MCT O/W system when SOR was 0:1.5 (Fig. 3.3a). The existence of large droplets in the system probably attributed to droplet growth caused by gravitational separation, coalescence, flocculation, and/or Ostwald ripening (Chang & McClements, 2014). The relative low disruptive forces generated by the rotor-stator homogenizer limited its ability in oil droplet breakup, so that couldn't prevent the droplets from aggregating and the emulsion produced had poor stability over time with some coalescence of oil droplets. Further increase of homogenization pressure facilitated droplet disruption, as seen in Fig. 3.3b. Microfluidization of this coarse emulsion could create finer emulsion with monomodal droplet size distribution. The formed emulsion was also relatively stable to droplet growth, with no significant change in mean droplet diameters.

The droplet size distribution in olive O/W system (SOR=1:1.5) was monomodal, with one peak representing a predominant size (Fig. 3.4). So the small molecule surfactant Tween 80 seemed to be more efficient in emulsion fabrication compare with gelatin. It could be rapidly adsorbed to the freshly formed surface of droplet during homogenization, forming a protective layer that stabilized the emulsion (Qian & McClements., 2011; Santana et al., 2013b).

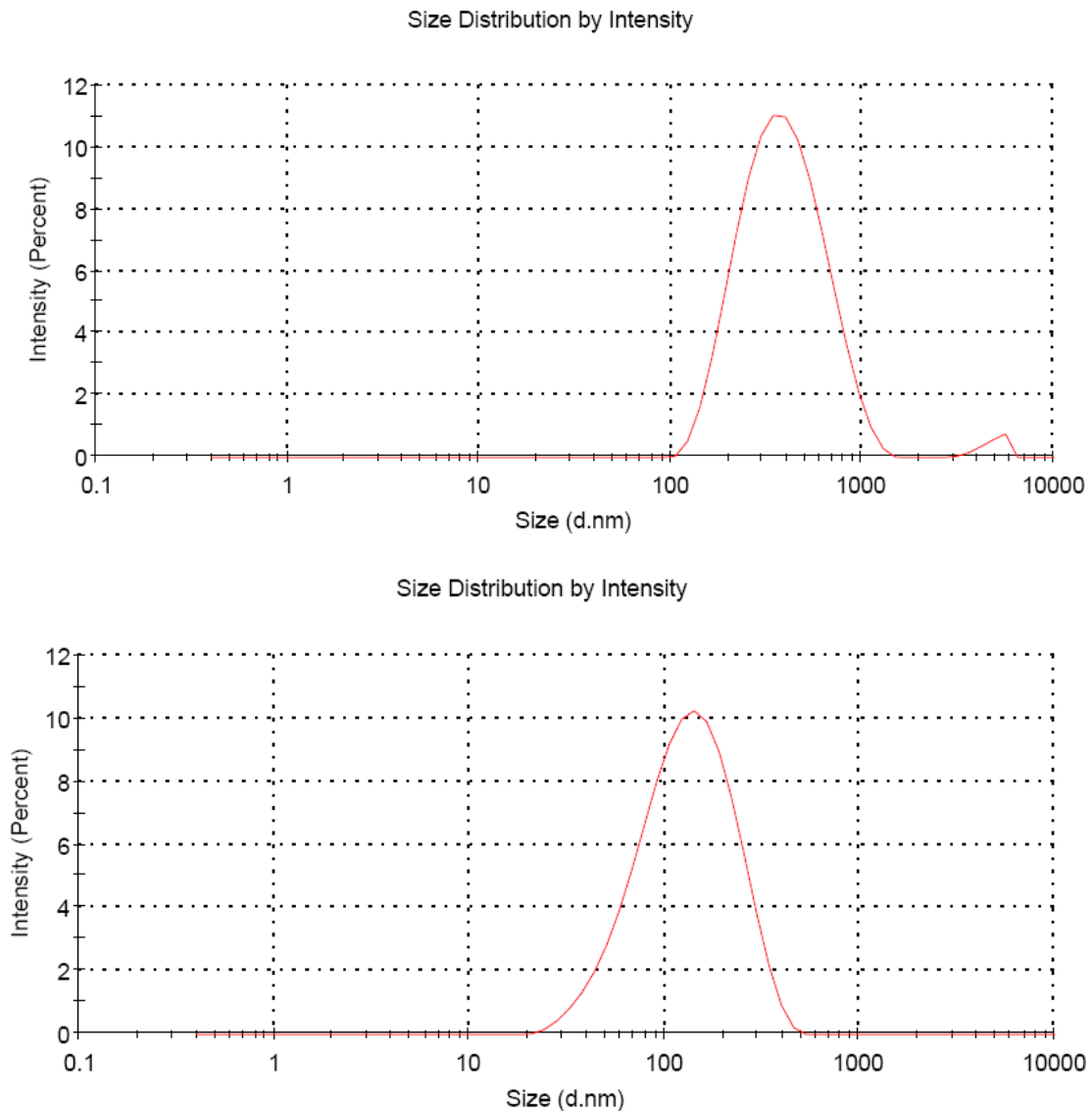


Fig. 3.3 Droplet size distribution of MCT oil-in-water emulsion formed by high-energy method when SOR=0:1.5. (top) Coarse emulsion before microfluidization, (bottom) Finer emulsion after microfluidization.

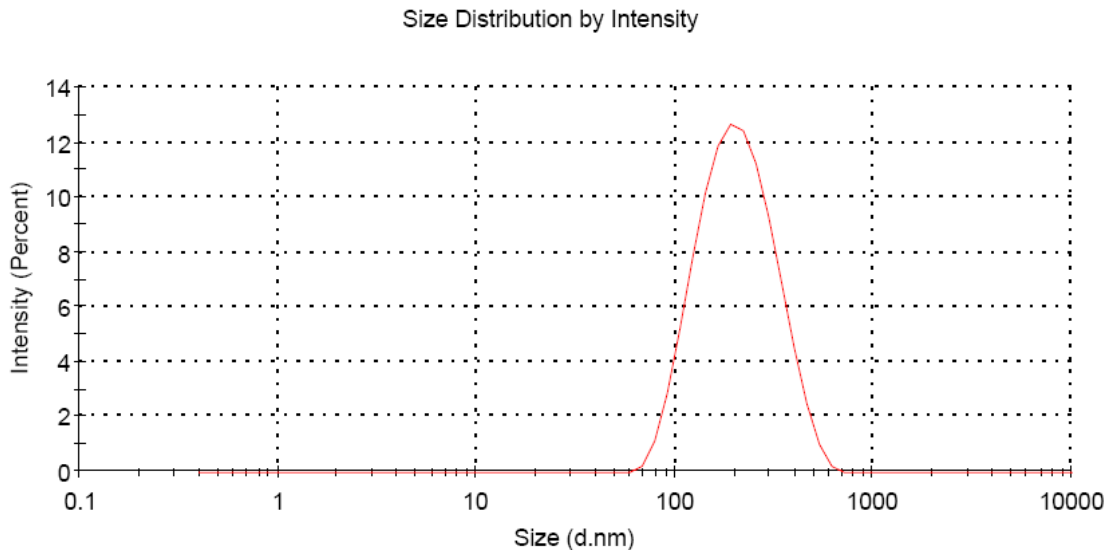


Fig. 3.4 Droplet size distribution of olive oil-in-water emulsion formed by high-energy method (no microfluidization) when SOR=1:1.5.

3.3.1.2 O/W emulsions by spontaneous emulsification (SE) method

In order to compare the results with high-energy method, the low-energy spontaneous emulsification (SE) method was also used to prepare O/W emulsions. Only MCT oil was selected as carrier oil since formation of emulsions with long-chain triglycerides oils (e.g. Olive oil) were often difficult to achieve in low-energy method (Flanagan & Singh, 2006; Hegde et al., 2013). A series of O/W emulsions was prepared using MCT as the oil and Tween 80 as the emulsifier (in the absence of gelatin). As seen in Fig. 3.5, the amount of Tween 80 present had a pronounced influence on the size of emulsion produced, with the smallest droplets being formed at the highest surfactant levels ($d = 200 \pm 3.0$ nm when SOR=1). At relatively low surfactant levels (SOR \leq 0.6), emulsion was formed with bimodal or even multimodal droplet distribution, relatively large droplets ($d > 1000$ nm) were observed and phase separation occurred quickly (Fig. 3.6a). On the other hand, the emulsions appeared less turbid at sufficiently high surfactant levels (SOR \geq 0.8), smaller droplets were formed with monomodal and narrower size distribution (Fig. 3.6b). This phenomenon was in agreement with earlier studies (Chang et al., 2013; Saberi et

al., 2013a) and could be attributed to a number of physicochemical mechanisms. First, higher surfactant concentrations at the oil-water boundary caused a larger reduction in the interfacial tension, which facilitates the formation of finer droplets (Lamaallam et al., 2005). Secondly, higher surfactant concentrations meant that a larger number of surfactant molecules diffuse from the organic phase into aqueous phase when they came into contact, thereby promoting the formation of finer oil droplets at the oil-water boundary (Anton & Vandamme, 2009).

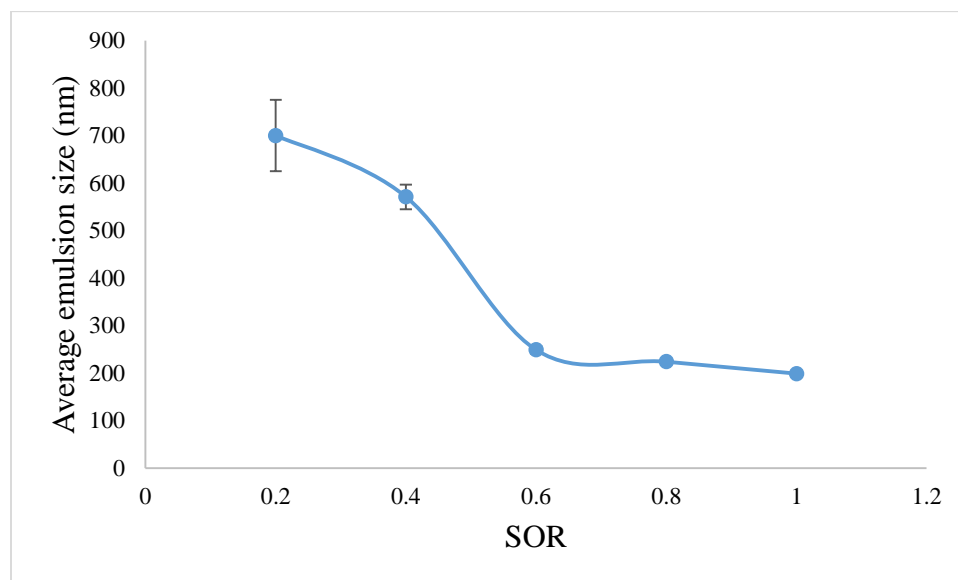


Fig. 3.5 Effect of SOR on mean droplet size of emulsion produced by spontaneous emulsification (SE).

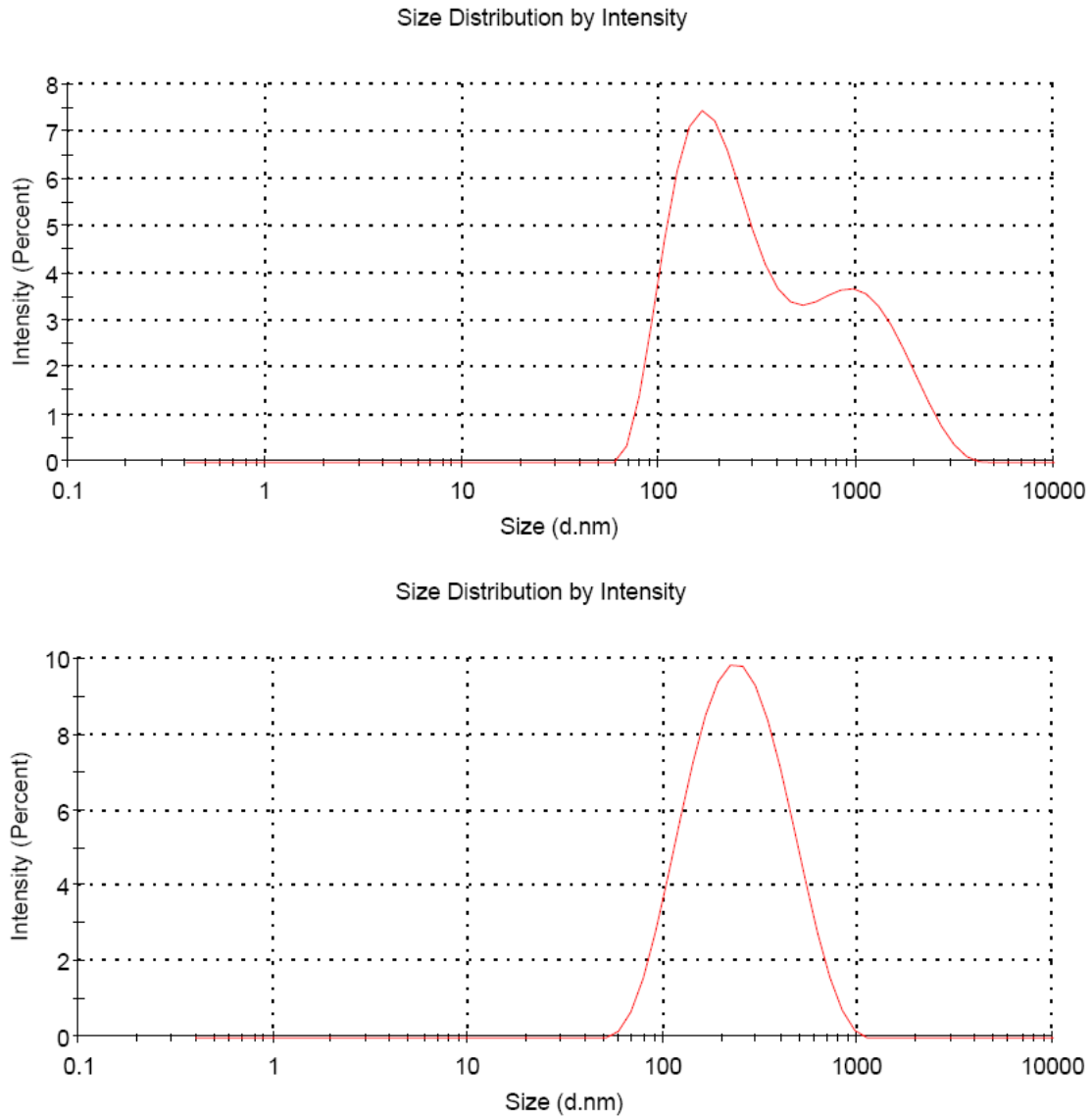


Fig. 3.6 Droplet size distribution of MCT oil-in-water emulsion formed by spontaneous emulsification when (top) SOR=0.6 (bottom) SOR=1.

The addition rate of the oil-surfactant mixture and stir speed of the oil-surfactant-water system also had influence on producing fine emulsions. It was observed that large clots were formed and difficult to disperse if the oil-surfactant mixture was poured into the water phase too quickly (Yang et al., 2012), so we used a slower addition rate (2 mL/min). Mild mixing of the oil-surfactant-water system was also required during the SE method to ensure different components

were thoroughly mixed. Too high mixing rates may lead to the promotion of droplet coalescence (Komaiko & McClements, 2014; Sol et al., 2010).

Since the synthetic surfactants are less favored in food products than natural emulsifiers, we tried to use gelatin as the emulsifier in the low-energy method. The emulsions produced were inhomogeneous and highly unstable to droplet growth. Gelatin is a poor emulsifier agent compared with surfactant, and the emulsion had a poor stability over time with some coalescence of oil droplets observed after about 1h. We therefore investigated the possibility of using a mixture of emulsifiers (gelatin and Tween 80) in the emulsion system in order to decrease the concentration of surfactants used. The emulsion was produced using the same SE method as described before, Tween 80/MCT oil mixture was titrated in to aqueous gelatin solutions instead of pure water solution with constant stirring. However, DLS measurements could not be carried out once gelatin was introduced, the emulsion produced was too polydisperse for analysis, and the large particles or aggregates presented were out of the range (limit) of the instrument. It had been postulated that the emulsion size increased above a certain level due to the formation of a highly viscous liquid crystalline phase, which made spontaneous breakup of the oil-water interface more difficult (Forgiarini et al., 2001; Saberi et al., 2013a; Wang et al., 2009).

3.3.1.3 Comparison of high- and low-energy homogenization methods

Fabrication of stable emulsions prior to spray drying process was crucial for encapsulating lipophilic core materials like carotenoids. Since smaller droplet size conferred advantages in terms of the emulsion stability (Rascon et al., 2011), as well as the bioavailability (Acosta, 2009; Hatanaka et al., 2010; Huang et al., 2010) and encapsulation efficiency of encapsulated

compounds. (Hogan et al., 2001; Soottitantawat et al., 2003), the initial emulsion size and its distribution became one of the most important factors to be considered (controlled) in this study. And as additional ~30-60 min were needed to complete the spray drying process, emulsions were stored and characterized 1 h after preparation.

Fig. 3.3, Fig. 3.4 and Fig. 3.6 shows that, with the help of sufficient amount of emulsifiers, the average emulsions size before spray drying could be decreased to less than 200 nm with a narrow size distribution. No phase separation and significant changes in emulsion size were observed by naked eyes (visual observation, data not shown). These results imply that the homogenization methods employed in this work were suitable to produce stable emulsions with fine droplet size (as evidenced by the small average droplet size). The low-energy homogenization method seemed to be more efficient in producing small droplets than the high-energy one since no expensive equipment was required. The emulsion size could be further reduced by adding some cosolvents or cosurfactants (such as ethanol, propylene glycol, and glycerol) (Saber et al., 2013b, 2013c). However, the use of gelatin in low-energy homogenization method was often challenging due to its high viscosity, which limits spontaneous surfactant movement from organic to aqueous phase, so that couldn't lower interfacial tensions between O/W phases and stabilize the emulsion system. By contrast, once the emulsion had been created by high-energy method, it was often highly physically stable. The mechanical forces within homogenizer facilitate droplet disruption, which favors the production of small droplets. The high viscosity of gelatin solutions might retard droplet movement, which helped to reduce droplet coalescence and/or sediment, resulting in good emulsion stability. Another disadvantage of the low-energy method was that more surfactant was required to form stable emulsions, sometimes at toxic

levels. The situation becomes even worse after spray drying, as the surfactants content would be highly concentrated because of the evaporation of water. The U.S Food and Drug Administration puts legal limits on the use of Tween 80 in various food applications, for example, not exceed 300 milligrams from the recommended daily dose of the preparations of fat-soluble vitamins (CFR, 2015). Therefore, the use of these relatively high surfactant levels may cause safety problems (concerns) in some food products. Novel “GRAS” surfactants or new approaches that can utilize existing emulsifiers more effectively in emulsion formation should be explored for future use in food industries (Mayer et al., 2013). High-energy method was thus selected to create stable emulsions for the spray drying processes of our studies. Though gelatin exhibits emulsifying properties, Tween 80 was included in all formulations to assure the stability of feed emulsions before spray drying.

3.3.2 Microcapsule characterization

Emulsions have been reported to be an appropriate system to encapsulate bioactive materials (Kim et al., 2012; Qian et al., 2012), however, it is still sensitive to the environment stresses, such as heating, freezing and altering pH, which would further tend to destabilize the encapsulated compounds. A spray drying process was conducted to overcome these limitations, following the emulsification process to produce powdered dry emulsions. This powdered form is stable and allows easier dosage and mixture with other powders, which helps to improve its long-term stability, facilitate its transport and utilization in some applications. Provided that infeed (feeding) emulsion was stable over the processing time, it was still important to optimize microencapsulation conditions in order to obtain higher production yield (Y) and encapsulation efficiency (EE). In this work, spray drying operating conditions were selected based on

preliminary experiments performed at different inlet temperatures, liquid feed rates and air flow rates. The drying air flow rate was set at the maximum gas flow rate (100% aspirator rate) to ensure complete solvent evaporation. Inlet air temperature was set from 150°C to 180°C, a compromise between high temperatures (water evaporation rates) and oil protections (Gallardo et al., 2013). The wall material to core ratio (w/w) was another variable to consider. It was generally accepted that a wall material to core ratio between 3 and 4 was suitable for most applications (Chen et al., 2013; Gallardo et al., 2013; Goula & Adamopoulos, 2012; Hojjati et al., 2011, 2014; Pérez-Alonso et al., 2008; Shen & Quek, 2014). A lower ratio would probably lead to insufficient amount of wall matrix to cover and stabilize all the dispersed oil droplets in the microcapsules, causing an unacceptable increase of surface oil, and consequently leading to poor EE of dried microcapsules. While a higher ratio would result in a very low oil loading in the microcapsule, which was not desirable for food applications (Hojjati et al., 2011, 2014). Therefore, the wall material (gelatin) to core (MCT oil) ratio (w/w) was kept at 5:1.5 for better encapsulation of the MCT oil.

3.3.2.1 Production yield (Y) and moisture content (MC)

The production yield (Y) in the current study varied from 50 to 70% (Table 3.2), which was consistent with many other studies (Santana et al., 2013a; Su et al., 2008). In contrast, Gallo et al. (2011) reported that higher yield (~85%) was achieved for the same kind of spray dryer (B-290). This difference might be due to difference in calculation of the yield. In this study, only powder recovered from the production vessel was considered in the calculation, powders attaching to the wall or the underside metal lid of cyclone was not regarded as part of the product. Those accumulated powder received more heat exposure so may have different properties (Goula &

Adamopoulos, 2012). This relatively low Y was also related to the dimensions of the spray dryer, the narrow dryer chamber of the B-290 makes the wet powders deposit in the chamber wall easier, and hence results in a reduced production yield. The use of larger scale spray dryer may lead to higher production yield. The MC of the powders was in the range of 5.5-7% (w/w, d.b.) (Table 3.2) and decreased with the increasing inlet temperatures. It has been observed that these low MCs are usually associated with low water activities and higher glass transition temperatures (T_g), which could prevent lipid oxidation and give microcapsules a more promising stability during storage (Chen et al., 2013; Gallardo et al., 2013; Klaypradit & Huang, 2008).

3.3.2.2 Encapsulation efficiency (EE)

For efficient encapsulation, the presence of unencapsulated oil on the microcapsule surface (higher surface oil) should be low. Current results (Table 3.2) showed that the EEs of MCT oil were around 90%. Considering the extraction procedure, the degree of encapsulation values were reasonably high, oil losses during the spray drying process can be regarded as low, which indicated the formation of an effective protective “shell” by the wall matrices gelatin to confer high level protection to the encapsulated core material MCT oil. EEs were also significantly affected by the drying temperature. At a high enough drying temperature ($T_i > 150^\circ\text{C}$), the oil retention (EE) could be improved once the drying temperature increased. This could be explained by that increasing drying temperature, which in turn increased drying rates, the duration of the constant-rate stage of the drying process was reduced, resulting in more rapid formation of the semi-permeable membrane on the droplet surface, which acted as a protective layer to encapsulate the bioactives (MCT oils) (Rascon et al., 2011). However, the EEs were decreased when drying temperature was raised to 180°C . These results are in agreement with

previous research (Chen et al., 2013; Shen & Quek, 2014), and may be due to excessive vapor evaporation from the wall materials at higher drying temperature, causing cracks, fissures or splits on the microcapsule surface, consequently increasing the risk of oil leakage to the surface (Drusch & Berg, 2008; Jafari et al., 2008; Paramita et al., 2010).

Table 3.2 Effect of drying temperature on the properties of the spray dried microcapsules containing MCT oil as core material and gelatin as wall material.

Drying Temperature (°C)	MC (%)	Y (%)	EE (%)	d ₅₀ (µm)	Span
150	6.8	50.7	90.3	9.8	1.36
160	6.2	54.8	91.5	10.6	1.26
170	6.0	59.4	87.7	10.7	1.29
180	5.7	66.8	83.2	10.8	1.14

3.3.2.3 Particle size and morphology

As seen in Fig. 3.7, the spray dried powders produced had a monomodal and relatively narrow size distribution, their volume median diameter d₅₀ was between 9.8 and 10.8 µm, with a span from 1.1 to 1.4, respectively (Table 3.2). Compared with the resultant microcapsules (d₅₀ ≈ 10 µm), the emulsion droplets (d_{avg} < 400 nm) were small enough to be encapsulated. However, the presence of those “big” drops in the coarse emulsion (d_{avg} > 1 µm) did not seem to be compatible with a good oil retention (Turchiuli et al., 2014). The breakdown of larger emulsion droplets during spray drying process could make the loss of core material easier (Hojjati et al., 2011, 2014). In the present work, we prepared both the coarse emulsions and finer emulsion. The reduction of emulsion size in the finer emulsion might be one of the main causes for the improvement in encapsulation efficiency (Gallardo et al., 2013). On the other hand, despite lower homogenization pressure indicated lower EE, the EE in the coarse emulsion remained

around 90%, probably due to the adequate wall material used for microencapsulation. The microfluidization step could be omitted for economic reasons (cost savings associated with energy savings).

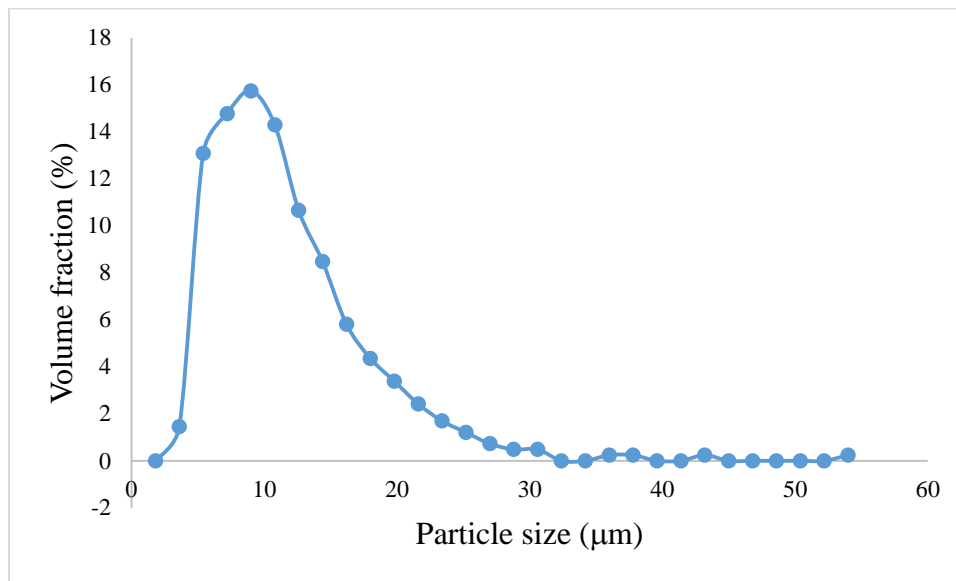


Fig. 3.7 Particles size distribution of spray dried powders when $T_i=150^\circ\text{C}$.

The surface morphology of the spray dried powders was observed by scanning electron microscope (SEM) at $5000\times$ magnification (Fig. 3.8). Most of the optimally produced microcapsules exhibited spherical shapes with certain degree of dimpled surfaces, which were the typical characteristics of spray dried particles (Table 3.1) (Gallardo et al., 2013; Tonon et al., 2011). The dimpled surfaces being more likely to occur could be attributed to the slower diffusion of water, allowing more time for structures to deform, shrink and even collapse (Aniesrani Delfiya et al., 2015; Chen & Mujumdar, 2008). Besides, this irregularity on the surface of the microcapsules might be desirable in terms of enhanced dispersibility and rehydration of the powders (Guadarrama-Lezama et al., 2012). In contrast, addition of hydrocarbon compounds (e.g. sucrose or mannitol), which could act as a plasticizer, may promote

the formation of a smoother surface (Bayram et al., 2005; Bruschi et al., 2003; Faria et al., 2010; Shu et al., 2006). Importantly, no cracks or fissures on the particle surfaces indicate complete coverage of gelatin, ensuring lower gas permeability, therefore providing better protection and retention of the core material (Rocha et al., 2012; Aniesrani Delfiya et al., 2015).

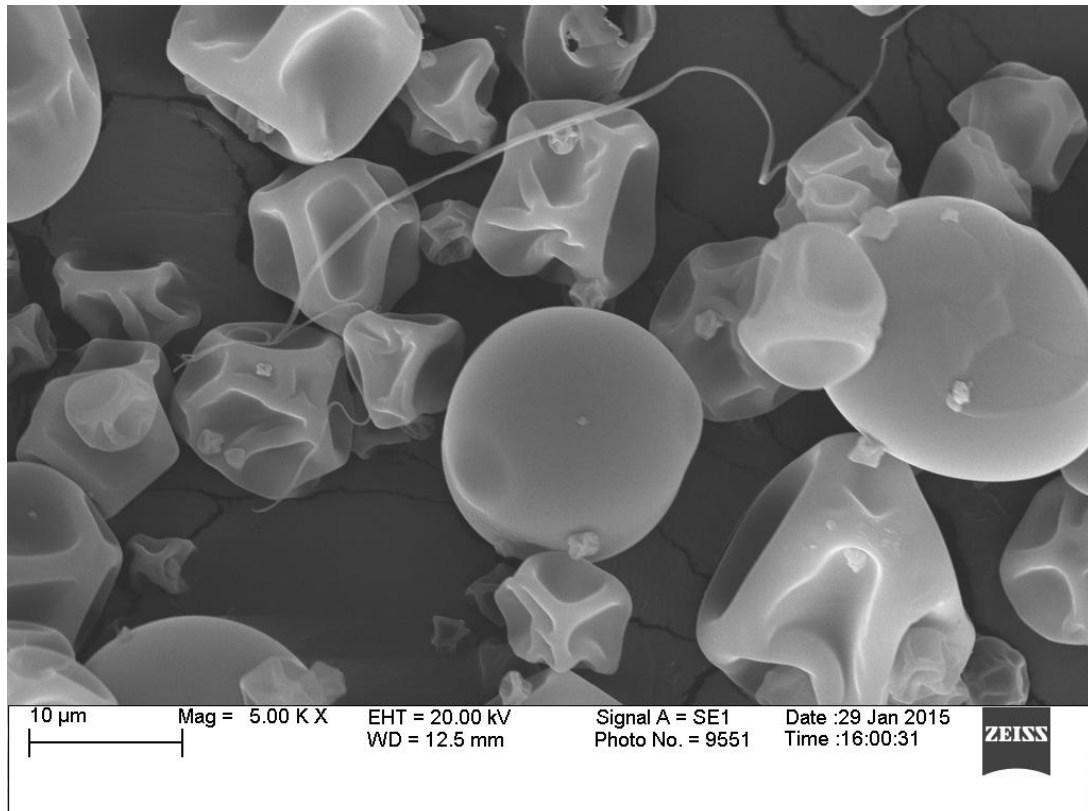


Fig. 3.8 SEM image of microcapsulated MCT oil with gelatin as wall materials

Conclusions

This study investigated the feasibility of microencapsulation of bioactive materials by spray drying. Stable O/W emulsion consisting of lipophilic components was successfully fabricated by both high- and low-energy methods. High-energy method was preferred for safety and health concerns, as it was able to produce fine stable emulsions at low SOR. The obtained emulsions were further spray dried and the results demonstrated gelatin was a good wall material to encapsulate powders with desired properties. So it is possible to apply this emulsion-based system to microencapsulate bioactive materials in the near future.

References

- Aaneby J, 2012. Iron Catalyzed Lipid Oxidation in Emulsions and the Influence of Antioxidants. Master thesis. Norwegian University of Science and Technology, Norway.
- Abidov M, Ramazanov Z, Seifulla R, Grachev S, 2010. The effects of Xanthigen in the weight management of obese premenopausal women with non-alcoholic fatty liver disease and normal liver fat. *Diabetes Obes Metab.* 12(1):72-81.
- Acosta E, 2009. Bioavailability of nanoparticles in nutrient and nutraceutical delivery. *Current Opinion in Colloid & Interface Science.* 14(1):3-15.
- Aniesrani DD, Thangavel K, Natarajan N, Kasthuri R, and Kailappan R, 2015. Microencapsulation of Turmeric Oleoresin by Spray Drying and In Vitro Release Studies of Microcapsules. *Journal of Food Process Engineering.* 38(1):37-48.
- Anton N & Vandamme TF, 2009. The universality of low-energy nano-emulsification. *Int J Pharm.* 377(1-2):142-7.
- Ax K, Schubert H, Briviba K, Rechkemmer G, Tevini M, 2001. Oil-in-water emulsions as carriers of bioavailable carotenoids. In: *PARTEC 2001, Nuremberg, 27-29.*
- Bae EK & Lee SJ, 2008. Microencapsulation of avocado oil by spray drying using whey protein and maltodextrin. *J Microencapsul.* 25(8):549-60.
- Bayram OA, Bayram M, Tekin AR, 2005. Spray drying of sumac flavour using sodium chloride, sucrose, glucose and starch as carriers. *Journal of Food Engineering.* 69(2):253-260.
- Brown MJ, Ferruzzi MG, Nguyen ML, Cooper DA, Eldridge AL, Schwartz SJ, White WS, 2004. Carotenoid bioavailability is higher from salads ingested with full-fat than with fat-reduced salad dressings as measured with electrochemical detection. *Am J Clin Nutr.* 80(2):396-403.

- Bruschi ML, Cardoso MLC, Lucchesi MB, & Gremião MPD, 2003. Gelatin microparticles containing propolis obtained by spray-drying technique: preparation and characterization. *International Journal of Pharmaceutics*. 264:45-55.
- Carranco Járegui ME, Calvo Carrillo Mde L, Romo FP, 2011. Carotenoids and their antioxidant function: a review. *Archivos latinoamericanos de nutrición*. 61(3):233-241. [Article in Spanish]
- CFR (2015). CFR- Code of Federal Regulations Title 21, Sec. 172.840 Polysorbate 80. Revised as of April 1, 2015. U.S. Food and Drug Administration. Silver Spring, MD.
- Chang YH, McLandsborough L, and McClements DJ, 2013. Physicochemical properties and antimicrobial efficacy of carvacrol nanoemulsions formed by spontaneous emulsification. *Journal of Agricultural and Food Chemistry*. 61(37):8906-8913.
- Chang YH & McClements DJ, 2014. Optimization of orange oil nanoemulsion formation by isothermal low-energy methods: influence of the oil phase, surfactant, and temperature. *J Agric Food Chem*. 62(10):2306-12.
- Chen XD & Mujumdar AS, 2008. *Drying Technologies in Food Processing*. Wiley-Blackwell. Hoboken, NJ.
- Chen Q, McGillivray D, Wen JY, Zhong F, Queka SY, 2013. Co-encapsulation of fish oil with phytosterol esters and limonene by milk proteins. *Journal of Food Engineering*. 117(4):505-512.
- Colle IJP, Buggenhout SV, Lemmens L, Van Loey AM, Hendrickx ME, 2012. The type and quantity of lipids present during digestion influence the in vitro bioaccessibility of lycopene from raw tomato pulp. *Food Research International*. 45(1):250-255.

- Drusch S & Berg S, 2008. Extractable oil in microcapsules prepared by spray-drying: localisation, determination and impact on oxidation stability. *Food Chemistry*. 109(1):17-24.
- Fang ZX & Bhandari B, 2010. Encapsulation of polyphenols – a review, *Trends in Food Science & Technology*. 21(10):510-523.
- Faria AF, Mignone RA, Montenegro MA, Mercadante AZ, and Borsarelli CD, 2010. Characterization and Singlet Oxygen Quenching Capacity of Spray-Dried Microcapsules of Edible Biopolymers Containing Antioxidant Molecules. *Journal of Agricultural and Food Chemistry*. 58(13):8004-8011.
- Flanagan J & Singh H, 2006. Microemulsions: A Potential Delivery System for Bioactives in Food. *Critical Reviews in Food Science and Nutrition*. 46(3):221-237.
- Forgiarini A, Esquena J, González C and Solans C, 2001. Formation of Nano-emulsions by Low-Energy Emulsification Methods at Constant Temperature. *Langmuir*. 17(7):2076-2083.
- Gallardo G, Guida L, Martínez V, López MC, Bernhardt D, Blasco R, Pedroza-Islasc R, Hermida LG, 2013. Microencapsulation of linseed oil by spray drying for functional food application. *Food Research International*. 52(2):473-482.
- Gallo L, Llabot JM, Allemandia D, Bucalab V, Piña J, 2011. Influence of spray-drying operating conditions on *Rhamnus purshiana* (Cáscara sagrada) extract powder physical properties. *Powder Technology*. 208(1):205-214.
- Gammone MA & D'Orazio N, 2015. Anti-obesity activity of the marine carotenoid fucoxanthin. *Marine Drugs*. 13(4):2196-2214.
- Garti N & McClements DJ, 2012. *Encapsulation Technologies and Delivery Systems for Food Ingredients and Nutraceuticals*, 1st Edition. Woodhead Publishing Ltd., Cambridge, UK.

- Gharsallaoui A, Roudaut G, Chambin O, Voilley A, Saurel R, 2007. Applications of spray-drying in microencapsulation of food ingredients: An overview. *Food Research International*. 40(9):1107-1121.
- Gonnet M, Lethuaut L, Boury F, 2010. New trends in encapsulation of liposoluble vitamins. *J Control Release*. 146(3):276-290.
- Goula AM & Adamopoulos KG, 2012. A New Technique for Spray-Dried Encapsulation of Lycopene. *Drying Technology*. 30(6):641-652.
- GRAS Substances (1975). GRAS Substances (SCOGS) Database. Select Committee on GRAS Substances (SCOGS) Opinion: Gelatin. Report Number: 58. Last Updated: 04/23/2013. U.S. Food and Drug Administration. Silver Spring, MD.
- Grootveld M, Silwood CJ, Addis P, Claxson A, Serra BB and Viana M, 2001. Health effects of oxidized heated oils. *Foodservice Research International*. 13:41-55.
- Guadarrama-Lezama AY, Dorantes-Alvarez L, Jaramillo-Flores ME, Pérez-Alonso C, Niranjana K, Gutiérrez-López GF, Alamilla-Beltrán L, 2012. Preparation and characterization of non-aqueous extracts from chilli (*Capsicum annum L.*) and their microencapsulates obtained by spray-drying. *Journal of Food Engineering*. 112(1-2):29-37.
- Gulotta A, Saberi AH, Nicoli MC, and McClements DJ, 2014. Nanoemulsion-Based Delivery Systems for Polyunsaturated (ω -3) Oils: Formation Using a Spontaneous Emulsification Method. *Journal of Agricultural and Food Chemistry*. 62(7):1720-1725.
- Halwanil M, Yebiol B, Suntres ZE, Alipour M, Azghani AO, Omril A, 2008. Coencapsulation of gallium with gentamicin in liposomes enhances antimicrobial activity of gentamicin against *Pseudomonas aeruginosa*. *Journal of Antimicrobial Chemotherapy* 62(6):1291-1297.

- Hanani ZAN, Roos YH, Kerry JP, 2014. Use and application of gelatin as potential biodegradable packaging materials for food products. *International Journal of Biological Macromolecules*. 71:94-102.
- Hanus MJ & Langrish TAG, 2007. Re-entrainment of wall deposits from a laboratory-scale spray dryer. *Asia-Pacific Jnl of Chem. Eng.* 2:90-107.
- Hashimoto T, Ozaki Y, Mizuno M, Yoshida M, Nishitani Y, Azuma T, Komoto A, Maoka T, Tanino A and Kanazawa K, 2012. Pharmacokinetics of fucoxanthinol in human plasma after the oral administration of kombu extract. *British Journal of Nutrition*, 107:1566-1569.
- Hatanaka J, Chikamori H, Sato H, Uchida S, Debari K, Onoue S, Yamada S, 2010. Physicochemical and pharmacological characterization of α -tocopherol-loaded nano-emulsion system. *International Journal of Pharmaceutics*. 396(1-2):188-193.
- Hegde RR, Verma A, and Ghosh A, 2013. Microemulsion: New Insights into the Ocular Drug Delivery. *ISRN Pharmaceutics*. Article ID 826798, 11 pages.
- Hogan SA, McNamee BF, O'Riordan ED, and O'sullivan M, 2001. Microencapsulating Properties of Sodium Caseinate. *Journal of Agricultural and Food Chemistry*. 49(4):1934-1938.
- Hojjati M, Razavi SH, Rezaei K, Gilani K, 2011. Spray drying microencapsulation of natural canthaxantin using soluble soybean polysaccharide as a carrier. *Food Science and Biotechnology*. 20(1):63-69.
- Hojjati M, Razavi SH, Rezaei K, Gilani K, 2014. Stabilization of canthaxanthin produced by *Dietzia natronolimnaea* HS-1 with spray drying microencapsulation. *J Food Sci Technol*. 51(9):2134-40.

- Hosokawa M, Kudo M, Maeda H, Kohno H, Tanaka T, Miyashita K, 2004. Fucoxanthin induces apoptosis and enhances the antiproliferative effect of the PPARgamma ligand, troglitazone, on colon cancer cells. *Biochim Biophys Acta*. 1675(1-3):113-119.
- Huang Q, Yu H, Ru Q, 2010. Bioavailability and Delivery of Nutraceuticals Using Nanotechnology. *Journal of Food Science*. 75(1):R50-R57.
- Israelachvili JN, 2011. *Intermolecular and Surface Forces*, third Edition. Academic Press. London, UK.
- Jafari SM, Assadpoor E, He YH, Bhandari B, 2008. Encapsulation efficiency of food flavours and oils during spray drying. *Drying Technology*. 26(7):816-835.
- Kang HJ & Connolly E, 2006. Method of improving immune function in mammals using lactobacillus strains with certain lipids. Patent: US20060251634 A1.
- Kapoor D & Dhawan S, 2013. *Biocompatible Nanomaterials for Targeted and Controlled Delivery of Biomacromolecules*. ASME. Momentum Press, New York. (Chapter 5 Biocompatible and biodegradable nanomaterials)
- Karim AA & Bhat R, 2008. Gelatin alternatives for the food industry: recent developments, challenges and prospects. *Trends in Food Science & Technology*. 19(12):644-656.
- Kasapisa S, Sablani SS, 2005. A fundamental approach for the estimation of the mechanical glass transition temperature in gelatin. *International Journal of Biological Macromolecules*. 36(1-2):71-78.
- Kemp IC, Wadley R, Hartwig T, Cocchini U, See-Toh Y, Gorringer L, Fordham K, Ricard F, 2013. Experimental Study of Spray Drying and Atomization with a Two-Fluid Nozzle to Produce Inhalable Particles. *Drying Technology*. 31(8):930-941.

- Kha TC, Nguyen MH, Roach PD, Stathopoulos CE, 2013. Effects of Gac aril microwave processing conditions on oil extraction efficiency, and β -carotene and lycopene contents. *Journal of Food Engineering*. 117(4): 486-491.
- Kha TC, Nguyen MH, Roach PD, Stathopoulos CE, 2014a. Microencapsulation of Gac Oil by Spray Drying: Optimization of Wall Material Concentration and Oil Load Using Response Surface Methodology. *Drying Technology*. 32(4): 385-397.
- Kha TC, Nguyen MH, Roach PD, Stathopoulos CE, 2014b. Microencapsulation of Gac oil: Optimisation of spray drying conditions using response surface methodology. *Powder Technology*. 264:298-309.
- Kim DM, Hyun SS, Yun P, Lee CH, Byun SY, 2012. Identification of an emulsifier and conditions for preparing stable nanoemulsions containing the antioxidant astaxanthin. *International Journal of Cosmetic Science*. 34(1):64-73.
- Klaypradit W & Huang YW, 2008. Fish oil encapsulation with chitosan using ultrasonic atomizer. *LWT - Food Science and Technology*. 41(6):1133-1139.
- Komaiko J & McClements DJ, 2014. Optimization of isothermal low-energy nanoemulsion formation: hydrocarbon oil, non-ionic surfactant, and water systems. *J Colloid Interface Sci*. 425:59-66.
- Kotake-Nara E, Kushiro M, Zhang H, Sugawara T, Miyashita K, Nagao A, 2001. Carotenoids affect proliferation of human prostate cancer cells. *J Nutr*. 131(12):3303-3306.
- Kotake-Nara E, Terasaki M, Nagao A, 2005. Characterization of apoptosis induced by fucoxanthin in human promyelocytic leukemia cells. *Biosci Biotechnol Biochem*. 69(1):224-227.

- Kotake-Nara, E., Sugawara, T. and Nagao, A, 2005. Antiproliferative effect of neoxanthin and fucoxanthin on cultured cells. *Fisheries Science*, 71: 459–461.
- Kuang P, Zhang H, Bajaj PR, Yuan Q, Tang J, Chen S, Sablani SS, 2015. Physicochemical properties and storage stability of lutein microcapsules prepared with maltodextrins and sucrose by spray drying. *Journal of Food Science*. 80(2):E359-69.
- Lamaallam S, Bataller H, Dicharry C, Lachaise J, 2005. Formation and stability of miniemulsions produced by dispersion of water/oil/surfactants concentrates in a large amount of water. *Colloids and Surfaces A: Physicochemical and Engineering Aspects*. 270–271:44-51.
- Lemmens L, Colle I, Buggenhout SV, Palmero P, Loey AV, Hendrickx M, 2014. Carotenoid bioaccessibility in fruit- and vegetable-based food products as affected by product (micro)structural characteristics and the presence of lipids: A review. *Trends in Food Science & Technology*. 38(2):125-135.
- Li DX, Oh YK, Lim SJ, Kim JO, Yang HJ, Sung JH, Yong CS, Choi HG, 2008. Novel gelatin microcapsule with bioavailability enhancement of ibuprofen using spray-drying technique. *Int J Pharm*. 355(1-2):277-84.
- Liang R, Huang QR, Ma JG, Shoemaker CF, Zhong F, 2013. Effect of relative humidity on the store stability of spray-dried beta-carotene nanoemulsions. *Food Hydrocolloids*. 33(2):225-233.
- Lipkie TE, De Moura FF, Zhao ZY, Albertsen MC, Che P, Glassman K, an. Ferruzzi MG, 2013. Bioaccessibility of Carotenoids from Transgenic Provitamin A Biofortified Sorghum. *Journal of Agricultural and Food Chemistry*. 61(24):5764-5771.

- Loksuwan J, 2007. Characteristics of microencapsulated β -carotene formed by spray drying with modified tapioca starch, native tapioca starch and maltodextrin, *Food Hydrocolloids*. 21(5-6):928-935.
- López-Montilla JC, Herrera-Morales PE, Pandey S & Shah DO, 2002. Spontaneous Emulsification: Mechanisms, Physicochemical Aspects, Modeling, and Applications. *Journal of Dispersion Science and Technology*. 23(1-3):219-268.
- Lucas L, Russell A, Keast R, 2011. Molecular mechanisms of inflammation. Anti-inflammatory benefits of virgin olive oil and the phenolic compound oleocanthal. *Curr Pharm Des*. 17(8):754-68.
- Ma JKH & Hadzija B, 2013. *Basic Physical Pharmacy*. Jones & Bartlett Publishers. Table 13-5. Required HLB values for the oil phase materials used in O/W and W/O emulsions.
- Maeda H, Hosokawa M, Sashima T, Funayama K, Miyashita K, 2005. Fucoxanthin from edible seaweed, *Undaria pinnatifida*, shows antiobesity effect through UCP1 expression in white adipose tissues. *Biochem Biophys Res Commun*. 332(2):392-7.
- Maeda H, Hosokawa M, Sashima T, Miyashita K, 2007a. Dietary combination of fucoxanthin and fish oil attenuates the weight gain of white adipose tissue and decreases blood glucose in obese/diabetic KK-Ay mice. *J Agric Food Chem*. 55(19):7701-6.
- Maeda H, Hosokawa M, Sashima T, Funayama K, Miyashita K, 2007b. Effect of Medium-chain Triacylglycerols on Anti-obesity Effect of Fucoxanthin. *Journal of Oleo Science*. 56(12):615-621.
- Maeda H, Tsukui T, Sashima T, Hosokawa M, Miyashita K, 2008. Seaweed carotenoid, fucoxanthin, as a multi-functional nutrient. *Asia Pac J Clin Nutr*. 17(Suppl 1):196-9.

- Maeda H, Hosokawa M, Sashima T, Murakami-Funayama K, Miyashita K, 2009. Anti-obesity and anti-diabetic effects of fucoxanthin on diet-induced obesity conditions in a murine model. *Mol Med Rep.* 2(6):897-902.
- Maeda H, 2015. Nutraceutical effects of fucoxanthin for obesity and diabetes therapy: a review. *J Oleo Sci.* 64(2):125-32.
- Mayer S, Weiss J, McClements DJ, 2013. Vitamin E-enriched nanoemulsions formed by emulsion phase inversion: factors influencing droplet size and stability. *J Colloid Interface Sci.* 402:122-30.
- McClements DJ, Decker EA, Weiss J, 2007. Emulsion-based delivery systems for lipophilic bioactive components. *J Food Sci.* 72(8):R109-124.
- McClements DJ & Rao J, 2011. Food-grade nanoemulsions: formulation, fabrication, properties, performance, biological fate, and potential toxicity. *Crit Rev Food Sci Nutr.* 51(4):285-330.
- McClements DJ, 2014. Nanoparticle- and Microparticle-based Delivery Systems: Encapsulation, Protection and Release of Active Compounds. CRC Press. Boca Raton, Florida.
- Mercadante AZ, 2008. Carotenoids in foods: sources and stability during processing and storage. In: Carmen S (ed.) *Food colorants: chemical and functional properties.* Boca Raton, CRC Press. 213-240.
- Nagao A, Kotake-Nara E, Hase M, 2013. Effects of Fats and Oils on the Bioaccessibility of Carotenoids and Vitamin E in Vegetables. *Bioscience, Biotechnology, and Biochemistry.* 77(5):1055-1060.
- Nazzaro F, Orlando P, Fratianni F, Coppola R, 2012. Microencapsulation in food science and biotechnology. *Current Opinion in Biotechnology.* 23(2):182-186.

- Nedovic V, Kalusevic A, Manojlovic V, Levic S, Bugarski B, 2011. An overview of encapsulation technologies for food applications. *Procedia Food Science*, Volume 1:1806-1815.
- Nesterenko A, Alric I, Silvestre F, Durrieu V, 2013. Vegetable proteins in microencapsulation: A review of recent interventions and their effectiveness. *Industrial Crops and Products*. 42:469-479.
- Ostertag F, Weiss J, McClements DJ, 2012. Low-energy formation of edible nanoemulsions: factors influencing droplet size produced by emulsion phase inversion. *J Colloid Interface Sci*. 388(1):95-102.
- Paramita V, Iida K, Yoshii H, Furuta T, 2010. Effect of feed liquid temperature on the structural morphologies of D-limonene microencapsulated powder and its preservation. *Journal of Food Science*. 75 (1):E39-E45.
- Parker RS, 1997. Bioavailability of carotenoids. *Eur J Clin Nutr* 51:86–90.
- Paudel A, Worku ZA, Meeus J, Guns S, Van den Mooter G, 2013. Manufacturing of solid dispersions of poorly water soluble drugs by spray drying: Formulation and process considerations. *International Journal of Pharmaceutics*. 453(1):253-284.
- Peng J, Yuan JP, Wu CF, and Wang JH, 2011. Fucoxanthin, a Marine Carotenoid Present in Brown Seaweeds and Diatoms: Metabolism and Bioactivities Relevant to Human Health. *Mar Drugs*. 9(10): 1806–1828.
- Pérez-Alonso C, Cruz-Olivares J, Barrera-Pichardo JF, Rodríguez-Huezob ME, Bález-González JG, Vernon-Carter EJ, 2008. DSC thermo-oxidative stability of red chili oleoresin microencapsulated in blended biopolymers matrices. *Journal of Food Engineering*. 85(4):613-624.

- Pignatello R, 2011. Biomaterials Applications for Nanomedicine. InTech. Rijeka, Croatia.
(Chapter 2 Collagen- vs. Gelatine-Based Biomaterials and Their Biocompatibility: Review and Perspectives by Gorgieva S & Kokol V)
- Prabhu HR, 2000. Lipid peroxidation in culinary oils subjected to thermal stress. *Indian J Clin Biochem.* 15(1):1-5.
- Prasad K, 2009. Flaxseed and cardiovascular health. *J Cardiovasc Pharmacol.* 54(5):369-77.
- Pu JN, Bankston JD, Sathivel S, 2011. Developing microencapsulated flaxseed oil containing shrimp (*Litopenaeus setiferus*) astaxanthin using a pilot scale spray dryer. *Biosystems Engineering.* 108(2):121-132.
- Qian C & McClements DJ, 2011. Formation of nanoemulsions stabilized by model food-grade emulsifiers using high-pressure homogenization: Factors affecting particle size. *Food Hydrocolloids.* 25(5):1000-1008.
- Qian C, Decker EA, Xiao H, McClements DJ, 2012. Physical and chemical stability of [beta]-carotene-enriched nanoemulsions: Influence of pH, ionic strength, temperature, and emulsifier type. *Food Chemistry.* 132(3):1221-1229.
- Rao AV & Rao LG, 2007. Carotenoids and human health. *Pharmacological Research.* 55(3):207-16.
- Rascón MP, Beristain CI, García HS, Salgado MA, 2011. Carotenoid retention and storage stability of spray-dried encapsulated paprika oleoresin using gum Arabic and Soy protein isolate as wall materials. 44(2):549-557.
- Rhein LD, Schlossman M, O'Lenick A, and Somasundaran P, 2006. Surfactants in Personal Care Products and Decorative Cosmetics, 3rd Edition. CRC Press, New York. Chapter 8.

Emulsions and Their Behavior. Somasundaran P, Farinato R, Mehta SC, Wines TH, and Garti N.

Rocha GA, Fávoro-Trindade CS, Grosso CRF, 2012. Microencapsulation of lycopene by spray drying: Characterization, stability and application of microcapsules, Food and Bioproducts Processing. 90(1):37-42.

Rodríguez-Huezo ME, Pedroza-Islas R, Prado-Barragán LA, Beristain CI and Vernon-Carter EJ, 2004. Microencapsulation by Spray Drying of Multiple Emulsions Containing Carotenoids. Journal of Food Science. 69:351–359.

Rosenberg M, Kopelman IJ, Talmon Y, 1985. A scanning electron microscopy study of microencapsulation. Journal of Food Science. 50(1):139-144.

Ruiz-Canela M & Martínez-González MA, 2011. Olive oil in the primary prevention of cardiovascular disease. Maturitas. 68(3):245-50.

Saberi AH, Fang Y, McClements DJ, 2013a. Fabrication of vitamin E-enriched nanoemulsions: factors affecting particle size using spontaneous emulsification. J Colloid Interface Sci. 391:95-102.

Saberi AH, Fang Y, McClements DJ, 2013b. Fabrication of vitamin E-enriched nanoemulsions by spontaneous emulsification: Effect of propylene glycol and ethanol on formation, stability, and properties. Food Research International. 54(1):812-820.

Saberi AH, Fang Y, McClements DJ, 2013c. Effect of glycerol on formation, stability, and properties of vitamin-E enriched nanoemulsions produced using spontaneous emulsification. J Colloid Interface Sci. 411:105-13.

- Saberi AH, Fang Y, McClements DJ, 2014. Stabilization of vitamin E-enriched mini-emulsions: Influence of organic and aqueous phase compositions. *Colloids and Surfaces A: Physicochemical and Engineering Aspects*. 449(1):65-73.
- Sachindra NM, Sato E, Maeda H, Hosokawa M, Niwano Y, Kohno M, Miyashita K, 2007. Radical scavenging and singlet oxygen quenching activity of marine carotenoid fucoxanthin and its metabolites. *J Agric Food Chem*. 55(21):8516-22.
- Santana AA, Kurozawa LE, de Oliveira RA, Park KJ, 2013a. Influence of Process Conditions on the Physicochemical Properties of Pequi Powder Produced by Spray Drying. *Drying Technology*. 31(7):825-836.
- Santana RC, Perrechil FA, Cunha RL, 2013b. High- and Low-Energy Emulsifications for Food Applications: A Focus on Process Parameters. *Food Engineering Reviews*. 5(2):107-122.
- Santos DT & Meireles MAA, 2010. Carotenoid Pigments Encapsulation: Fundamentals, Techniques and Recent Trends. *The Open Chemical Engineering Journal*. 4: 42-50.
- Shen Q & Quek SY, 2014. Microencapsulation of astaxanthin with blends of milk protein and fiber by spray drying. *Journal of Food Engineering*. 123:165-171.
- Sheu TY & Rosenberg M, 1998. Microstructure of microcapsules consisting of whey proteins and carbohydrates. *Journal of Food Science*. 63(3):491-494.
- Shu B, Yu WL, Zhao YP, Liu XY, 2006. Study on microencapsulation of lycopene by spray-drying, *Journal of Food Engineering*. 76(4):664-669.
- Sluijs I, Cadier E, Beulens JW, van der A DL, Spijkerman AMW, van der Schouw YT, 2015. Dietary intake of carotenoids and risk of type 2 diabetes. *Nutrition, Metabolism and Cardiovascular Diseases*. 25(4):376-381.

- Solè I, Pey CM, Maestro A, González C, Porrás M, Solans C, Gutiérrez JM, 2010. Nano-emulsions prepared by the phase inversion composition method: preparation variables and scale up. *J Colloid Interface Sci.* 344(2):417-23.
- Song D, Zhang W, Gupta RK, Melby EG, 2011. Role of operating conditions in determining droplet size and viscosity of tackifier emulsions formed via phase inversion. *AIChE Journal.* 57(1):96-106.
- Soottitawat A, Yoshii H, Furuta T, Ohkawara M and Linko P, 2003. Microencapsulation by Spray Drying: Influence of Emulsion Size on the Retention of Volatile Compounds. *Journal of Food Science.* 68(7):2256-2262.
- Su YL, Fu ZY, Zhang JY, Wang WM, Wang H, Wang YC, Zhang QJ, 2008. Microencapsulation of Radix salvia miltiorrhiza nanoparticles by spray-drying. *Powder Technology.* 184(1):114-121.
- Talegaonkar S, Azeem A, Ahmad FJ, Khar RK, Pathan SA, Khan ZI, 2008. Microemulsions: a novel approach to enhanced drug delivery. *Recent Pat Drug Deliv Formul.* 2(3):238-257.
- Tanaka T, Shnimizu M, Moriwaki H, 2012. Cancer chemoprevention by carotenoids. *Molecules.* 17(3):3202-3242.
- Tantra R, Schulze P, Quincey P, 2010. Effect of nanoparticle concentration on zeta-potential measurement results and reproducibility. *Particuology.* 8(3):279-285.
- Tonon RV, Brabet C, Hubinger MD, 2008. Influence of process conditions on the physicochemical properties of açai (*Euterpe oleraceae* Mart.) powder produced by spray drying. *J. Food Eng.* 88(3):411-418.

- Tonon RV, Grosso CRF, Hubinger MD, 2011. Influence of emulsion composition and inlet air temperature on the microencapsulation of flaxseed oil by spray drying. *Food Research International*. 44(1):282-289.
- Tontul I & Topuz A, 2013. Mixture Design Approach in Wall Material Selection and Evaluation of Ultrasonic Emulsification in Flaxseed Oil Microencapsulation. *Drying Technolog*. 31(12):1362-1373.
- Truong V, Bhandari BR, Howes T, 2005. Optimization of co-current spray drying process of sugar-rich foods. Part I—moisture and glass transition temperature profile during drying. *J. Food Eng*. 71(1):55-65.
- Turchiulia C, Jimenez Munguiad MT, Hernandez Sancheza M, Cortes Ferrea H, Dumoulin E, 2014. Use of different supports for oil encapsulation in powder by spray drying. *Powder Technology*. 255:103-108.
- Vaio CD, Graziani G, Gaspari A, Scaglione G, Nocerino S, Ritieni A, 2010. Essential oils content and antioxidant properties of peel ethanol extract in 18 lemon cultivars. *Scientia Horticulturae*. 126(1):50-55.
- Verma A & Singh SV, 2015. Spray drying of fruit and vegetable juices--a review. *Crit Rev Food Sci Nutr*. 55(5):701-19.
- Vos P, Faas MM, Spasojevic M, Sikkema J, 2010. Encapsulation for preservation of functionality and targeted delivery of bioactive food components, *International Dairy Journal*, 20(4):292-302.
- Wang LJ, Dong JF, Chen J, Eastoe J, Li XF, 2009. Design and optimization of a new self-nanoemulsifying drug delivery system. *Journal of Colloid and Interface Science*. 330(2):443-448.

- Wang YF, Ye H, Zhou CH, Lv FX, Bie XM, Lu ZX, 2012. Study on the spray-drying encapsulation of lutein in the porous starch and gelatin mixture. *European Food Research and Technology*. 234(1):157-163.
- Yang Y, Marshall-Breton C, Leser ME, Sher AA, McClements DJ, 2012. Fabrication of ultrafine edible emulsions: Comparison of high-energy and low-energy homogenization methods. *Food Hydrocolloids*. 29(2):398-406.
- Zhang H, Tang YB, Zhang Y, Zhang SF, Qu J, Wang X, Kong R, Han CH, and Liu ZQ, 2015. Fucoxanthin: A Promising Medicinal and Nutritional Ingredient. *Evidence-Based Complementary and Alternative Medicine*. Volume 2015, Article ID 723515, 10 pages.
- Zuidam NJ & Nedovic V, 2010. *Encapsulation Technologies for Active Food Ingredients and Food Processing*. Springer-Verlag New York.

Chapter 4

Monitoring moisture content of spray dried powders using capacitance sensor

Keywords

Moisture content, Capacitance sensor, Spray drying

Abstract

The moisture content (MC) of spray dried powders is of great importance to define the product quality, since it is directly related to drying conditions and it affects particle deposition and yield. Several methods such as oven drying, near infrared spectroscopy (NIR) have been developed to measure MC offline. However, these methods are not appropriate for spray drying where an online (real-time) assessment of MC is required. The objective of this study was to develop a sensor for measuring moisture content of a moving stream of spray dried powders. A capacitance sensor was built for this purpose using pairs of copper plate electrodes attached to the perimeter of the spray dryer product collection vessel. The plates formed capacitors that were sensitive to changes in dielectric properties of the material within the collection vessel, which in turn were related to MC. Each electrode was connected to a capacitance-to-voltage transducer, the output of which was sampled using a commercial data acquisition system. The amplitude of the sensor output signal was calculated using software LabVIEW and correlated with MC. The self-built system was tested in two modes: a) an offline (non-moving sample) mode in which a mass-based MC prediction model was built to validate the capability of the sensor to measure variation in MC; and b) an online (moving sample) mode to measure MC of sample moving through the sensor enclosure. Tests were made on spray dried gelatin powders ranging in moisture content of

5% to 50% (w.b.). Results indicated a high correlation between sensor output and moisture content. The capacitance sensor also showed the ability to characterize the distribution of MC (permittivity) within the sensor enclosure, which could reflect spatial variation in deposition of dried powders during spray drying. Overall, the capacitance sensor system was shown to measure MC for online sampling with acceptable accuracy, and can be applied in quality control applications for continuous spray drying processes.

4.1 Introduction

Moisture content (MC) analysis is critical for spray drying process since it greatly influences the physical properties (T_g) and the quality (yield, deposition) of the spray dried product. Several methods (oven drying, NIR) have been developed to measure MC offline. However, many of them are not appropriate for spray drying where an online (real-time) assessment of MC is required. For example, the oven drying method is a traditional way of measuring MC. It is thermogravimetric based and very accurate. But it is also destructive and time consuming. Typically it takes 24 hours to fully dry a sample. In a spray dryer system, one must turn off the machine and collect samples to test the MC, which makes the whole process time-consuming. The near infrared radiation (NIR) method is also considered an effective way to detect MC in the food, chemical and pharmaceutical industries as O-H bond (hydroxyl bonds) of water shows significant absorptions at NIR wavelength (Adedipe & Dawson-Andoh, 2008; Brink et al., 2010). However, it is a spot and surface measurement, so a single measurement (measured sample) might not be representative of the whole population inside the measuring vessel. In addition, it is imprecise in measuring MC during spray drying process when deposits are formed on the wall, the NIR measures the MC for deposits rather than spray dried powders moving inside the vessel. The goal of this study was to develop a sensor for measuring moisture content of a moving stream of spray dried powders. It is desired to employ non-contact methods that have advantages for dynamic MC determination (Table 4.1).

Table 4.1 Comparison of various MC measurement methods

	Oven drying	NIR	Capacitance Sensor
Advantage	Accurate	Non-contact	Online
Disadvantage	Time consuming	Surface, Spot	Mass dependency

Based on Gauss's law, for dielectric material like gelatin, its dielectric property can be greatly affected by the presence of water, so any permittivity change/variation within the capacitance sensor's measuring/enclosed area should be observable as a capacitance change, and therefore as a change in its output voltage (Johana et al., 2011). A capacitance sensor was built for this purpose using pairs of copper plate electrodes attached to the perimeter of the spray dryer measuring vessel (e.g. collection vessel, cyclone, side outlet tube). The plates formed capacitors that were sensitive to changes in dielectric properties (permittivity) of the material between two electrodes, which in turn is greatly affected by the presence of water. The formed capacitors can measure variation in dielectric properties of a material occupying the enclosed place, thereby sensing variation in MC. The approach relies on observing the change in capacitance between two electrodes as the material between them varies. The permittivity of water ($\epsilon = 80$) is significantly larger than air ($\epsilon = 1$) and gelatin ($\epsilon = 6-7$ or $20-30$). Based on Gauss's law, any permittivity change within the ECT sensor's measuring area should be observable as a capacitance change, and therefore as a change in its output voltage.

4.2 Capacitance sensing system configuration

A capacitance sensor system generally consists of capacitance sensors, signal processing and a data acquisition system/circuit, and a computer to collect data and control the experiment (for image reconstruction and display) (Pan, 2014). Copper plate electrodes were attached to the

perimeter of the measuring cylinder, either on the production collection vessel, cyclone or the side outlet tube for different testing modes. A waveform generator (Keysight 33621A, Agilent Technologies, Santa Rosa, CA) was used to generate input signal (500 or 800 kHz, 10 vpp amplitude sine wave) for capacitance measurement. Each electrode was connected to a capacitance-to-voltage transducer so that the output signal could be collected using a commercial data acquisition device (NI 6210, National Instruments, Austin, TX) and analyzed by data processing software LabVIEW (National Instruments, Austin, TX).

As most data acquisition systems available can measure voltages quickly and inexpensively, it was necessary to develop a means to convert the input capacitance signal to a voltage signal so that could be sampled. Therefore, each electrode was connected to a capacitance-to-voltage transducer so that the amplitude of the sensor output signal (high frequency sine wave) could be collected using a commercial data acquisition device (NI 6210, National Instruments, Austin, TX). This device allowed sampling outputs at 2 MHz. Data processing software LabVIEW (National Instruments, Austin, TX) was used to determine the amplitude of the high frequency sensor output signal and correlated it with MC.

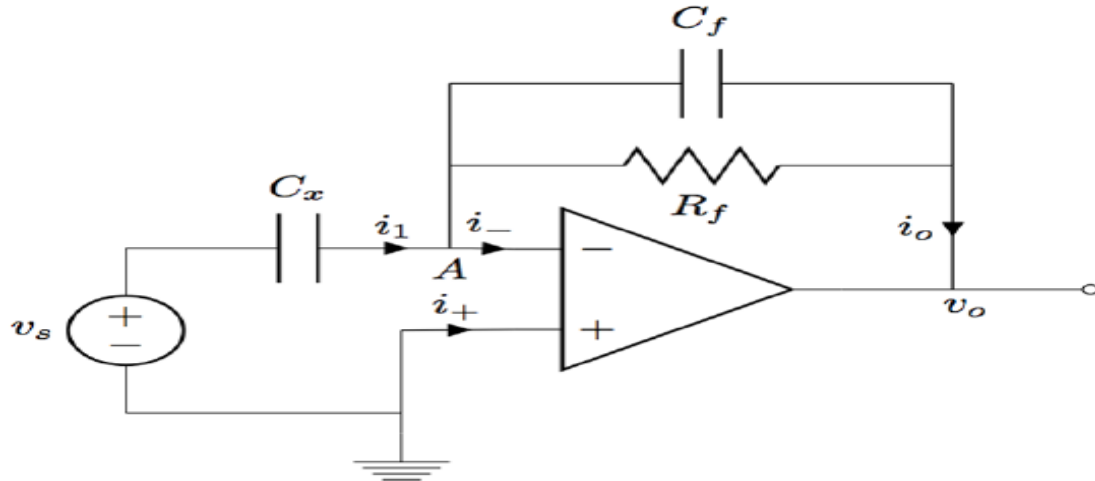


Fig. 4.1 Schematic diagram of the capacitance-to-voltage transducer circuit (AD844 Op-amp, sample capacitance (C_x), feedback capacitor (C_f), feedback resistor (R_f), input voltage (V_s), output voltage (V_o), adapted from Pan (2014)).

Fig. 4.1 shows the schematic diagram of the capacitance-to-voltage conversion circuit. It consists of an Op-amp (AD844, Analog Devices, Norwood, MA), a feedback resistor (R_f) and feedback capacitor (C_f) and a power supply (E3630A, Keysight (Agilent) Technologies, Santa Rosa, CA) to charge the Op-amp. C_x is the sample capacitance resulting from the material within the sensor enclosure between any pair of copper plate. For such a transducer, the input excitation voltage (V_s) is a sine wave, when $|j\omega C_f R_f| \gg 1$, the amplitude of the output voltage V_o can be proportional to the ratio of the sample capacitance C_x to the feedback capacitance C_f ($V_o \approx -C_x/C_f \cdot V_s$). So C_f was selected as 10 pf to be necessarily small to sufficiently amplify the output signal V_o . R_f should be selected as large as possible but limited by the cut-off frequency. In this study, R_f was set as 680 Ω .

Multiple strategies were applied to stabilize power variations and minimize noise in the system. All output circuits were fixed on a printed circuit board (PCB) to eliminate undesirable variation resulting from non-constant stray interaction between the individual elements. The length of lead

wires between test circuits and electrodes was also fixed. All wires for signals were shielded to eliminate stray capacitance between adjacent conductors. With the protection of the copper shield, the response indicated the grounded shield successfully protected the circuit signal from outside disturbances, which increased the sensor robustness. To obtain capacitances between electrodes, each electrode should be able to connect either to the source signal or to the capacitance-to-voltage transducer to form a measurement pair. This function was achieved by a switching network (ADG419, Analog Devices, Norwood, MA), so that the status of each electrode could be controlled by the data acquisition system. Any undesirable signals would be led to ground so as to minimize stray capacitance in the system. A 5V regulator was used to convert the input 15 V to 5 V that supported ADG419. To avoid any instability arising from very quick changes in power levels in the circuit (due to the switching network), multiple capacitors were installed into the ECT data acquisition circuits to act as charge pumps. When the power supply for the circuits pulsed, these capacitors could provide, or absorb, current to eliminate that specific source of measuring error.

4.3 Materials and Methods

The self-built system (Fig. 4.2) was applied to a lab scale spray dryer (B-290, BÜCHI Labortechnik AG, Flawil, Switzerland) and MC measuring tests were made on spray dried gelatin powders in three different modes:

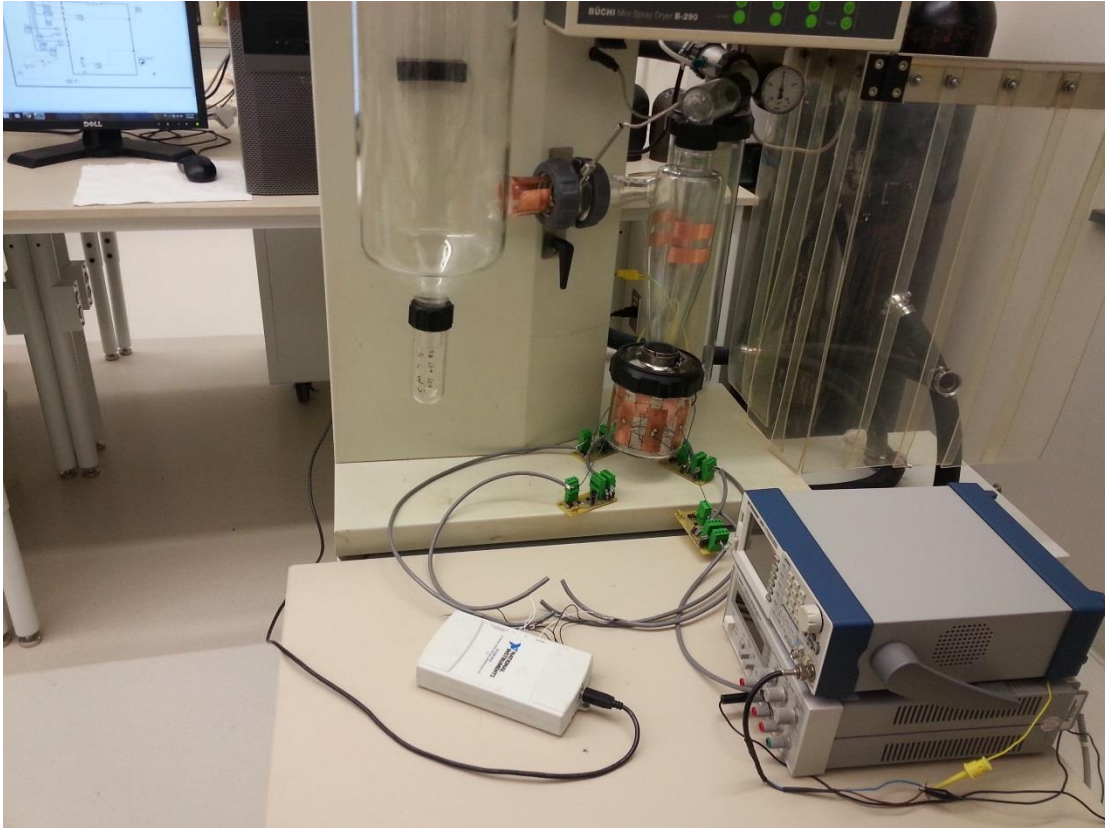


Fig. 4.2 Image showing experiment setup for MC measurement. Measuring cylinder: collection vessel for offline mode, cyclone for online mode, side outlet tube for ECT mode.

4.3.1 Offline mode (4-electrode capacitance sensing system)

Two copper plates are able to form a capacitance sensor and measure MC of a dielectric material. However, additional electrodes could provide redundancy (higher accuracy) in measurements. A 4-electrode electrical capacitance sensor system (6 combinations of electrodes pairs) was built to validate the accuracy of the sensor in static mode (Fig. 4.3), with each unique

pair of electrodes then used to generate the electric field and detect the permittivity of the test material would be available to characterize the distribution of dielectric constant of the material within the measurement enclosure. Sensor electrodes were formed from copper plates and attached at uniform intervals around the external perimeter of the product collection vessel. Each pair of sensors was connected to a capacitance-to-voltage transducer and provided an independent capacitance value (C_{12} , C_{14} , C_{23} , C_{24} , C_{34} , and C_{31}). A switching network was embedded in all electrode circuits and used to control their state of operation. The AC output of each sensor was sampled using a commercial data acquisition system (NI 6210) and the amplitude of the signal was implemented in the software LabVIEW.

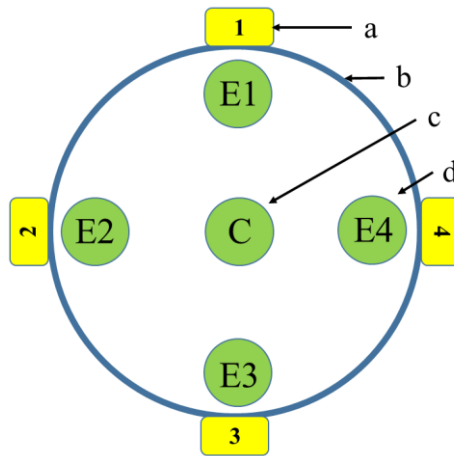


Fig. 4.3 Illustration of the offline mode. (a) Electrodes, (b) Measuring cylinder: collection vessel, (c) Center location, (d) Edge location. 4 electrodes form 6 different electrode combinations and provide 6 independent capacitance values (C_{12} , C_{14} , C_{23} , C_{24} , C_{34} , C_{31}).

Responses of the 6 different electrode combinations were collected to verify consistency in sensor output. Data was collected when the sensor was in an empty state (nothing but air in the sensing area) and a full state (the measuring area was fully occupied by a test material). To avoid unnecessary air gaps between spray dried powders, water was used as the test material. The

system noise level was evaluated by signal-to-noise ratio (SNR) values (Lu et al., 2004; Pan, 2014) with each capacitance combination (C_{12} , C_{14} , C_{23} , C_{24} , C_{34} , and C_{31}) having 500 repeats. Location test (ANOVA test) was undertaken to investigate the influence of material location on the sensor response. Sensitivity tests were undertaken to determine the minimum quantity of material (water and spray dried gelatin powder) that could be observed using the capacitance sensor. Student's t-test was used to check if a sensor reading was significantly different from the reference level at a 95% confidence level (the first observation with $P < 0.05$). Once identified, that volume of water significantly different from a background reading was defined as the system resolution, or minimum sensible amount, for test materials. The sum of 6 capacitances was used as the sensor response. For measuring MC for non-moving samples, the capacitance sensor system was used along with a commercial moisture analyzer Moisture Analyzer (MF-50, A&D, San Jose, CA) to estimate the MC of gelatin powders. A mass-based MC prediction model was built to establish a relationship between sensor output (readings) and water/gelatin quantity in order to validate the capability of the sensor. To exclude the effect of water, pre-dried gelatin powders and free water were used in the test. To explore the effect of water inside the spray dried powders, samples consist of fixed quantity of dried gelatin (10 g) and varying amounts of water was performed in the test. A mass-based MC prediction model was built to establish a relationship between sensor output and water/gelatin quantity. The input signal used in the tests was an 800 kHz sine with 20 vpp amplitude. Data were sampled using the one source/one detector mode at 1.99 MHz. Peak-to-peak amplitude was measured with 100 replications and the values were averaged.

4.3.2 Online mode (Dual frequency capacitance sensing system)

MC of static samples could be measured accurately if the weight of the bulk sample was known. However, it was impossible to measure mass or mass flow rate in a dynamic application of the capacitance sensor. A dual frequency capacitance sensor method was developed by using two input signals at two distinct excitation frequencies to remove dependency on sample mass (Fig. 4.4). According to the parallel electrode capacitance calculating method ($C = \epsilon_r \epsilon_0 A / 4\pi d$), the difference in capacitance at two frequencies can be written as $(C_1 - C_2) = (\epsilon_{r1} - \epsilon_{r2}) \epsilon_0 A / 4\pi d$. To be an effective sensor, the difference in the dielectric constant should be related to MC, and independent of other variables including sample weight and location, which could be a good indicator of the moisture present in the material. In the current study, sensor measurement was tested in series that a second excitation frequency (800 kHz) was taken after the regular measurement at 500 kHz. Readings at both 500 kHz and 800 kHz were processed in the same manner. The dual frequency output result was calculated as the average response at 800 kHz minus that at 500 kHz. The output from the sensor was a voltage signal proportional to capacitance and was read using a USB-6210 data acquisition module. The data (ECT readings) were sampled at 10 kHz and recorded using a LabVIEW program.

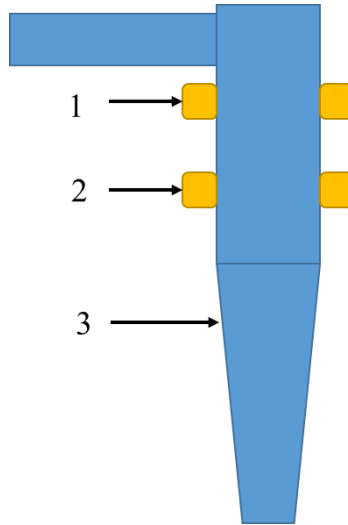


Fig. 4.4 Illustration of online mode. Sensor measurement was tested in series (a second excitation frequency after the regular one). 1. Electrode excited by 500 kHz signal, 2. Electrode excited by 800 kHz. 3. Measuring cylinder: cyclone.

4.3.3 Electric capacitance tomography (ECT) mode

The distribution of the sample's dielectric properties within the measurement enclosure can be reconstructed by tomography (ECT), the same principle applied in X-ray tomography applications. For the multiple electrode system, capacitances for each pair of electrodes were used individually to compute a 2-D image representing the distribution (variation) of permittivity within the measurement enclosure. The 2-D image can be reconstructed by adding all capacitor combinations together. The cross-section image could directly show location plus quantity/volume of objects inside the closed vessel. Once the spray dried powder deposit is formed at the wall of the side outlet tube, permittivity distribution inside the sensor enclosure will be increased significantly, so the previous 4-electrode capacitance sensor system (in the offline mode) was extended to reflect spatial variation in deposition of spray dried gelatin powders. The commonly used approach for image reconstruction is the linear back projection (LBP) algorithm. With LBP, the relationship between capacitance combination (C) and vector-

based electric field (G) can be seen $C=SG$, S is the sensitivity matrix, which was simulated by ANSYS Mechanical APDL (ANSYS, Inc, Canonsburg, PA). A Landweber iteration algorithm was applied to improve the simulation accuracy. PYTHON (Python Software Foundation, Delaware, U.S.A) was used to convert vector-based G estimates to reconstructed image using an interpolation scheme.

4.4 Results and Discussion

4.4.1 Validation of the capability of the sensor

Since all electrodes and circuits were designed exactly the same, the single paired parallel plate capacitance measurements should provide the same result under the same conditions. As seen from Fig. 4.5, the capacitance values were almost the same if the two electrodes were separated at the same distance (e.g. C_{12} and C_{23} , C_{13} and C_{24}). Those variations were relatively small and within an acceptable range. Sources of variation that might have introduced errors could have been associated with size or placement differences between electrodes, or response variability between electronic components used in the sensor circuits. Capacitance values decreased when the separation between two electrodes increase (e.g. $C_{12} > C_{13}$, $C_{23} > C_{24}$). The result highlights the consistency in sensor response for the various combinations of excitation/response electrodes and between the empty and full states, which strongly suggested the arrangement of electrodes and the data processing circuits were correctly designed and adequately built.

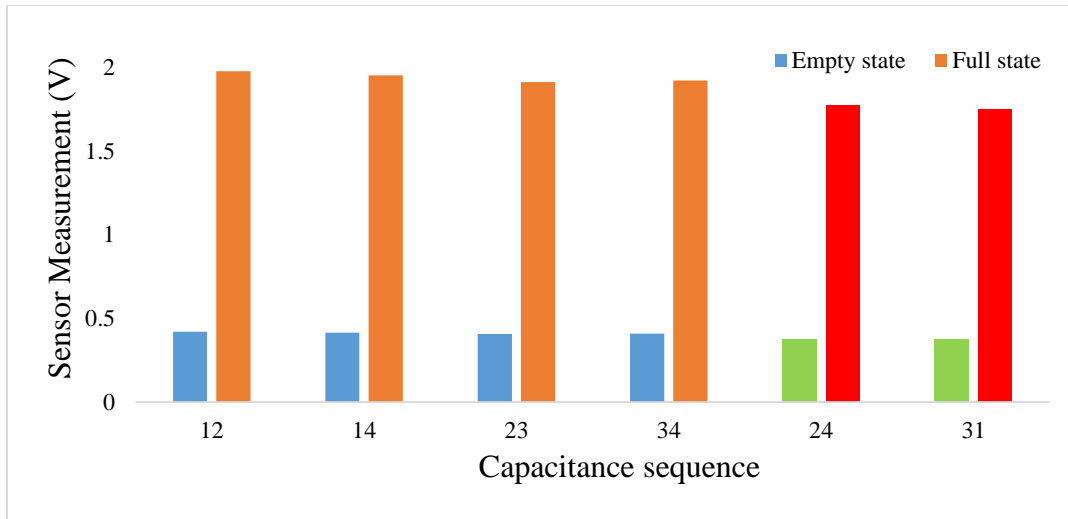


Fig. 4.5 Sensor output at empty and full state

Table 4.2. SNR for each electrode combination

C_{12}	C_{14}	C_{23}	C_{24}	C_{34}	C_{31}	Sum
43.53	46.16	45.95	46.06	46.25	45.73	59.36

As seen from Table 4.2, signal-to-noise ratio (SNR) values were large enough to support the conclusion that the capacitance sensor as built was a stable and low noise system. The variation in summed capacitances was significantly smaller than any single capacitance. It was, therefore, reasonable to use the capacitance (or voltage) sum as the sensor output predicting overall average permittivity change within the entire sensing area. This implied the use of the multiple-electrode system was equivalent to a single-paired-plate capacitance sensor, but perhaps provided greater stability in the presence of variability in the material being tested.

Table 4.3 Sensitivity test (t-test) and location test (ANOVA test) of the sensor output

	Sensitivity test		Location variation	
	Edge	Center	Original	Normalized
Water	0.32 g	0.4 g	P=0.0718	P=0.4236
Gelatin	1 g	1.4 g	P=0.0832	P=0.2928

The sensor response was different for the same sample placed at varying horizontal locations (Table 4.3). The sensor response at the central location tended to be smaller than the edge locations for the same object, which referred to the different sensitivity at central and edge locations. This effect reduces sensor accuracy, e.g. 50% MC powders at an edge location might have the same sum with a 55% MC powders at the center. Based on this, a ratio normalization method was developed to eliminate variations in sensor output. The normalized sensor response (V_n) was calculated as $V_n(i, j) = (V(i, j) - V_e(i, j)) / (V_f(i, j) - V_e(i, j))$, where $V(i, j)$ was the direct reading between electrode i and j , $V_e(i, j)$ and $V_f(i, j)$ were measurements from paired electrode i and j at empty and full states, respectively. Suppose the amplitude of the output signal was proportional to the measured capacitance ($V_0 = -V_s \cdot C_x / C_f$), so that the normalized sensor output would therefore be the normalized capacitance. After normalization, the sensor output variation in sample location was greatly reduced.

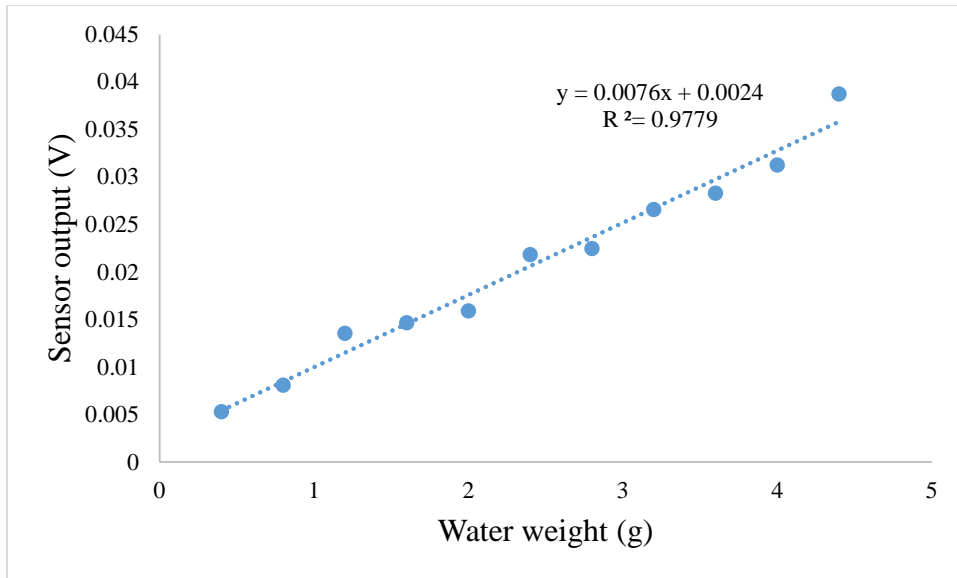


Fig. 4.6 Measured sensor output (V) against water content (g)

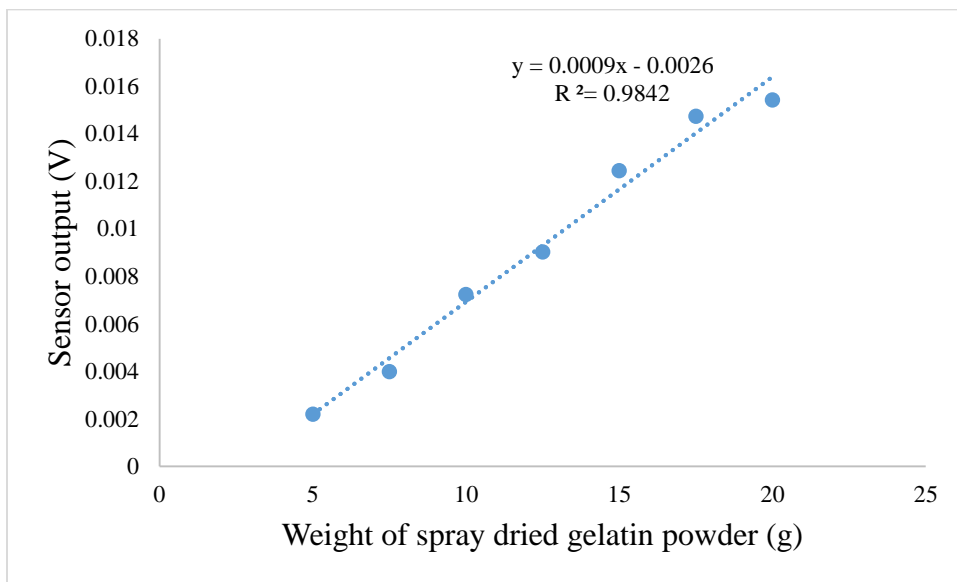


Fig. 4.7 Measured sensor output (V) against spray dried gelatin content (g)

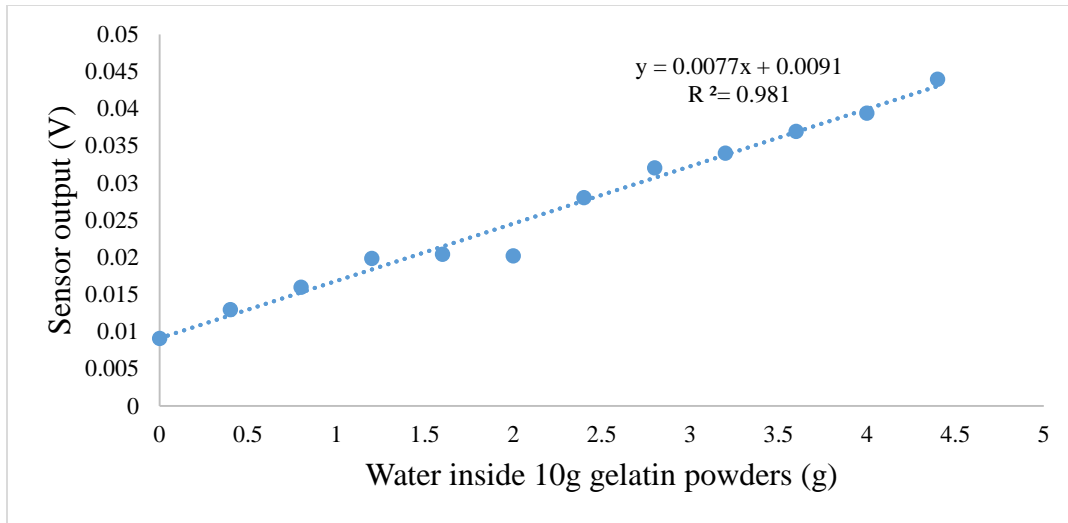


Fig. 4.8 Measured sensor output (V) against spray dried gelatin plus water content (g)

As can be seen from Fig. 4.6-4.8, a highly correlated linear relationship (R^2) between weight of materials tested and sensor output was observed which suggested that the capacitance measuring circuit was reliable. Water slope (Fig. 4.6) was significantly bigger than spray dried gelatin (Fig. 4.7) as the permittivity of water is larger than gelatin. So the relationship among sensor response, water and gelatin quantity for mixed test samples could be modeled as $V = k_1W_g + k_2W_w + k_3W_gW_w + k_4$. The statistical analysis (Table 4.4) showed p-values for water and gelatin weight coefficients were < 0.0001 , which again proved the significant influence on capacitance from both materials, and that they were individually discernible when mixed. However, the p-value for the interaction term (water effect in gelatin), indicated as W_gW_w , was 0.6787, and was therefore deemed as being insignificant in estimating capacitance. After removing the interaction effect, both water and gelatin remained significantly related to the sensor output. Since the wet weight of gelatin (W) was simply the sum of its constituents ($W_g + W_w$), $W_g/W = 1/(1+MC)$. Based on these results, the relationship among capacitance, MC and the wet weight of gelatin W can be revised to $1/(1+MC) = \alpha \cdot V/W + \beta \cdot 1/W + \gamma$. Knowing the wet weight of a sample W , and the

sum of 6 capacitance readings V , MC could be estimated. So a mass-based MC prediction mode was built $1/MC = -137.977 \bullet V/W + 0.107 \bullet 1/W + 1.101$ (Fig.3.8).

Table 4.4 P-value of the coefficient in the regression model

	With interaction $W_g W_w$	Without interaction $W_g W_w$
Water W_w	<0.0001	<0.0001
Gelatin W_g	<0.0001	<0.0001
Interaction $W_w W_g$	0.6787	

4.4.2 Measurement of MC of moving samples

The sampling rate would be the first consideration for measuring MC for moving samples, especially in cases where rapid determination of MC was required. When the 4-electrode system was used, 6 combinations among electrodes are simultaneously measured using the NI 6210, the effective device sampling rate is divided by 6, which would be much lower than necessary.

During measurement, some data was missed due to the low sampling rate. Two single paired parallel-plate electrode sensors were therefore used in the on-line mode. Here in this mode, the cyclone was selected as the measuring vessel for several reasons. Firstly, gas and spray dried powders were separated at the cyclone, so the MC measured would solely refer to gelatin, rather than gelatin and gas mixture. Secondly, the centrifugal force and inertia in cyclone causes the particles to move outward, collide with the outer wall, and then slide down to the bottom wall, so that samples could be placed on the edge of the sensor enclosure, no location shift from edge to center. No location normalization was thus needed and higher test sensitivity could be obtained. The strong centrifugal force also resulted in few deposits formed in the cyclone area, so that the accuracy of the MC measurement would not be affected by the deposits.

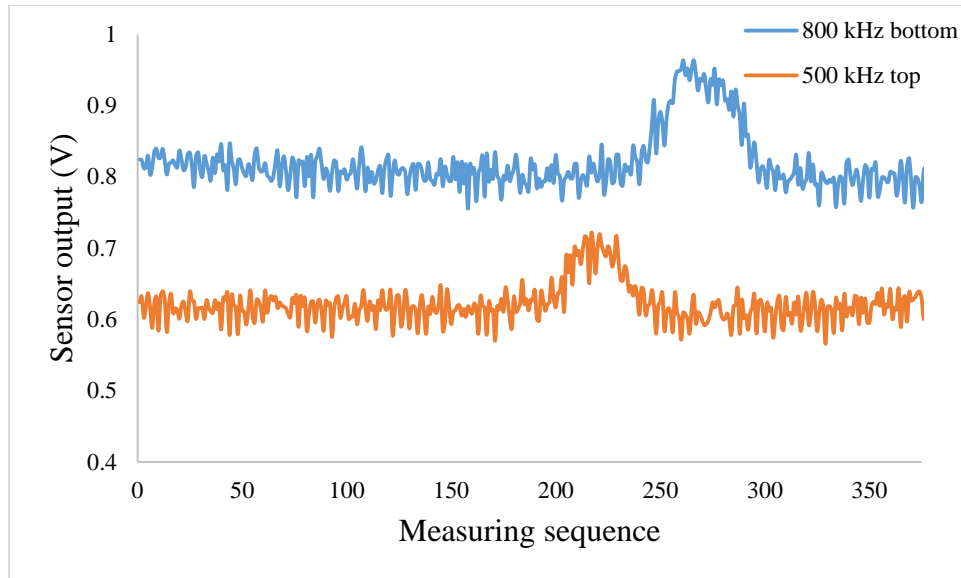


Fig. 4.9 Online MC prediction with dual frequency method

Results (Fig. 4.9) indicated a relative low correlation compare with offline mode. Time duration for powders passing through the sensing area was $<0.1s$, so that the effective sampling rate would be lower than necessary. The output signal could be amplified by an Op-amp circuit so that the detection limit could be even lower. Future work should mainly focus on approaches to enhance the sampling rate. An envelope detector that converts AC signal to DC signal to increase the effective sampling rate could also be used in the future.

4.4.3 Visualization of the deposition status of spray dried powders

As can be seen from Fig. 4.10, the ECT system was used to describe the permittivity distribution at a fixed discrete point (55) inside the measuring enclosure (side outlet tube), which could be thought of as a vector element (55) associate with some fixed location. The resulting permittivity distribution vector elements were used as the gray scale values for a reconstructed image (G). Change in electrode capacitance due to the change in distribution of dielectric properties in the sensing region were measured, so that a cross-sectional image representing the permittivity

distribution inside the vessel was reconstructed (Fig. 4.11). This reconstructed image was expected not only to detect the area and location of the deposits, but also the MC of the powders. MC information could be extracted from the color in the image. The blue indicated low electric potential and red was high electric potential. The central part was always in a low energy state, which could be explained by the presence of air. Increasing the electrode numbers could divide the sensing area into more segments, which would improve the resolution of reconstructed images. However, it may also decrease the sampling rate achievable for a given data acquisition system, which reduces the number of frames per second that can be imaged.

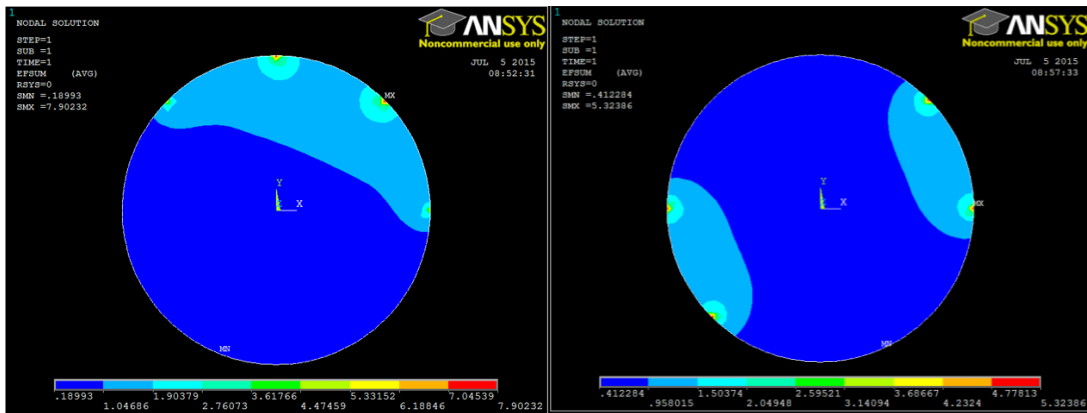


Fig. 4.10 Sensitivity matrix (S) simulated by ANSYS APDL for (left) C₁₂ and (right) C₁₃

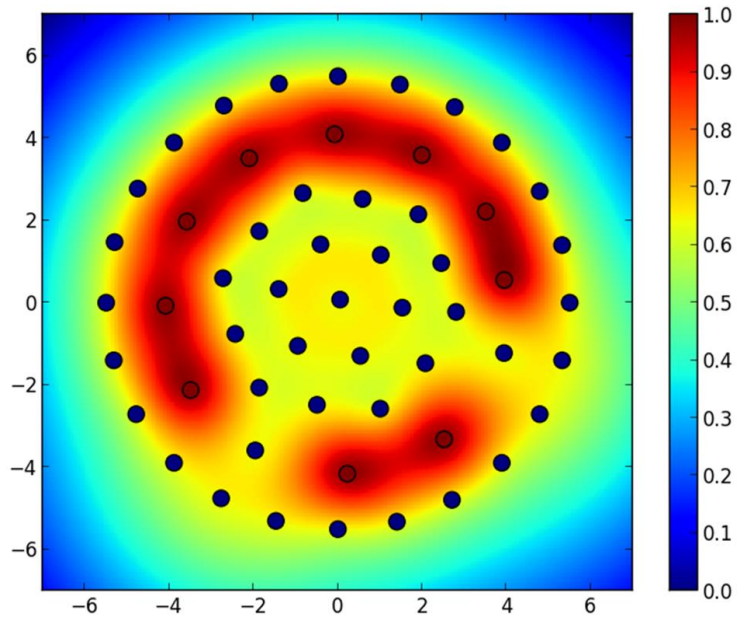


Fig. 4.11 Simulated deposition status (G) inside the spray dryer when $C_{12}=0.003618$, $C_{14}=0.018417$, $C_{23}=0.00124$, $C_{24}=0.016047$, $C_{34}=0.014142$, $C_{31}=0.003615$.

Conclusion

A self-built capacitance sensor system was shown to be feasible to measure MC of gelatin powders both statically (not moving) and dynamically (moving through the sensor enclosure) with acceptable accuracy. The sensor has potential to be applied in quality control applications for continuous spray drying processes. Future work should focus on approaches to enhance system accuracy and stability, and to increase the sampling rate. Envelop detector that convert original AC signal to DC signal which could reduce the sampling rate of data acquisition circuit greatly could be used in the future. All wires and circuits could be put in a printed board to improve system's stability.

References

- Adedipe OE & Dawson-Andoh B, 2008. Prediction of yellow poplar (*Liriodendron tulipifera*) veneer stiffness and bulk density using near infrared spectroscopy and multivariate calibration. *Journal of Near Infrared Spectroscopy*. 16(5):487-496.
- Brink M, Mandenius CF, Skoglund A, 2010. On-line predictions of the aspen fibre and birch bark content in unbleached hardwood pulp, using NIR spectroscopy and multivariate data analysis. *Chemometrics and Intelligent Laboratory Systems*. 103(1):53-58.
- Johana E, Yunus FRM, Rahim RA, Chan KS, 2011. Hardware development of electrical capacitance tomography for imaging a mixture of water and oil. *Journal Teknologi*. 54:425-442.
- Pan PM, 2014. Monitoring moisture content and mass flow of wood chips using electrical capacitance tomography. Doctoral dissertation, Auburn University.

Chapter 5

PIV measurements of airflow patterns in a lab-scale spray dryer

Keywords:

Airflow pattern, Particle image velocimetry, Computational fluid dynamics, Spray dryer

Abstract:

To evaluate the airflow pattern (velocity field) inside a co-current lab scale spray dryer, air velocity magnitudes were measured by a particle image velocimetry (PIV) system at numerous locations in the spray dryer chamber in the absence of spray. Analysis at varied drying air flow rate strongly suggested the flow in the chamber has high turbulence intensity. The PIV analysis provided information on how drying air flow rate affects fluid flow profiles, which could be used to validate the CFD simulated results.

5.1 Introduction

During spray drying, the airflow pattern inside the spray chamber influences the trajectories of the particles, which subsequently affects the particle residence time and particle deposition or escape from the wall (Kuriakose & Anandharamakrishnan, 2010; Woo et al., 2010). Knowledge of the airflow pattern is essential to predict the performance of a spray dryer. Since the introduction of computational fluid dynamics (CFD) in the past decades, it is now possible to simulate the airflow pattern in spray dryers (Gabites et al., 2010; Guo & Maghirang, 2012; Langrish et al., 2004; Toschkoff et al., 2012; Wawrzyniak et al., 2012). However, the CFD simulations are conducted based on many assumptions. Accurate experimental measurement of airflow quantities such as global air distribution or local air velocity are still needed in order to validate or calibrate simulated results (Yoshida et al., 2015).

Several different techniques are now available for this purpose in measuring airflows. The most frequently used methods are point-wise based techniques, such as hot-wire anemometry (Kieviet et al., 1997), and laser Doppler velocimetry (LDV) (Kumara et al., 2010; Mychkovsky et al., 2012; Pfeifer et al., 2011). Nevertheless, the traditional point-wise anemometry can only yield airflow information for a few predefined measurement points (Hagemeier et al., 2015).

Furthermore, it is not possible to conduct accurate and detailed airflow field measurement with point-wise velocimetry, where large velocity fluctuations, non-symmetrical recirculation, and strongly unstable airflow occurs. Many point-wise techniques are intrusive, such as hot-wire anemometry and ultrasonic anemometry, and are thought to interfere with the local airflow. Even those non-intrusive point-wise techniques (e.g. LDV), it is still excessively difficult and time-consuming to conduct global airflow field measurements point by point. For these reasons, the

optical-based method, such as particle image velocimetry (PIV), have become an alternative tool for airflow field studies (Raffel et al., 2007). The use of such velocimetry avoids the need for intrusive probes, allowing visualization of airflow pattern in a global domain without disturbing the airflow (Cao et al., 2014).

PIV is a non-intrusive laser-based imaging technique for characterizing flows in the study of fluid dynamics (Adrian & Westerweel, 2010). It is used to measure flow velocity and related flow properties (e.g. detailed flow structures) across the entire flow field of interest. The basic principle of PIV is that a laser light sheet is used to illuminate the flow field being studied, which is usually seeded with tracer particles. A double shutter camera is synchronized with the double pulsed laser to record two successive frames closely separated in time so that the movement of the flow (particle displacement) within this short time interval is visualized. The technique has found wide acceptance because it allows researchers to accurately characterize high speed flows in two dimensions (2D-PIV), or even three dimensions (3D-PIV (Angarita-Jaimes et al., 2012)), useful for analyzing transient and turbulent flow (Pawar et al., 2014; van Hooff et al., 2012), and validating numerical CFD simulations (Cao et al., 2014), where previous techniques (such as hot-wire anemometry, LDV) only allowed single-point characterization (Hagemeier et al., 2015; Khodarahmi, 2015). A typical PIV setup consists of the seeding particles, a double-pulse laser system with an optical arrangement to convert the laser to a light sheet, a double shutter camera, a synchronizer for control of both the camera and laser, and the software to post-process the captured images. More details about the PIV system will be described in the next several sections.

5.1.1 Seeding

To facilitate visualization of the flow, most applications require seeding the flow with appropriate tracer particles. Tracer particles play a key role in airflow measurement, because PIV actually measures the movement of tracer particles instead of the real airflows. Therefore, the seeded particles should be sufficiently small and light so they are able to satisfactorily follow the motion of the flow. On the other hand, if seeded particles are too small they do not scatter enough light, and hence produce weak images (Melling, 1997). Any particles that are small enough to achieve good tracking behavior, yet large enough to scatter a significant quantity of the incident laser light can be used as tracer particles (Bosbach et al., 2009; Melling, 1997; Raffel et al., 2007). In addition, the tracer particles should be seeded into airflow at a steady and high enough rate to meet the spatial resolution requirement for the PIV experiment. Generally, a higher seeding concentration is preferred to obtain evenly spatially distributed particles. However, excessively high density seeding may lead to poor scattering performance. The ideal concentration of the tracer particles is 10-20 particles in an interrogation area (Adrian, 1983). A uniform seeding size is also desirable in order to avoid excessive intensity from larger particles and background noise from smaller particles. Various methods are now available to generate tracer particles (Kahler et al., 2002; Meyers, 1991). The most commonly used is the fog machine, with which it is feasible to generate large number of smoke particles. However, the initial velocity of seeded smoke particles need to be considered as it may lead to perturbations on the original airflow velocity.

5.1.2 Laser and optics

For the PIV measurement, a high intensity light source, normally a laser pulse or conventional light source (e.g. strobe light), is required to illuminate those tracer particles and enable their location be to imaged. To avoid blurred images while analyzing fast flows, pulsed laser is preferred due to its ability to generate high-power light beams with short pulse durations, easily freezing any motion. Either Nd:YLF (neodymium-doped yttrium lithium fluoride) or Nd:YAG (neodymium-doped yttrium aluminium garnet; $\text{Nd:Y}_3\text{Al}_5\text{O}_{12}$) lasers could be used in PIV system, with the plane within the flow of interest is illuminated twice within a short time interval, straddling the two frames as shown in Fig. 5.1. Commonly, the PIV measurements must be performed in a dark room, so that when the laser illumination is off, the image is completely dark. This provides an excellent contrast between tracer particles and background to ensure accurate results. The other reason to use pulsed laser is that only laser light can be focused into a thin enough light sheet so that only particles in a plane are illuminated and imaged. Otherwise the scattered light from particles in other planes would make the measurement inaccurate. The light sheet can be formed from a collimating laser beam using spherical and cylindrical lenses in combination. The spherical lens compresses the plane into a thin sheet with desired thickness, while the cylindrical lens expands the laser into a straight line in one dimension, which is essential for the generation of a light sheet. It should be noted that the spherical lens cannot compress the laser sheet into an actual 2-dimensional plane. To guarantee the measured flow field can be kept in a plane, the thickness of the light sheet in the measurement area is typically about 1-3 mm or less (Cao et al., 2014; Sun and Zhang, 2007). However, using such a thin light sheet as the illumination method also brings about a challenge for measuring a strong three-dimensional flow field. In this case, some particles recorded by the cameras in the first frame

may move out of the measured plane and cannot be captured in the next frame. That will limit the accuracy of PIV measurement to the regions of the thin plane flow (Hart, 2000).

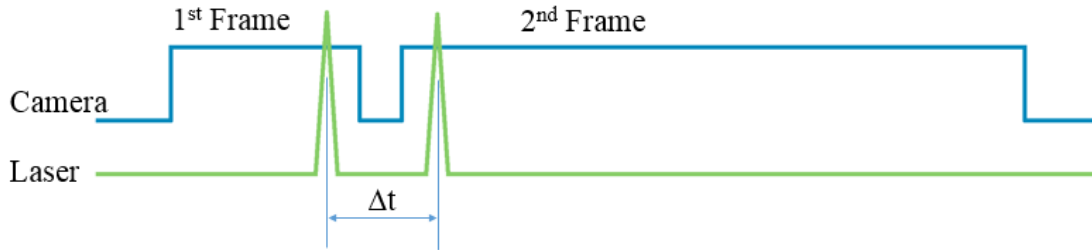


Fig. 5.1 Timing diagram for double shutter camera and double pulsed laser

5.1.3 Camera and synchronization

The light scattered by the tracer particles in the field of interest are captured by a double shutter camera. The unique feature of this double shutter camera is the ability to acquire coupled pairs of separated frames in a very short time interval which can be set down to a few hundred ns. This allows each exposure to be isolated on its own frame for more accurate cross-correlation analysis of the airflows. The most common cameras used in PIV measurements are coupled charged devices (CCD) cameras and complementary metal oxide semiconductor (CMOS) cameras. A CCD camera sensor normally consists of an array of many individual CCD elements, which also called pixels. Each pixel has a size on the order of $10 \times 10 \mu\text{m}$. The CCD camera has been widespread used in PIV experiments for its increased spatial resolution, better image quality and wider applied range. Today, commercially available CCD cameras typically have the sensor resolution range from 2 M ($1600 \text{ pixels} \times 1200 \text{ pixels}$) to 29 M ($6576 \text{ pixels} \times 4384 \text{ pixels}$), which makes it necessary to obtain the complete airflow structures in a large-scale measurement. (FlowSense EO Camera Series, 2012, Dantec Dynamics, www.dantecdynamics.com). A CMOS sensor allows for high-speed recording of up to a few thousand frames per second, which is very

promising for study of turbulent characteristics within airflows. However, the low spatial resolution has become the main obstacle for CMOS cameras to completely replace the CCD cameras. This critical drawback limits the applications of CMOS cameras only to small-scale measurements. Thus, one should make a trade-off between the spatial resolution and the temporal resolution, and select the proper cameras depend on certain applications (Hain et al., 2007). The correct lens for the camera should also be selected to properly focus and visualize the particles within the investigation area. The scattered light from each particle should be in the region of 2 to 4 pixels across on the image. If too large an investigation area is recorded, particle image size drops and may result in loss of sub pixel precision in PIV analysis.

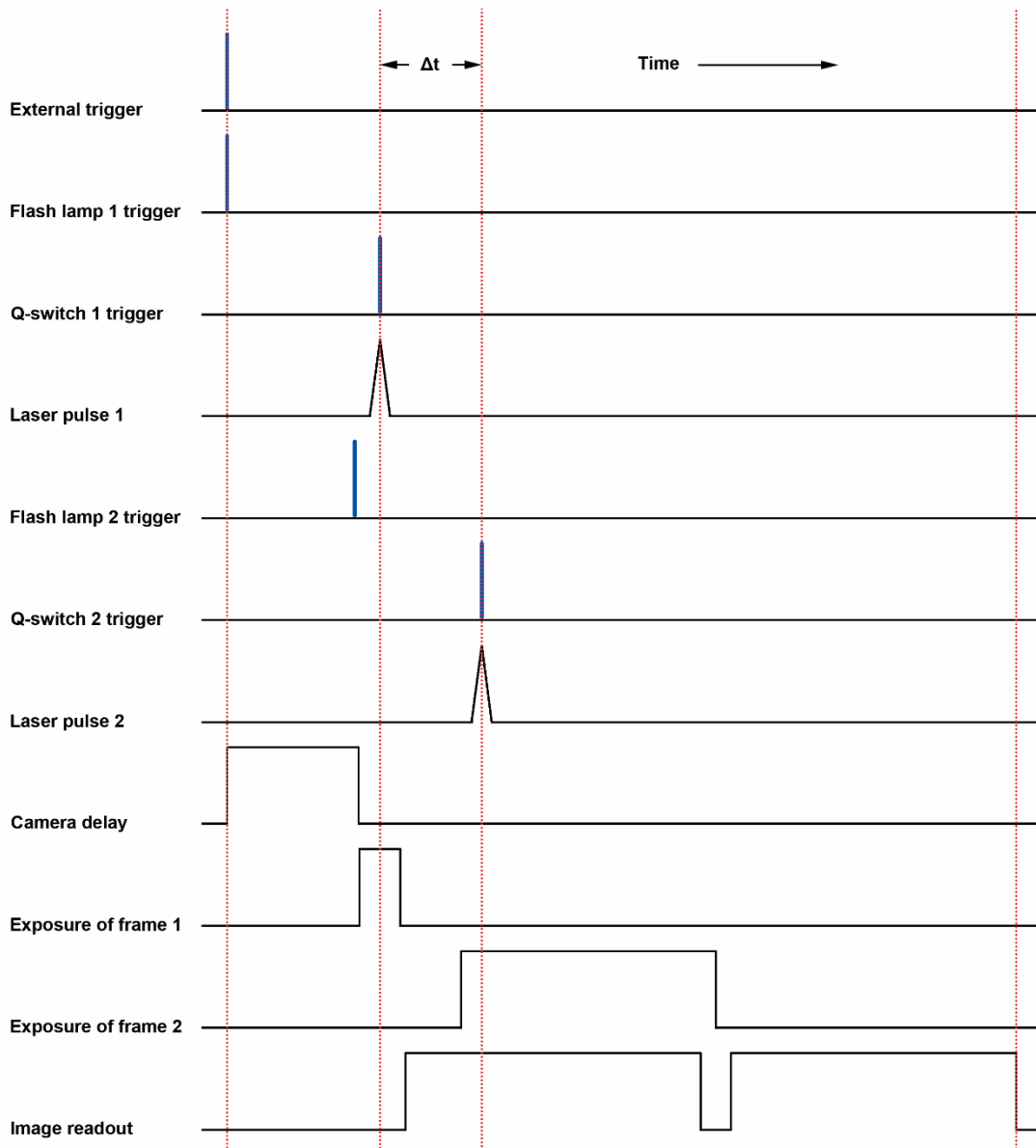


Fig. 5.2 Timing diagram for a PIV system consisting double-pulsed laser and double-shutter camera.

Before such cameras can be used, they must be precisely time-coordinated with the laser to ensure the laser pulses straddle the frame, so that the first laser pulse can illuminate the object during the first image integration, and the second laser pulse can illuminate the object during the second image integration (Fig. 5.1). This time correlation is usually achieved by a synchronizer.

Fig. 5.2 shows a timing diagram for a PIV system consisting double shutter camera and double

pulsed laser. In this example, the synchronizer acts as an external trigger for both the camera and the laser system, which firstly sends a trigger signal to the laser system to initiate the emission of the flash lamp 1. To warm the flash lamps to thermal equilibrium, a “Q- Switch” is employed to prevent the laser from emitting until the energy intensity reaches to its maximum level, then the Q-switch 1 is triggered, and the laser pulse 1 is emitted. Typically, the time delay between the initiation of the light flash and the Q-switch is between 180 and 240 μs . The flash lamp 2 is also triggered after the flash lamp 1 initiate but with an appropriate delay. A short time later, Q-switch 2 trigger will begin, so that two laser light pulses with a predefined time delay (Δt) are generated (Adrian & Westerweel, 2010). The synchronizer system also trigger the double shutter camera. As PIV system requires the initiation of the flash lamp prior to the recording of the PIV image, the camera’s build-in delay function was used in response to the trigger pulse, then the camera starts the exposure process of the first frame. After certain interval, the second picture is exposed. The exposure time is controlled by the synchronizer so that the laser pulses can be triggered within the period that the shutter is open and straddle the frame. As it is desirable in PIV applications to minimize the time separation between the successive illuminating laser pulses, it is standard to trigger a laser pulse at the end of the first pulse and then again at the beginning of the second exposure (Raffel et al., 2007). And for the double shutter camera, after the completion of the recording of the first frame, the image data must be read-out from the CCD sensor and transferred and stored to the frame grabber before next frame can be transferred. So the actual limitation is that whether the camera can store the first image fast enough to be ready for the second exposure. As a result, the integration time (recording period) of the second frame is usually set to be longer than the first one to ensure enough time for read-out the image information, whereas the interframe time is very short. The short interframe time makes it

possible to use PIV for high speed airflow observations that require record the particle images on separated frames with very short exposure time delays.

For accurate PIV analysis, the time delay between the two pulses (Δt) have to be chosen such that adequate particle displacement on the images as a function of time are obtained. The time delay (Δt) should be long enough that able to identify the displacement of the tracer particles between the two pulses, but also need to be short enough to avoid particles travelling out of the light sheet plane during subsequent frames. According to Cao's recommendation (Cao et al., 2010a, 2010b), the separation of the particle images (in pixels) should be larger than the accuracy of the peak detection and smaller than a quarter (1/4) of the selected interrogation area size (32×32 pixels). Therefore, depending on the airflow velocity (U), the magnification of the camera lens setup (in pixel), and the desired interrogation area size (d_{int} , in pixels), the optimum pulse delay will be in the range of: $pixel/U_{max} < \Delta t = \Delta x/U_{max} < 1/4 d_{int}/U_{max}$. So after successive images are captured, the particle flow vector can be computed.

5.1.4 Imaging analysis

Once the images are successfully recorded, the next step is the imaging analysis. The displacement field is determined from the motion of the seeding particles between the two successive images. As it is impossible to directly determine the displacement for each particle due to the high density of particles within the flow plane being imaged, the preferred evaluation method is to subdivide the full image area into many small subareas called interrogation windows (or area), with each ideally containing ~10-20 particles. The size of the interrogation window should be sufficiently small such that there is no significant displacement gradient

within the interrogation area, so typically the size is set at 32×32 pixels. As the location of the interrogation windows in images is the same, assuming all particles inside interrogation windows move homogeneously, the mean local displacement vector (ΔX) between the two exposures can then be determined using cross-correlation techniques (Fig. 5.3).

The computation of the cross-correlation function is commonly based on Fast-Fourier Transform (FFT) algorithms. The interrogation windows are spatially shifted, when the corresponding two images align with each other, the pixel intensities will be larger than elsewhere, so a signal peak can be produced by the cross-correlation function, providing the magnitude and direction of the displacement vector. In the general case, when all particles inside the interrogation window do not have uniform displacement, the spatial shift that yields the maximum in the correlation function, which is the most probable location of the destination of the particle displacement, is regarded as the mean particle displacement over the interrogation window. Many other processing algorithms (e.g. adaptive correlation (Theunissen et al., 2010), least squares matching (LSM) (Brücker et al., 2013; Kitzhofer et al., 2012)) with additional features (e.g. size, shape, orientation) have also been developed for PIV analysis, aimed at improving processing accuracy, enhancing signal-to-noise ratio (SNR), reducing image distortion and removing spurious vectors (Cao et al., 2014; Fansler & Parrish, 2014). To convert the displacement field from image coordinates to real laboratory coordinates, length calibration procedure is usually performed with a calibration sheet. Calibration sheet is a set of grid points on which the distance between two grid points is known. By putting the calibration sheet at the image plane, the image of the grid is captured and superimposed on the PIV image. Taking into account the time delay between the images, once the displacement field is determined, the instantaneous velocity field for the entire

cross-section area of flow of interest can be obtained. By analyzing large quantity of image pairs, averaged airflow information can also be gained.

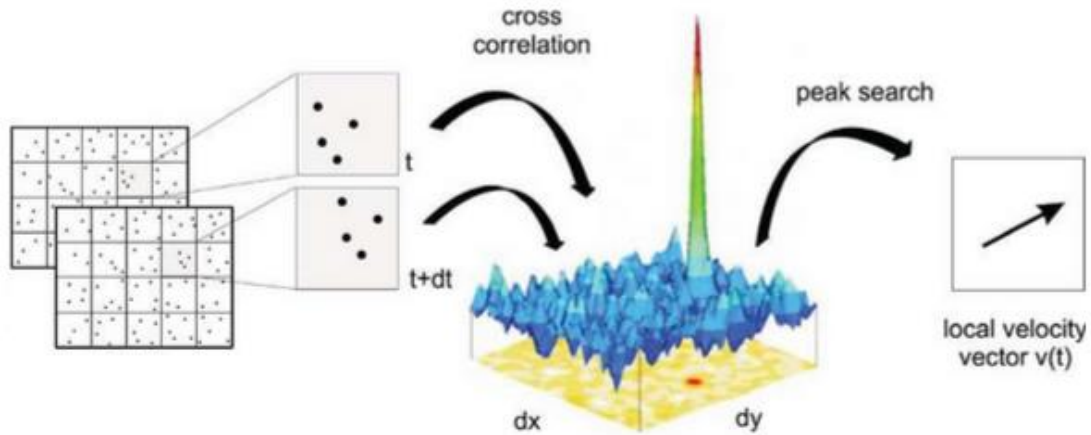


Fig. 5.3 PIV data analysis via cross correlation (adapted from Pawar et al. (2014))

Accurate predictions of flow patterns inside the spray dryer are essential for validation of the CFD simulation result. Although LDA and hot wire anemometry have been frequently used (Kieviet et al., 1997; Kumara et al., 2010; Mychkovsky et al., 2012; Pfeifer et al., 2011), there is a lack of experimental data for airflow measurements in spray dryer using PIV (Meyer et al., 2011; Stafford et al., 1997). As most parts of B-290 are manufactured from glassware, the complete airflow inside the dryer chamber was visible, which enables PIV measurements to be performed. We thus aim to characterize the airflow pattern inside the spray dryer chamber using PIV. Results will be useful to gain more insight into the detailed airflow pattern information and to validate turbulence models used in CFD simulations.

5.2 Materials and Methods

The schematic overview of the experimental set-up in this work is depicted in Fig.4.4 and Fig. 5.5. It consists of a spray dryer and a PIV system. The spray dryer used is a lab scale co-current

cylinder-on-cone spray dryer (B-290, BÜCHI Labortechnik AG, Flawil, Switzerland). The spray dryer chamber was made of transparent 3.3 borosilicate glass and consists of two sections: a cylindrical section (0.49m in height, 0.165m in diameter), and a conical section that reduces in diameter from 0.165 m to 0.03 m over a height of 0.06 m. The chamber has a side outlet (0.04 m in diameter) at the bottom (mounted at 0.0825 m from the center axis in the side, 0.415m from the top). The drying air enters the dryer chamber through an annulus at the top with the nozzle as its center. The airflow rate is controlled by an aspirator. According to the calculated Reynolds numbers, the airflow type inside the chamber significantly varies at different aspirator settings (Table 5.1). To achieve uniform airflow rate, after switching on the current, the spray dryer is conditioned until use.

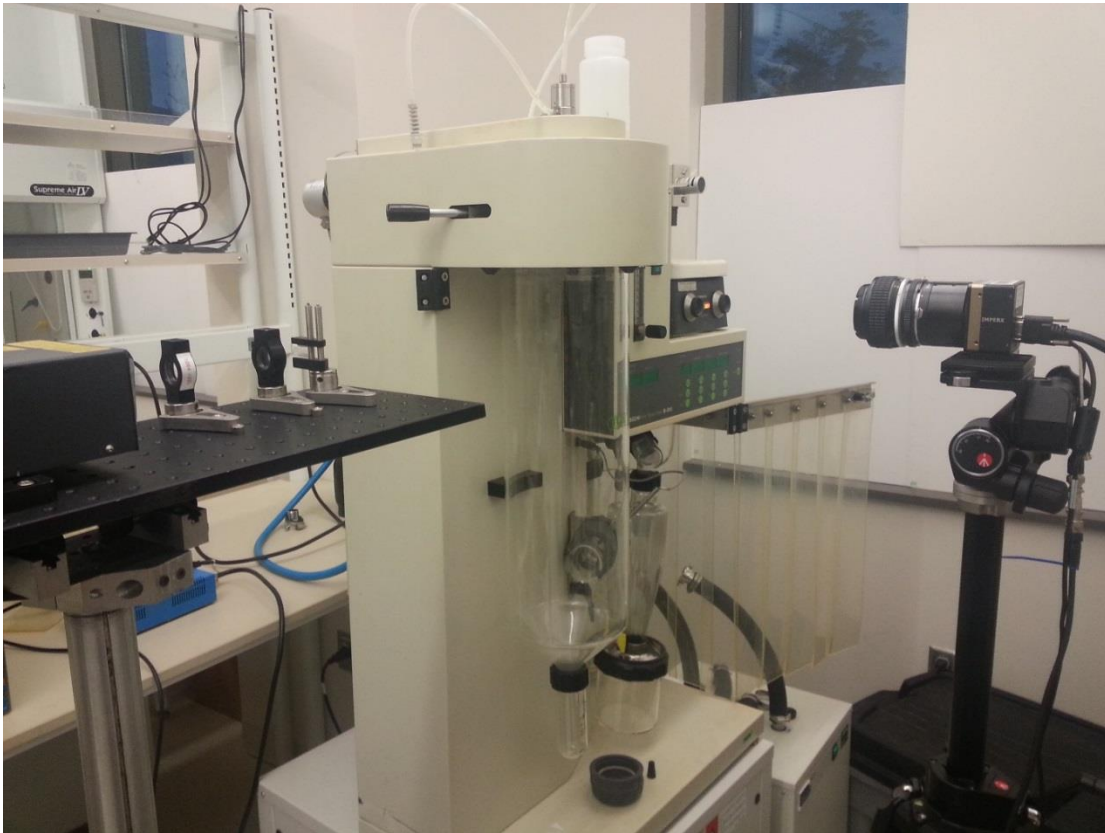


Fig. 5.4 PIV setup along with the spray dryer B-290

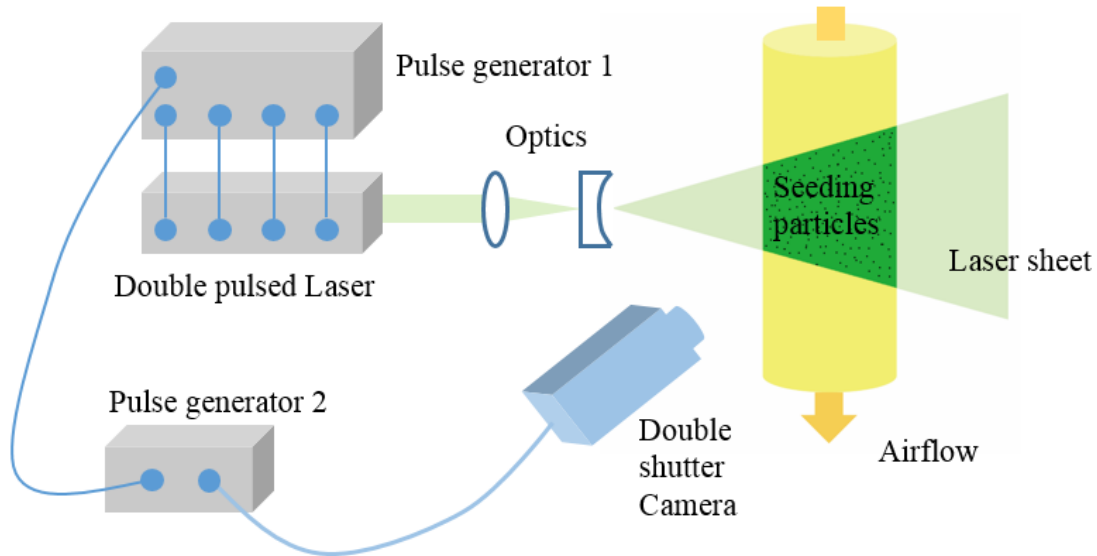


Fig. 5.5 Schematic diagram of the PIV system apparatus setup

Table 5.1 Effect of aspirator settings on airflow

Aspirator	Airflow velocity	Re	Flow type*
%	m/s		
50	0.25	2145	Laminar
60	0.31	2547	Transient
70	0.36	2949	Transient
80	0.41	3351	Transient
90	0.45	3753	Transient
100	0.5	4155	Turbulent

Note: The airflow rate values were provide by manufacturer (Buchi). The diameter of the spray chamber cylinder is 0.165m. Air kinematic viscosity at 60°C is $18.9 \times 10^{-6} \text{ m}^2/\text{s}$, so the Re number can be calculated. The flow is laminar when Reynolds number (Re) < 2300, transient when $2300 < \text{Re} < 4000$, and turbulent when $\text{Re} > 4000$.

The PIV measurement system consists of double-pulsed Nd:YAG laser and a double-shutter CCD camera, which are synchronized by a digital delay pulse generator. The airflow is seeded with tracer particles (smoke), which are provided by a fog machine. The laser beam is modified by a spherical and cylindrical lens combination to create a thin laser sheet to illuminate the tracer particles on the vertical central plane of the dryer chamber, parallel to the flow direction. A tripod is used to guide the laser sheet to the target position and direction during the experiment,

any minor misalignment was easily corrected by manipulating the laser and optics. In this way, all axial positions of the chamber could be reached. The CCD camera is placed perpendicular to the laser sheet plane to capture the light scattered from the tracer particles. The camera is mounted on another tripod and located at the same height with laser to ensure the targeted laser sheet areas are in focus. The equipment used in the experiment setup is shown in Table 5.2. Details about the PIV equipment are available in publications from Melnick & Thurow (2011, 2012).

Table 5.2 Detailed information about the PIV system set-up

Component	Model	Manufacturer
Spray dryer	B-290	Buchi, Flawil, Switzerland
Laser	Solo III-15 PIV Laser system	New Wave, Fremont, CA
Camera	B4020 CCD Camera	Imperx Inc, Boca Raton, FL
Lens	AF DC-Nikkor 135mm f/2D	Nikon Inc, Melville, NY
	SP AF 60mm F/2.0	Tamron, Commack, NY
Extension tube	Kenko auto extension tube set	Kenko, Huntington Beach, CA
Optics	Spherical and cylindrical lens	Thorlabs, Newton, NJ
Synchronizer	9514 digital pulse generator	Quantum, Bozeman, MT
Smoke	Z-800II Portable Fog Machine	Antari, Taoyuan, TW, China

The airflow pattern visualization experiments were carried out at two different aspirator rates (airflow rates) of 50% and 100%, in the absence of liquid spray (without considering the effects of liquid atomization in the airflow pattern). In order to overcome the limitation of the laser powder to cover the relatively large area of dryer chamber and improve the spatial measuring resolution, the entire flow domain (measurement area) was divided into several sub-regions

located at 13 levels in the axial direction of the dryer chamber. PIV measurement was performed in each of these small sub-regions of interest, focusing on the vertical central plane of the chamber (0.165m×0.04m (W × H), 4008×2672 pixels with one pixel being 9µm), and analyzed in terms of instantaneous (mean) velocity magnitude in the entire flow domain, and in terms of turbulence intensity and vorticity. Since the view of object was set at 3 cm, the field of view in the digital camera was 2672 pixel × 9 µm/pixel = 2.4048 cm, the magnification should be $2.4048/3 = 0.8016$. As the particle was expect to move no more than 1/4 of the interrogation window (typically 32 × 32 pixel), the movement of particles in the image should be no more than 8 pixel × 9 µm/pixel =72 µm, the actual object movement should be $72/0.8016 = 89.82 \mu\text{m}$. Thus, the optimum time delay between exposures must be set at $89.82 \mu\text{m}/250000 \mu\text{m/s} = 0.00035928 \text{ s}$ and $89.82 \mu\text{m}/500000 \mu\text{m/s} = 0.00017964 \text{ s}$ for 50% and 100% aspirator rate, respectively.

After images were taken, the PIVlab software was used to perform the data analysis (Thielicke & Stamhuis, 2014, 2015) in order to determine the displacement of the particles. Paired images were divided into interrogation windows and processed by a multi-pass cross-correlation algorithm, which operated the cross-correlation multiple times with different window sizes to make the results more accurate. The initial window size was generally the largest, and the final pass generally had the smallest window size. This essentially serves as a refining of the results with each new pass. In this experiment, we began with 256×256. The final output (vector map) of the PIV algorithm is a qualitative understanding of the true airflow field in the dryer chamber. The PIV algorithm often does not account for the magnification of the image. If it is desired to obtain the flow field in true units such as m/s, one must multiply the data by the following factor:

(distance in object space per pixel)/(time between image pairs). The results of the PIV algorithm are vectors with units of pixels. The factor that we multiply by is (meters/pixel)/(seconds).

Therefore, the result of this multiplication is velocity vectors with magnitude m/s. Vector field files are processed using Tecplot 360 to modify the manner in which the vector file is presented.

5.3 Results and discussion

In a spray dryer, particle trajectories, and thus where and when the particles hit the chamber walls, are greatly influenced by the airflow pattern. To simplify the complexity of the particle/air mixing in a spray dryer chamber, Langrish & Premarajah (2013) assumed the particles and the airflow move in parallel to each other in plug flow inside the Buchi B-290 spray dryer and simulated the spray drying process by Matlab. The calculated Re values from Table 5.1 indicated the presence of a transitional/turbulent flow regime inside the chamber, which could be distinguished from laminar flow (or plug flow) by the presence of vortex structures. PIV experiments were thus conducted at 50% and 100% aspirator rates to validate the assumptions. Fig. 5.6 shows that unsteady vortices were clearly visible even at 50% aspirator rate. Therefore, the assumption of steady and isotropic plug flow inside the spray dryer chamber is unreasonable. Further simulation of the airflow pattern should take consideration of the complexity of turbulent/transitional flow inside the chamber.

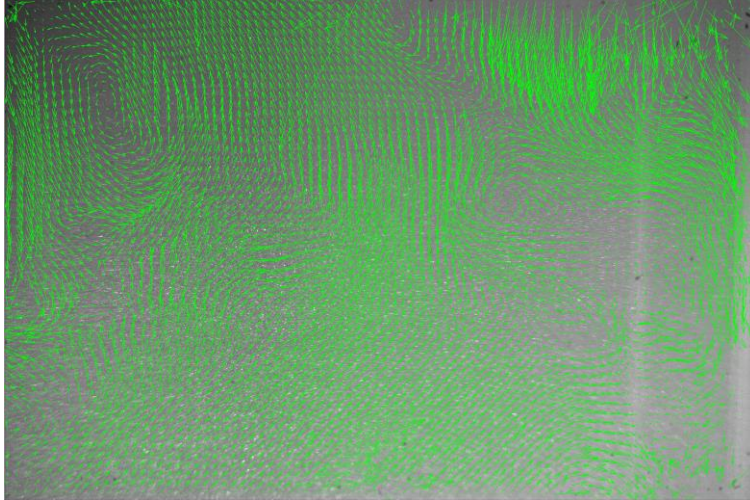


Fig.5.6 PIV image of the region 14 to 17 cm from the nozzle inlet for 50% aspirator rate.

In order to obtain qualitative information of the airflow pattern at 100% aspirator rate, PIV measurement was performed at different fields of view in the vertical center plane of the chamber. Due to apparatus obstructions at the top of the chamber, it was not possible to analyze the flow in the area just below the nozzle (0-5 cm vertical distance from the nozzle). Fig. 5.7-Fig. 5.10 show instantaneous airflow images obtained by PIV at 4 different axial locations. Colors of the vectors indicated the relative magnitude of the particle displacement. For this aspirator rate, a transitional/turbulent flow regime was anticipated. The airflow pattern for 13 sub-regions of interest show remarkable differences. The major features observable were: the laminar-like downward flow nearby the air inlet (Fig. 5.7), a recirculation pattern zone at the upper part of the chamber (Fig. 5.8), a half circle airflow pattern at the lower part of the chamber (Fig. 5.10, 5.11) and horizontal air movement near the side outlet (Fig. 5.12). Fig. 5.7 shows the instantaneous airflow map in the field of view 5-8 cm from the nozzle. The downward airflow was dominant in this region and had a laminar-like symmetric distribution around the centerline, which was in accordance with the expectations that the inlet air penetrated the top of the chamber and produced a downward axial airflow through the chamber. The airflow field appeared non-

symmetrical in regions further away from the inlet as air flowed down toward the bottom of the chamber. Large clock-wise recirculation zones were observed in the area 8-26 cm vertical distance from the nozzle. The vector incoming from the left side of the measurement window (Fig.5.8) was slightly inclined in the upward direction, and moved in the downward direction when passing through the right side of the measurement window. High recirculation could enhance the mixing between the drying air and the feed, which would increase the drying rate. Two counter-rotating vortices can be observed in the image at 14-17 cm region (Fig. 5.9). In addition, there was a difference in direction of airflow motion between 29-32 cm region (Fig. 10) and 38-41 cm region (Fig. 11). Airflow moved from the upper right corner to the lower left corner, and then turned back moving from the upper left corner to the lower right corner. For the region near the side outlet (41-44 cm region) (Fig. 5.12), airflow moved horizontally to the side outlet, magnitude of the vertical vector was close to zero in the outlet.

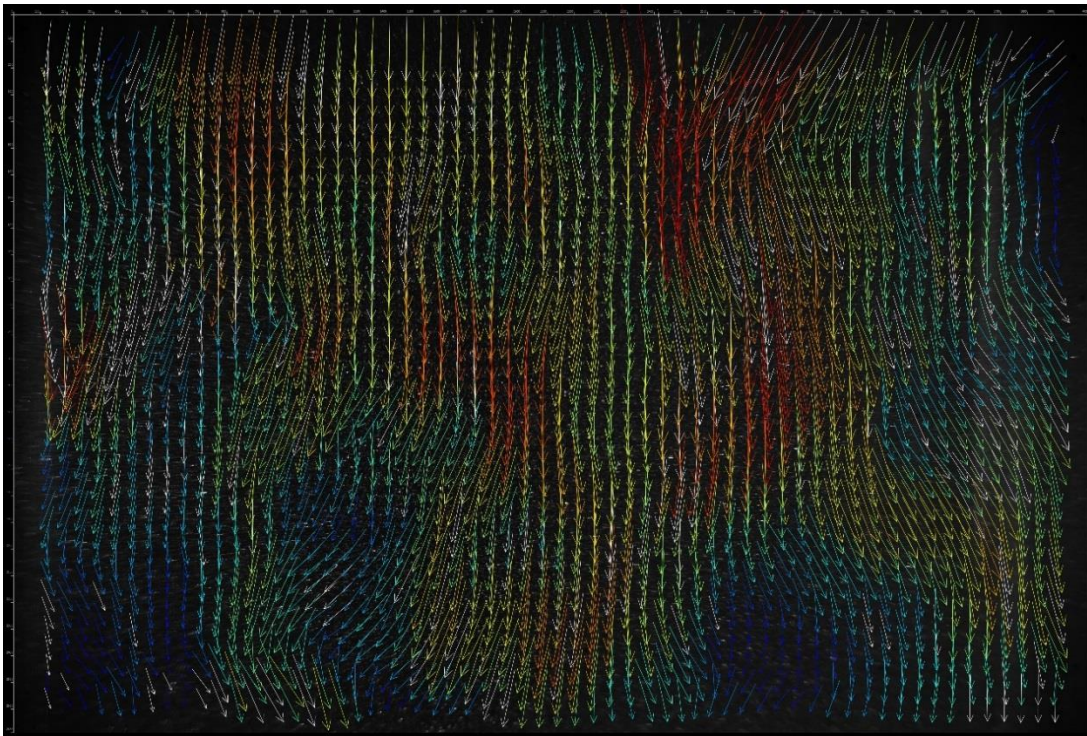


Fig.5.7 PIV image of the region 5 to 8 cm from the nozzle inlet for 100% aspirator rate

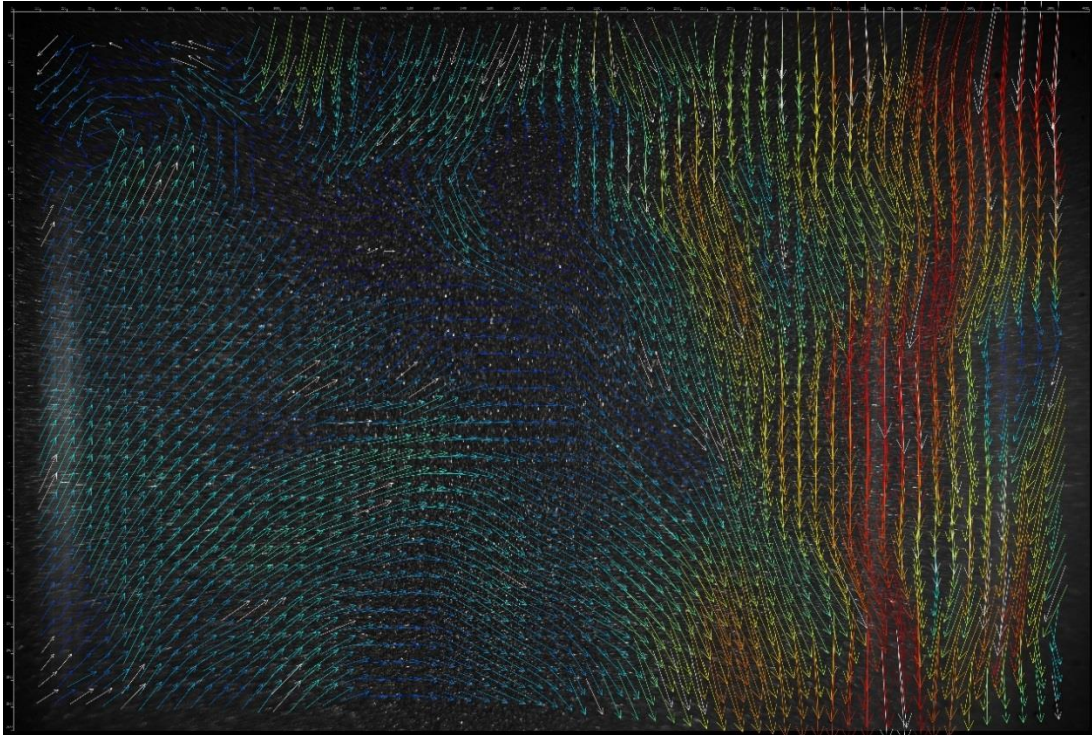


Fig.5.8 PIV image of the region 8 to 11 cm from the nozzle inlet for 100% aspirator rate

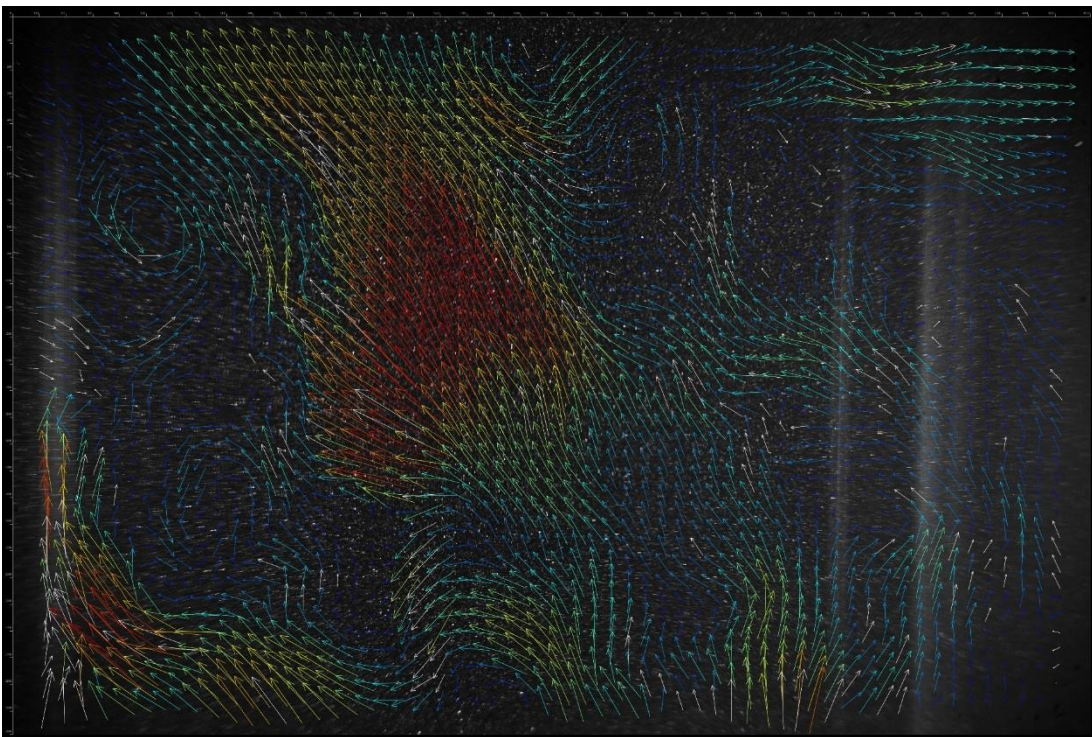


Fig.5.9 PIV image of the region 14 to 17 cm from the nozzle inlet for 100% aspirator rate

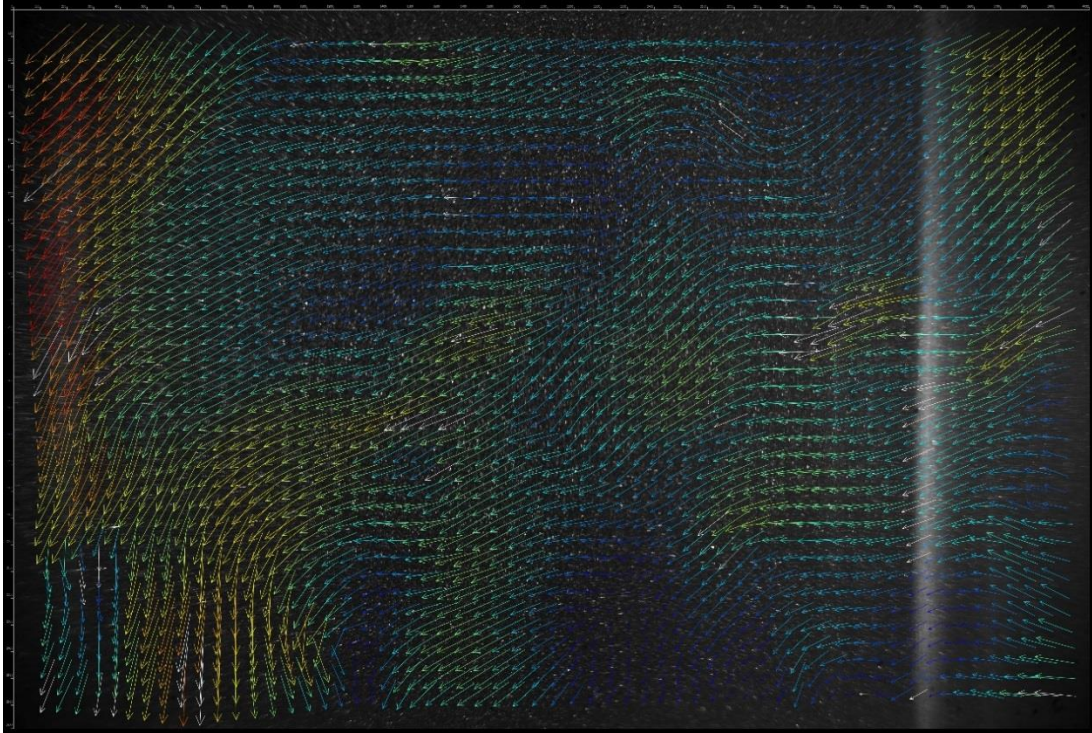


Fig.5.10 PIV image of the region 29 to 32 cm from the nozzle inlet for 100% aspirator rate

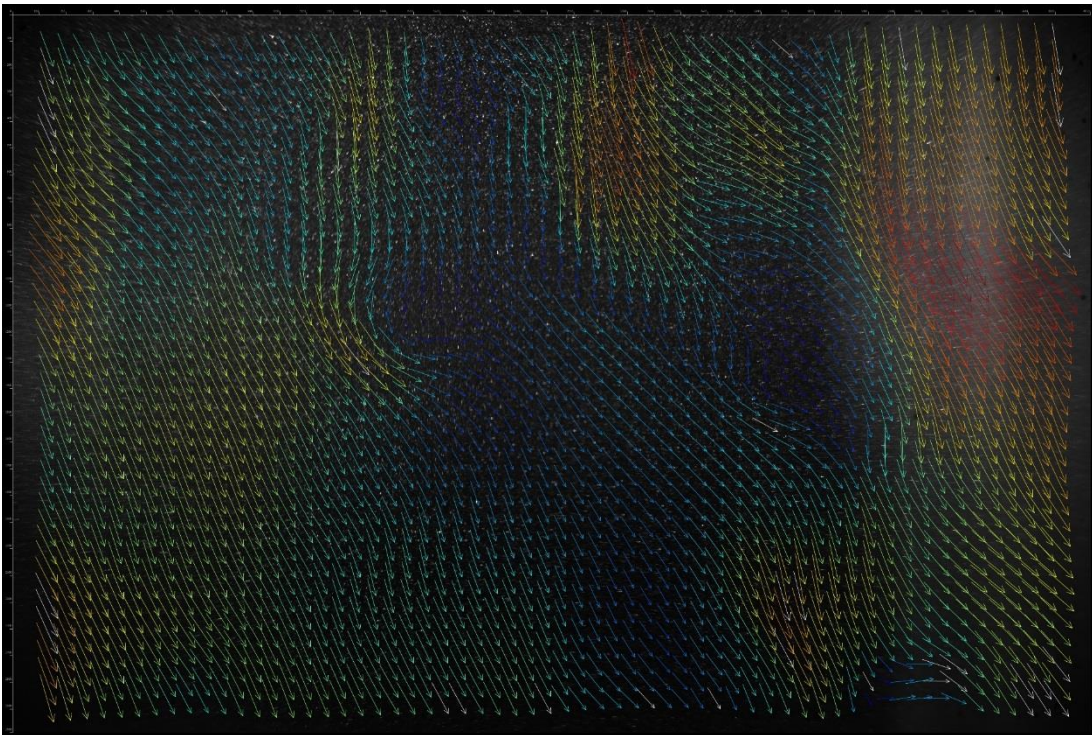


Fig.5.11 PIV image of the region 38 to 41 cm from the nozzle inlet for 100% aspirator rate

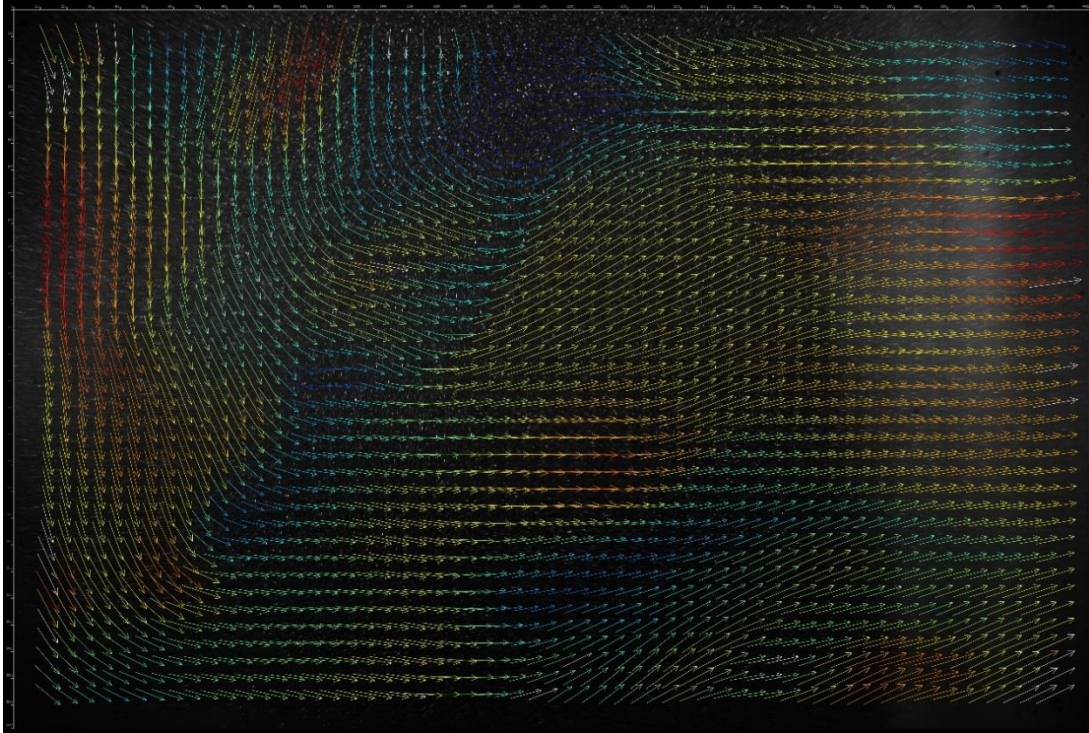


Fig.5.12 PIV image of the region 41 to 44 cm from the nozzle inlet for 100% aspirator rate

It is shown from the present work that the PIV measurements of the airflow pattern in the spray dryer reveal a turbulent/transitional dominant flow condition. The application of PIV in the chamber provides an overall visualization of the flow behavior that could serve for the validation of future CFD numerical results. However, there is still lack of quantitative experimental data on airflow information to allow selection or validation of appropriate turbulence models. Additional PIV experiments are necessary to characterize the flow fields in the spray dryer, including studies to determine the three-dimensional flow structures.

Conclusion

The airflow pattern in the spray dryer chamber were evaluated using PIV analysis at several locations in the spray dryer chamber in the absence of spray. Large recirculation zones and vortices were observed in the dryer chamber which strongly suggested the flow in the chamber has high turbulence intensity. When operated at 100% aspirator rate, the observed airflow pattern included a laminar-like downward flow near the air inlet, recirculation pattern zones at the upper part of the chamber, half circle airflow patterns at the lower part of the chamber and horizontal air movement near the side outlet. These results have potential to be used for validation of CFD simulations.

References

Adrian RJ, 1983. Laser velocimetry. *Fluid Mechanics Measurements*. Taylor & Francis. 155-244.

Adrian RJ & Westerweel J, 2010. *Particle Image Velocimetry*. Cambridge: Cambridge University Press.

Angarita-Jaimes D, Towers CE and Towers DP, 2012. Three component multi-phase velocimetry measurements on a GDI spray using optically efficient fluorescent tracers. *Experiments in Fluids*. 52(4):949-962.

Bosbach J, Kühn M, Wagner C, 2009. Large scale particle image velocimetry with helium filled soap bubbles. *Experiments in Fluids*. 46(3):539-547.

Brücker C, Hess D, Kitzhofer J, 2013. Single-view volumetric PIV via high-resolution scanning, isotropic voxel restructuring and 3D least-squares matching (3D-LSM). *Measurement Science and Technology*. 24(2):024001.

Cao GY, Sivukari M, Kurnitski J, Ruponen M, Seppanen O, 2010a. Particle Image Velocimetry (PIV) application in the measurement of indoor air distribution by an active chilled beam. *Building and Environment*. 45(9):1932-1940.

Cao GY, Sivukari M, Kurnitski J, Ruponen M, 2010b. PIV measurement of the attached plane jet velocity field at a high turbulence intensity level in a room. *International Journal of Heat and Fluid Flow*. 31(5):897-908.

Cao XD, Liu JJ, Nan J, Chen QY, 2014. Particle image velocimetry measurement of indoor airflow field: A review of the technologies and applications. *Energy and Buildings*. 69(2014):367-380.

Dantec Dynamics, FlowSense EO Camera Series, 2012, www.dantecdynamics.com.

- Elsinga GE & Ganapathisubramani B, 2013. Advances in 3D velocimetry. *Measurement Science and Technology*. 24(2):020301.
- Fansler TD & Parrish SE, 2015. Spray measurement technology: a review. *Measurement Science and Technology*. 26:012002.
- Gabites JR, Abrahamson J, Winchester JA, 2010. Air flow patterns in an industrial milk powder spray dryer. *Chemical Engineering Research and Design*. 88(7):899-910.
- Gui L, Longo J, Stern F, 2001. Biases of PIV measurement of turbulent flow and the masked correlation-based interrogation algorithm. *Experiments in Fluids*. 30(1):27-35.
- Guo L & Maghirang RG, 2012. Numerical Simulation of Airflow and Particle Collection by Vegetative Barriers. *Engineering Applications of Computational Fluid Mechanics*. 6(1):110-122.
- Hagemeier T, Börner M, Bück A, Tsotsas E, 2015. A comparative study on optical techniques for the estimation of granular flow velocities. *Chemical Engineering Science*. 131(2015):63-75.
- Hain R, Kahler CJ, Tropea C, 2007. Comparison of CCD, CMOS and intensified cameras. *Experiments in Fluids*. 42(3):403-411.
- Hart, 2000. PIV error correction. *Experiments in Fluids*. 29(1):13-22.
- Hoomans BPB, Kuipers JAM, MohdSalleh MA, Stein M, Seville JPK, 2001. Experimental validation of granular dynamics simulations of gas-fluidised beds with homogenous in-flow conditions using positron emission particle tracking. *Powder Technol*. 116(2-3):166-177.

- Hreiz R, Abdelouahed L, Fünfschilling D, Lopicque F, 2015. Electrogenerated bubbles induced convection in narrow vertical cells: PIV measurements and Euler–Lagrange CFD simulation. *Chemical Engineering Science*. 134(2015):138-152.
- Kähler C, Sammler B, Kompenhans J, 2002. Generation and control of particle size distributions for optical velocity measurement techniques in fluid mechanics. *Experiments in Fluids*. 33(2002):736–742.
- Langrish TAG & Premarajah R, 2013. Antioxidant capacity of spray-dried plant extracts: Experiments and simulations. *Advanced Powder Technology*. 24(4):771-779.
- Langrish TAG, Williams J, Fletcher DF, 2004. Simulation of the effects of inlet swirl on gas flow patterns in a pilot-scale spray dryer. *Chemical Engineering Research & Design*. 82(A7):821-833.
- Khodarahmi I, 2015. Comparing velocity and fluid shear stress in a stenotic phantom with steady flow: phase-contrast MRI, particle image velocimetry and computational fluid dynamics. *Magnetic Resonance Materials in Physics, Biology and Medicine*. 28(4):385-393.
- Kieviet FG, Van Raaij J, De Moor PPEA, Kerkhof PJAM, 1997. Measurement and Modelling of the Air Flow Pattern in a Pilot-Plant Spray Dryer. *Chemical Engineering Research and Design*. 75(3):321-328.
- Kim HT, 2015. Preliminary test results and CFD analysis for Moderator Circulation Test (MCT). *Annals of Nuclear Energy*. 85(2015):386-393.
- Kitzhofer J, Nonn T, Brückner C, 2011. Generation and visualization of volumetric PIV data fields. *Experiments in Fluids*. 51(6):1471–1492.

- Kitzhofer J, Ergin F, Jaunet V, 2012. 2D least squares matching applied to PIV challenge data (Part 1). Proceedings of 16th International Symposium on Applications of Laser Techniques to Fluid Mechanics, Lisbon, Portugal.
- Kumara WAS, Elseth G, Halvorsen BM, Melaaen MC, 2010. Comparison of Particle Image Velocimetry and Laser Doppler Anemometry measurement methods applied to the oil-water flow in horizontal pipe. *Flow Measurement and Instrumentation*. 21(2):105-117.
- Kuriakose R, Anandharamakrishnan C, 2010. Computational fluid dynamics (CFD) applications in spray drying of food products. *Trends in Food Science & Technology*. 21(8):383-398.
- Ma R, Dong B, Yu ZQ, Zhang T, Wang Y, Li WZ, 2015. An experimental study on the spray characteristics of the air-blast atomizer. *Applied Thermal Engineering*. 88(2015):149-156.
- Melling A, 1997. Tracer particles and seeding for particle image velocimetry. *Measurement Science and Technology*. 8(12):1406-1416.
- Melnick MB & Thurow BS, 2011. Simultaneous 3-D Flow Visualization with 2-D PIV to Observe a Turbulent Boundary Layer. 49th AIAA Aerospace Sciences Meeting including the New Horizons Forum and Aerospace Exposition. P750.
- Melnick MB & Thurow BS, 2012. Experimental Investigation of a Turbulent Boundary Layer Using Simultaneous 3-D Flow Visualization and 2-D PIV. 50th AIAA Aerospace Sciences Meeting including the New Horizons Forum and Aerospace Exposition. P752.
- Meyerss JF, 1991. Generation of particles and seeding. VKI for Fluid Dynamics, Lecture Series 1991-08, Laser Velocimetry.
- Meyer KE, Velte CM, Ullum T, 2011. PIV measurements of flow structures in a spray dryer. 9th International symposium on Particle Image Velocimetry - PIV11, Kobe, Japan, July 21-23, 2011.

- Mychkovsky A, Rangarajan D, Ceccio S, 2012. Ldv measurements and analysis of gas and particulate phase velocity profiles in a vertical jet plume in a 2D bubbling fluidized bed part1: a two-phase LDV measurement technique. Powder Technol. 220 (2012):55-62.
- Pawar SK, Abrahams RHM, Deen NG, Padding JT, van der Gulik GJ, Jongsma A, Innings F, Kuipers JAM, 2014. An experimental study of dynamic jet behavior in a scaled cold flow spray dryer model using PIV. The Canadian Journal of Chemical Engineering. 92(12):2013-2020.
- Pfeifer C, Bruzzese C, Fast G, Kuhn D, Class AG, 2011. Application of the Tomographic Laser Doppler Anemometry (TDLA) to a fuel spray. Flow Measurement and Instrumentation. 22(5):456-460.
- Raffel M, Willert CE, Wereley ST, Kompenhans J, 2007. Particle Image Velocimetry: A Practical Guide. Springer-Verlag Berlin Heidelberg.
- Roustapour OR, Hosseinalipour M, Ghobadian B, Mohaghegh F, Azad NM, 2009. A proposed numerical–experimental method for drying kinetics in a spray dryer. Journal of Food Engineering. 90(1):20-26.
- Saarenrinne P, Piirto M, Eloranta H, 2001. Experiences of turbulence measurement with PIV. Measurement Science and Technology. 12(11):1904-1910.
- Southwell DB & Langrish TAG, 2001. The effect of swirl on flow stability in spray dryers. Chemical Engineering Research & Design. 79(A3):222-234.
- Stafford RA, Fauroux O, Glass DH, 1997. Flow visualisation and instantaneous velocity measurements of spray dryer gas and spray flows using particle image velocimetry. Drying Technology. 15(6-8):1661-1671.

- Sun YG & Zhang YH, 2007. An Overview of Room Air Motion Measurement: Technology and Application. HVAC&R Research. 13(6):929-950.
- Theunissen R, Scarano F, Riethmuller ML, 2010. Spatially adaptive PIV interrogation based on data ensemble. Experiments in Fluids. 48(5):875–887.
- Thielicke, W. & Stamhuis, EJ, 2014. PIVlab-Towards User-friendly, Affordable and Accurate Digital Particle Image Velocimetry in MATLAB. Journal of Open Research Software. 2(1):e30.
- Thielicke, W. and Stamhuis, EJ, 2015. PIVlab - Time-Resolved Digital Particle Image Velocimetry Tool for MATLAB (version: 1.4).
- Toschkoff G, Suzzi D, Tritthart W, Reiter F, Schlingmann M and Khinast JG, 2012. Detailed analysis of air flow and spray loss in a pharmaceutical coating process. AIChE Journal. 58(2):399-411.
- van Hooff T, Blocken B, Defraeye T, Carmeliet J, van Heijst GJF, 2012. PIV measurements and analysis of transitional flow in a reduced-scale model: Ventilation by a free plane jet with Coanda effect. Building and Environment. 56(2012):301-313.
- Wawrzyniak P, Podyma M, Zbicinski I, Bartczak Z, Rabaeva J, 2012. Modeling of Air Flow in an Industrial Countercurrent Spray-Drying Tower. Drying Technology. 30(2):217-224.
- Westerweel J, 2000. Theoretical analysis of the measurement precision in particle image velocimetry. Experiments in Fluids. 29(1):S003–S012.
- Woo MW, Mujumdar AS, Daud WRW, 2010. Spray drying technology. ISBN - 978-981-08-6270-1, Published in Singapore.

Yoshida H, Kuwana A, Shibata H, Izutsu K-i, Goda Y, 2015. Particle Image Velocimetry
Evaluation of Fluid Flow Profiles in USP 4 Flow-Through Dissolution Cells.
Pharmaceutical Research. 32(9):2950-2959.

Chapter 6

Conclusion and future work

In this dissertation, spray drying technology was developed for microencapsulation of bioactive materials. The contributions of this work include the following.

1. The potential of gelatin as wall material for encapsulation was investigated. The droplet shrinkage behavior of gelatin droplets during spray drying was visualized by a high magnification imaging system, which provided understanding of the gelatin drying behavior that benefits the production of gelatin-based microcapsules by spray drying.
2. Stable O/W emulsion consisting of lipophilic components was successfully fabricated by both high and low-energy methods. High energy method was preferred for safety and health concerns. The emulsions were further spray dried and the results demonstrated that this emulsion-based system was suitable for encapsulation of bioactive materials.
3. The feasibility of the self-built capacitance sensor system to measure MC was well supported in three different modes. Future work should focus on approaches to enhance system accuracy.
4. Turbulent behavior of the airflow pattern inside the spray dryer was visualized by the PIV system, which was useful to guide the selection of turbulence models for the airflow. Future work should be done to collect more data for validation of CFD simulation results.